Swansea University E-Theses

Aeroelastic methodology for flight vehicles.

Bach, Can T

How to cite:

Bach, Can T (2004) *Aeroelastic methodology for flight vehicles..* thesis, Swansea University.
http://cronfa.swan.ac.uk/Record/cronfa42259

Use policy:

This item is brought to you by Swansea University. Any person downloading material is agreeing to abide by the terms of the repository licence: copies of full text items may be used or reproduced in any format or medium, without prior permission for personal research or study, educational or non-commercial purposes only. The copyright for any work remains with the original author unless otherwise specified. The full-text must not be sold in any format or medium without the formal permission of the copyright holder. Permission for multiple reproductions should be obtained from the original author.

Authors are personally responsible for adhering to copyright and publisher restrictions when uploading content to the repository.

Please link to the metadata record in the Swansea University repository, Cronfa (link given in the citation reference above.)

http://www.swansea.ac.uk/library/researchsupport/ris-support/

Aeroelastic Methodology For Flight Vehicles

by

Can T. Bach

Thesis submitted to the University of Wales
In candidature for the degree of Doctor of Philosophy

Department of Civil Engineering
University College of Swansea

JANUARY 19, 2004

ProQuest Number: 10797967

All rights reserved

INFORMATION TO ALL USERS
The quality of this reproduction is dependent upon the quality of the copy submitted.

In the unlikely event that the author did not send a complete manuscript
and there are missing pages, these will be noted. Also, if material had to be removed,
a note will indicate the deletion.

ProQuest 10797967

Published by ProQuest LLC (2018). Copyright of the Dissertation is held by the Author.

All rights reserved.
This work is protected against unauthorized copying under Title 17, United States Code
Microform Edition © ProQuest LLC.

ProQuest LLC.
789 East Eisenhower Parkway
P.O. Box 1346
Ann Arbor, MI 48106 – 1346

DECLARATION

This work has not previously been accepted in substance for any degree and is not being submitted in candidature for any degree.

....
Candidate

Jan 22, 04
Date

STATEMENT 1

This thesis is the result of my own investigations, except where otherwise stated. Other sources are acknowledged by footnotes giving explicit references. A bibliography is appended.

....
Candidate

Jan 22, 04
Date

STATEMENT 2

I hereby give consent for my thesis, If accepted, to be available for photocopying and for inter-library loan, and for the title and summary to be made available to outside organisations.

....
Candidate

Jan 22, 04
Date

Acknowledgement

I would like to express my most sincere gratitude to Dr. Kajal Gupta for his valuable guidance and continual support during the most difficult times of the research work. This work was primarily carried out at the NASA Dryden Flight Research Center and I gratefully acknowledge the assistance I received from the center in the preparation of the work. I would like to thank Mr. Marty Brenner for their help and knowledge in control systems, Dr. Andrew Arena and his students Mr. Tim Cowan and Cole Stephens for the help with ARMA code and the BACT wing control models. I like to express many thanks to Mr. Ed Hahn, Tim Doyle, Roger Truax and Tom Walsh for their help with STARS. I wish to thank Professor Ken Morgan for his continued encouragement and much patience during the tenure of this work. I most grateful to Dr. John Meek for his help and interest in seeing the completion of this thesis. Finally, I would like to express my deepest gratitude to my parents, husband and family for their constant support and encouragement.

Abstract

This thesis is set out as follows: In Chapter 1, the definition of flutter is given, together with a brief history and a short summary of some of the well know methods used in modeling and formulating the components of the equations of motion that have been employed previously. Chapter 2 includes the formulation of the numerical equations of motion for different types of structure and the numerical techniques used to solve these system of equations to obtain the structural characteristic eigensolution. Chapter 3 demonstrates the linear methods used in the panel method to compute the components of aerodynamic forces in the equations of motion, and their application in the solution of aeroelastic and aeroservoelastic problems. Chapter 4 shows the formulation of the nonlinear aerodynamic force component and its integration with the aeroelastic and aeroservoelastic multidiscipline. The formulation of the sensor and control systems and their integration are also detailed in this chapter. Chapter 5 gives the example test cases used for the aeroelastic and aeroservoelastic analysis. Chapter 6 is a short conclusion and is a summary of the study presented herein. A Matlab independent modeling of the aeroservoelastic integration is included in Appendix A. Appendix B and C give the example problem modeling data and formats.

TABLE OF CONTENTS

FIGURES AND TABLES

Nomenclature

$\mathbf{A}$	=	plant dynamics matrix in body fixed coordinates
$\mathbf{A}_c, \mathbf{B}_c, \mathbf{C}_c, \mathbf{D}_c$	=	analog control state-space matrices
$\mathbf{A}_s, \mathbf{B}_s, \mathbf{C}_s, \mathbf{D}_s$	=	analog structural state-space matrices
$\mathbf{A}_e(k)$	=	aerodynamic influence coefficient matrix
$\hat{\mathbf{A}}$	=	plant dynamics matrix in inertial frame of reference
ARMA	=	autoregressive moving average model
ASE	=	aeroservoelasticity
$\mathbf{B}$	=	control influence matrix in body-fixed coordinates
$\hat{\mathbf{B}}$	=	control influence matrix in inertial frame of reference
$\mathbf{C}$	=	control output state matrix in body fixed coordinates
$C, \hat{\mathbf{C}}$	=	standard and generalized structural damping matrix
$\mathbf{C}_c$	=	Coriolis acceleration matrix
$\mathbf{C}_d$	=	elastic damping matrix
c	=	mean aerodynamic chord
$\mathbf{D}$	=	control output matrix in body-fixed coordinates
E	=	Young's Modulus
f_a	=	generalized aerodynamic force vector
$\hat{f}_a$	=	scaled generalized aerodynamic force vector
f_I	=	generalized impulse force input vector
g	=	aeroelastic or structural damping
$\mathbf{G}_a, \mathbf{H}_a, \mathbf{C}_a, \mathbf{D}_a$	=	digitized aerodynamic state-space matrices

$\mathbf{G}_c, \mathbf{H}_c, \mathbf{C}_c, \mathbf{D}_c$	=	digitized control state-space matrices
$\mathbf{G}_s, \mathbf{H}_s, \mathbf{C}_s, \mathbf{D}_s$	=	digitized structural state-space matrices
$\mathbf{G}_{sa}, \mathbf{H}_{sa}, \mathbf{C}_{sa}, \mathbf{D}_{sa}$	=	digitized aeroelastic state-space matrices
$\mathbf{G}_{sac}, \mathbf{H}_{sac}, \mathbf{C}_{sac}, \mathbf{D}_{sac}$	=	digitized aeroservoelastic state-space matrices
i^*	=	$\sqrt{-1}$, imaginary number
$\mathbf{K}$	=	elastic stiffness matrix
$\mathbf{K}_G$	=	geometric stiffness matrix
$\hat{\mathbf{K}}$	=	generalized stiffness matrix ($\Phi^T \mathbf{K} \Phi$)
k	=	reduced frequency
k_i	=	discrete set of reduced frequencies
$\mathbf{M}$	=	elastic mass or inertia matrix
$\hat{\mathbf{M}}$	=	generalized mass matrix ($\Phi^T \mathbf{M} \Phi$)
$\mathbf{Q}$	=	generalized aerodynamic force matrix
$\hat{\mathbf{Q}}$	=	linear approximation of $\mathbf{Q}$
$\hat{\mathbf{Q}}_R, \hat{\mathbf{Q}}_I$	=	real and imaginary components of $\hat{\mathbf{Q}}$
$\mathbf{q}$	=	generalized displacement vector
$\bar{q}$	=	dynamic pressure $\frac{1}{2}\rho V^2$
$\dot{\mathbf{q}}, \ddot{\mathbf{q}}$	=	generalized velocity and acceleration
s	=	Laplace transform variable
T, dt, Δt	=	sampling time for digital control system
u,$\mathbf{U}$	=	real displacement vector

$\boldsymbol{u}_c$	=	control system input vector for single input control system/ control system input matrix for multi input control system
$\mathbf{x}$	=	system state vector
$\mathbf{x}_a$	=	aerodynamic system state vector
$\mathbf{x}_c$	=	control system state vector
$\mathbf{x}_s$	=	structural system state vector $(\mathbf{q}, \dot{\mathbf{q}})$
$\boldsymbol{y}_c$	=	control system output vector
$\boldsymbol{y}_s$	=	structural system output vector $(\mathbf{q}, \dot{\mathbf{q}})$
α	=	angle of attack
β_i	=	aerodynamic lag terms
δ	=	angle of deflection for control surface
η	=	generalized coordinate vector
λ	=	natural frequencies
ν	=	Poisson's ratio
ρ	=	density
$\hat{\rho}$	=	training density used for ARMA model
$\mathbf{\Phi}$	=	structural vibration mode shapes
ω	=	frequency

CHAPTER 1

A BRIEF DESCRIPTION OF AEROELASTICITY DEVELOPMENT

1.1 Definition of Aeroelasticity

The term aeroelasticty[1] is used to define phenomena that involve the interaction between inertial forces, aerodynamic forces and elastic forces. Aeroelasticity is commonly divided into static and dynamic analysis. Dynamic aeroelasticity includes phenomena such as flutter, gust response and limit cycle analysis while static aeroelasticity includes divergence, flight loads and control surface effectiveness analysis.

Static aeroelasticity includes the fundamental physics of two distinct phenomena, (1) 'divergence' or static instability and (2) loss of aerodynamic effectiveness usually known as 'control surface reversal'. The particular case of an oscillation with zero frequency, in which the structural frame is rigid and the inertia force may be neglected, is called the steady-state, or static aeroelastic instability. Static aeroelasticity is an interaction between the fluid mechanics and solid mechanics disciplines.

A major problem occurs when small disturbances of an incidental nature induce more or less violent uncontrollable oscillations. This is a case of dynamic aeroelasticity termed 'flutter' and has been known to affect, for example, airplanes and suspension bridges. Flutter is characterized by the interactions between aerodynamic, elastic and inertia forces as shown in Figure 1.1. Dynamic aeroelasticity involves external self-induced airloads that vary with time. Dynamic loads on the airplane structure not only produce translation and rotation of the structure but also tend to excite vibration of the elastic structure, which in turn generates new airloads. Initial excitement of the dynamic loads usually comes from atmospheric turbulence or gusts. Dynamic aeroelasticity is concerned with the physical phenomena known as 'flutter' or dynamic instability and dynamic response to various dynamic loads as modified by aeroelastic effects.

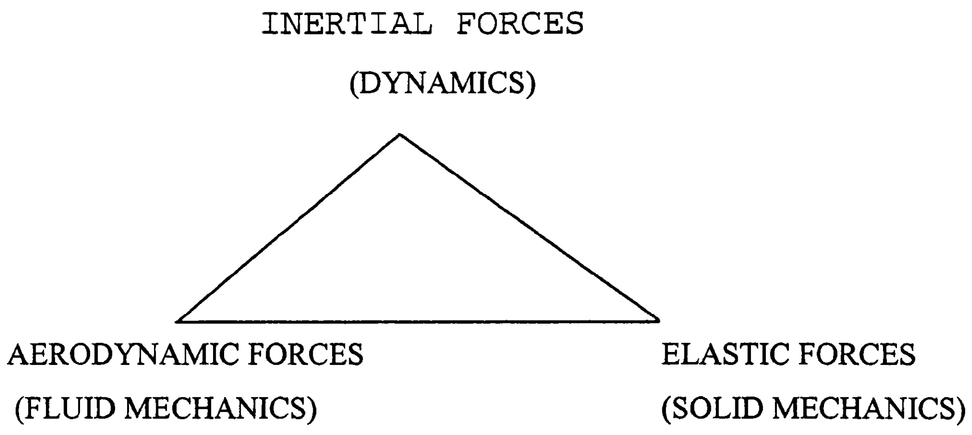

Figure 1.1 The disciplines of aeroelasticity.

Combining the vertices of the triangle in Figure 1.1 one can identify other important technical fields. For example,

Stability and control (flight mechanics)= dynamics (inertial forces)+ aerodynamics

Structural vibrations= dynamics (inertial forces)+ solid mechanics (elastic forces)

1.2 Formulation of the Dynamic Equations of Motion

The theoretical model of dynamic aeroelasticity starts with the formulation of the theoretical dynamic model [2,3]. This model has the general form

$$M\ddot{X} + C\dot{X} + KX = F_a \tag{1.1}$$

The dynamic model is represented by the left-hand side of the equation (1.1), which includes the inertia force ($M\ddot{X}$), the damping force ($C\dot{X}$), and the elastic force (KX) components. The aerodynamic forces (F_a), which are on the right hand side of the equation, will be discussed in the next section. In the case when F_a is zero in equation (1.1), the elastic vibration problem will be solved for the aeroelastic system and eigenvalues and eigenvectors will be computed from this equation. The principle of superposition is applied to the analysis of all linearized systems. This implies that the total linear deformation and angular deflection of any point is the sum of the deflections at the point produced by the individual forces and moments separately.

Historically, simple formulations were developed for the deflection of a beam element and, gradually, these formulations were developed to provide more complicated models, such as a wing planform. The deformation, x, of the beam is expressed in terms of a summation of a series of continuous sine and cosine functions that satisfy the boundary constraints and the initial conditions.

Principle of Minimum Potential Energy: Among all possible deformation configurations compatible with the geometric constraints, the configuration, which satisfies the equations of static equilibrium, is the one that minimizes the potential energy

$$\delta U_e - \delta W = \delta(U_e - W) = 0 \tag{1.2}$$

where δW is the virtual work done by the external forces and δU_e is the strain energy resulting from a small virtual displacement of the body. This is the principle of minimum potential energy applied to conservative systems. This principle of minimum potential energy is based upon the principle of virtual displacements. The principle of virtual displacements, applied to deformable bodies, may be stated as follows: if a body is in equilibrium under the action of prescribed forces, the work (virtual work) done by these forces in a small additional displacement compatible with the geometric constraints (virtual displacement) is equal to the change in strain energy.

$$\delta U_e = \delta W \tag{1.3}$$

Normally, Newton's 2nd law ($F = ma = m\frac{d^2x}{d^2t}$) together with Hooke's law ($F = kx$) are sufficient to obtain the equations of motion of any elastic body. For a system with a large number of degrees of freedom, an alternative procedure based on Hamilton's principle or Lagrange's equation may be used to formulate the generalized equations of motion for an aeroelastic system. Energy methods are widely used in aeroelastic problems for determining the deformation of the structural shape under static and dynamic loads and in the calculation of the stiffness influence functions and coefficients.

1.2.1 Hamilton's Principle

Hamilton's Principle starts from Newton's Second Law of motion[3], expressed in the form

$$F = m\frac{d^2x}{d^2t} \tag{1.4}$$

where $\boldsymbol{F}$ is the force vector and $\boldsymbol{x}$ is the displacement vector. Consider a particle with mass m which moves a finite small displacement of amount δx, which is referred to as a small 'virtual displacement'. We form the dot product of the force $\boldsymbol{F}$ with the displacement $\boldsymbol{x}$ and integrate from t_1 to t_2, to give

$$\int_{t_1}^{t_2}(m\frac{d^2\boldsymbol{x}}{d^2t}\cdot\delta x-\boldsymbol{F}\cdot\delta x)dt=0 \qquad (1.5)$$

where the term $\boldsymbol{F}\cdot\delta x$ denotes the 'virtual work'. The virtual work is defined as the work done by the actual forces being moved through the virtual displacement. Since δx is zero at t_1 and t_2, it follows that the first term of the above equation may be integrated by parts to give

$$m\int_{t_2}^{t_1}\frac{d^2\boldsymbol{x}}{dt^2}\cdot\delta\boldsymbol{x}dt=m\frac{d^2\boldsymbol{x}}{dt^2}\cdot\delta x\,|_{t_2}^{t_1}-m\int\frac{d\boldsymbol{x}}{dt}\cdot\frac{d}{dt}(\delta\boldsymbol{x})dt$$

$$=-m\int_{t_2}^{t_1}\frac{d\boldsymbol{x}}{dt}\cdot\delta\frac{d\boldsymbol{x}}{dt}dt$$

$$=-\frac{m}{2}\int_{t_2}^{t_1}\delta(\frac{d\boldsymbol{x}}{dt}\cdot\frac{d\boldsymbol{x}}{dt})dt$$

With this result, equation (1.5) now be written as

$$\int_{t_1}^{t_2}(-\tfrac{1}{2}m\delta(\frac{d\boldsymbol{x}}{dt}\cdot\frac{d\boldsymbol{x}}{dt})-\boldsymbol{F}\cdot\delta x)dt=0 \qquad (1.6)$$

or

$$\int_{t_1}^{t_2}\delta(\boldsymbol{T}+\boldsymbol{W})dt=0 \qquad (1.7)$$

where $\delta\boldsymbol{T}$ is the 'virtual kinetic energy' and $\delta\boldsymbol{W}$ is the 'virtual work'. The problem has now been cast into a scaled energy form. Equation (1.7) is Hamilton's Principle and it is equivalent to Newton's Second Law. As this has been derived for an individual particle, the elastic energy is not included.

For an assembly of particles, the basic principle remains the same, with the work and energy expressions changed according to

$$\delta\boldsymbol{T}=\sum_i\frac{m_i}{2}\delta(\frac{dx_i}{dt}\cdot\frac{dx_i}{dt}) \qquad (1.8)$$

$$\delta W = \sum_i F_i \cdot \delta x_i \tag{1.9}$$

1.2.2 Lagrange's Equations

If the process to obtain Hamilton's Principle is reversed, Lagrange's[3] equations may be obtained. The concept of generalized coordinates is introduced with this method. The generalized coordinates are arbitrary and independent of the other coordinates. The equation of motion describing the dynamical system is represented by a set of generalized coordinates.

The displacement of a particle, or a point in a continuous body, is given as

$$\boldsymbol{x} = x(q_1, q_2, q_3, \cdots, t) \tag{1.10}$$

where q_i is the i^{th} generalized coordinate. It follows that

$$\boldsymbol{T} = \boldsymbol{T}(\dot{q}_i, q_i, t) \tag{1.11}$$

$$\boldsymbol{U}_e = \boldsymbol{U}_e(\dot{q}_i, q_i, t) \tag{1.12}$$

where $\boldsymbol{U}_e$ is the potential energy of an elastic body. Noting that equation (1.7) was derived for isolated particles, for an elastic body with internal forces connecting the masses, Hamilton's Principle may be written as

$$\int_1^2 [\delta(\boldsymbol{T} - \boldsymbol{U}_e) + \delta W_{NC}]dt = 0 \tag{1.13}$$

or

$$\sum_i \int_1^2 \left[\frac{\partial(\boldsymbol{T} - \boldsymbol{U}_e)}{\partial \dot{q}_i} \delta\dot{q}_i + \frac{\partial(\boldsymbol{T} - \boldsymbol{U}_e)}{\partial q_i} \delta q_i + \boldsymbol{Q}_i \delta q_i \right] dt = 0 \tag{1.14}$$

where $\boldsymbol{Q}_i$ is the i^{th} generalized force and $\delta W_{NC} = \sum_i \boldsymbol{Q}_i \delta q_i$ and the subscript *NC* denotes non–conservative.

Integrating (1.14) by parts, the equation may be recast in the form

$$\sum_i \int_1^2 \left[-\frac{d}{dt} \frac{\partial(\boldsymbol{T} - \boldsymbol{U}_e)}{\partial \dot{q}_i} + \frac{\partial(\boldsymbol{T} - \boldsymbol{U}_e)}{\partial q_i} + \boldsymbol{Q}_i \right] \delta q_i dt = 0 \tag{1.15}$$

and, since δq_i is independent and arbitrary, it follows that the term inside the square brackets must be zero i.e.

$$-\frac{d}{dt}\frac{\partial(T-U_e)}{\partial\dot{q}_i}+\frac{\partial(T-U_e)}{\partial q_i}+Q_i=0 \qquad \text{i=1,2, 3, ...} \qquad (1.16)$$

These are Lagrange's equations.

1.2.3 Rayleigh Ritz method

Using the principle of minimum potential energy, the components of the displacement vector for the structure can be expressed, as functions of the generalized coordinates, as

$$\begin{aligned} u &= u\ (x,y,z,q_1,q_2,...,q_n) \\ v &= v\ (x,y,z,q_1,q_2,...,q_n) \\ w &= w\ (x,y,z,q_1,q_2,...,q_n) \end{aligned} \qquad (1.17)$$

The work done by the surface forces of an arbitrary virtual displacement may them be written as

$$\delta W_e = \int_S (F_x \delta u + F_y \delta v + F_z \delta w)dS$$

$$\delta W_e = \sum_{i=1}^{n}\{\int(F_x\frac{\partial u}{\partial q_i} + F_y\frac{\partial v}{\partial q_i} + F_z\frac{\partial w}{\partial q_i})dS\}\delta q_i = \sum_{i=1}^{n} Q_i\delta q_i \qquad (1.18)$$

where Q_i is the generalized force which corresponds to the generalized coordinate q_i. The strain energy due to an arbitrary virtual displacement of the generalized coordinates may be written as

$$\delta U_e = \sum_{i=1}^{n}\frac{\partial U_e}{\partial q_i}\delta q_i$$

and, applying these equations to the principle of minimum of potential energy of equation (1.2), yields

$$\sum_{i=1}^{n}\left\{Q_i - \frac{\partial U_e}{\partial q_i}\right\}\delta q_i = 0 \qquad (1.19)$$

Since the δq_i are independent and arbitrary, it follows that

$$\sum_{i=1}^{n}\left\{Q_i - \frac{\partial U_e}{\partial q_i}\right\} = 0 \qquad (1.20)$$

This equation is the equivalent form of the principle of minimum potential energy that is applicable to systems in which the space can be described by a set of discretized generalized coordinates. When n is finite, this process is called the Rayleigh–Ritz approximate solution method. If n is increased without limit, it is possible for the equilibrium equation (1.20) to yield an exact solution.

1.3 Methods of Computing the Aerodynamic Forces

In this section, a brief summary is given of some of the well known conventional approximate methods that may be used to compute and linearize the aerodynamic force components in the aeroelastic problem [4,5]. Usually, simplifying assumptions are made with respect to the spatial or temporal dependence of the aerodynamic forces.

Strip Theory Approximation: Reference 3 defines this as follows "*In this approximation, the known results for 2–dimensional flow (infinite span airfoil) are used to compute the aerodynamic forces on the lifting surface of finite span. The essence of the approximation is to consider each spanwise station as if it was a portion of an infinite span wing with uniform spanwise properties. From this assumption, the lift (or, generally, the chordwise pressure distribution) at any spanwise station depends only on the downwash at that station as given by two–dimensional aerodynamic theory and to be independent of the downwash at any other spanwise station. 'Strip theory' includes methods such as doublet lattice and Mach box or constant pressure method. These methods use a kernel function to calculate the influence coefficients in the computation of the downwashes*".

Quasi–Steady Approximation: The strip theory approximation discussed above is clear and its meaning is generally accepted. However, this is not the case for the quasi–steady approximation. The qualitative meaning is generally accepted, if the temporal memory effect in the aerodynamic model is ignored and it assumes the aerodynamic forces at any time depend only on the motion of the airfoil at the same time and are independent of the motion at any earlier time. The history of the motion is neglected as far as determining the aerodynamic forces. The piston theory aerodynamic approximation is inherently a quasi–steady approximation. For a high speed case (Mach number >> 1), the aerodynamic piston theory computes, at time t, the local pressure which depends only on the motion at that point without dependence on the motion history of this point or any other point.

Slender Body or Slender (Low Aspect Ratio) Wing Approximation: Reference 3 defines this methodology as "*Another approximation based upon spatial considerations is possible when the lifting surface has a low aspect ratio or one is dealing with a slender body. In such a case, the chordwise spatial rates of change (derivatives) may be neglected compared to spanwise rates of change and, hence, the chordwise coordinate effectively becomes a parameter rather than an independent coordinate. This approach is generally attributed to R. T. Jones. It is useful as an asymptotic check on numerical methods for slender bodies and low aspect ratio wings. However, it is useful for only a modest range of quantitative predictions of practical lifting surfaces.*"

1.4 Rationale for the Thesis

It is apparent, from a consideration of the history of structures in service, that the design of modern high speed aircraft, and slender structures, (for example, suspension bridges and electric power lines and even the submarine periscope) needs to consider the effects of elastic instability.

Their design requires a multidisciplinary approach, involving

Structural analysis

Aerodynamic analysis

Control analysis

It is the purpose of this thesis to delineate and further develop the general theory for the aeroservoelastic discipline problem and to demonstrate the validity of the proposed theory by including example problems involving practical flight vehicles. Related work in the area of aeroelasticity and aeroservoelasticity disciplines can be found in the research of Batina[6], Bendiksen[7] and Farhat[8]. Farhat and company use the three–field formulation to represent the coupled fluid and structure. The structure is represented by a finite element model, while the fluid is modeled in terms of an arbitrary Lagrangian–Eulerian form of the Euler equations[9], to enable the modeling of the interface between the solid and fluid for a frequency damping aeroelastic solution of an F–16 fighter configuration. Batina and Farhat have undertaken extensive work on aeroelastic analysis using dynamic meshes. Bendiksen treated the fluid–structure as a single continuum dynamics problem and switched from Eulerian to Lagrangian formulations at the fluid–

structure boundary[10,11-15].

1.5 Outline of Chapters 2–7

Chapter 2. A structural, solid mechanics numerical model using the finite element method is formulated for different dynamic loads. Solution techniques used in STARS to solve the system of equations of motion are discussed. The finite element method is used to discretize the structural continuum to obtain the simultaneous algebraic equations of equilibrium for static analysis, elastic buckling analysis, free vibration analysis of damped or undamped, spinning and nonspinning structures, dynamic response analysis and dynamic elements. Stability analysis and the determination of the dynamic response are vital components in ensuring the safe design of aerospace structures. The process of obtaining a reliable assessment of the structural natural frequency, and its associated free vibration mode shapes, is important in the determination of the dynamic response character for a structure subjected to external time dependent external forces, such as aerodynamic pressure. This presents an aeroelastic or aeroservoelastic type of problem. This chapter provides an over view of the class of structural dynamic systems that can be formulated and solved in the finite element STARS[16] code. To be able to carry out any additional type of multidisciplinary analysis, it is necessary to obtain a reliable structural dynamic behavior and this information is contained in the natural frequencies and mode shapes. When the equations of motion have been formulated and assembled, this chapter presents some of the most useful solution processes used in STARS for these system of equations. These include the Sturm sequence method and the Lanczos iteration[16,17].

Chapter 3. This Chapter considers the construction of the linear model to compute the aerodynamics component of the equations of motion. This is the time dependent external excitation that has to be applied on the right hand side of the equations of motion. The aerodynamic forces can be determined using a linear approximation method, such as a panel method. Panel methods include the doublet lattice and constant pressure methods. The aerodynamic force can be computed using the doublet lattice method for subsonic cases and the central pressure method is employed for supersonic flight conditions. When all components of the linearized equations of motion are obtained for the aeroelastic multidisciplinary problem, the stability analysis can then proceed. The K and PK stability solutions are most commonly used to determine the aeroelastic stability characteristics of a system. The methods provide the equivalent flutter speed and frequency for the structure at a specified flying condition. To touch upon the linear aeroservoelastic type of solution, the coupled aero–structure system of equations are converted to the Laplace (or *s*) domain. The generalized aerodynamic forces are curve fitted using Padé and least square approximations and rearranged into a state–space formulation. The controller, sensor and actuator systems of the structure can be augmented to the plant's state–space matrices using the control module in STARS, which yields a aeroservoelastic state–space matrix system of equations. The plant's state–space matrices can be formulated in the continuous or the discretized time domain. Automated steps to integrate of the control elements into the plant are built for STARS. The structural closed–loop stability is obtained by computing the eigenvalues of the closed loop structural state matrices. Frequency response is performed to obtain the necessary Bodé plots that are also calculated from the closed loop structural state-space matrices.

Chapter 4. In this chapter, the aerodynamic components in the system of equations of motion are computed using a nonlinear method. The aerodynamic force is computed for using an Euler computational fluid dynamics code. The chapter will describe the nonlinear aeroelastic and nonlinear aeroservoelasticity formulations and solution schemes. The key ingredients for a successful nonlinear multidisciplinary analysis tool are a 3–D unstructured tetrahedral grid generation, with adaptive mesh capability, and an explicit 3-D finite element Euler computational fluid dynamics code. The 3–D Euler flow solver provides the aerodynamic information in place of the linear constant pressure panel method that was discussed previously. The structural vibration characteristics must be interpolated into the aerodynamics mesh for the nonlinear aeroelastic and nonlinear aeroservoelastic analysis. This chapter is concerned with the modification of the finite element based analysis STARS program to integrate the structure–aero (aeroelasticity) disciplines into the program's simulation capabilities. The nonlinear aeroelasticity capability in STARS is based upon the implementation of the transpiration boundary condition method into the CFD flow solver. This approximation technique enables the boundary condition appropriate to the deformed structure to be applied in a computationally efficient manner, without changing or deforming the structure or the surrounding mesh.

A considerable amount of CPU time is required for a CFD based unsteady solution in an aeroelastic simulation analysis. This is even more pronounced when control analysis is coupled into the formulations. Part of the research effort has been devoted to speeding up the aerodynamic solution or to minimizing the CPU time required for the CFD analysis. To reduce the CPU time required for the aerodynamic model solution, an alternative unsteady analysis procedure is investigated. This procedure utilizes the system identification technique, to obtain a mathematical modeling of the aerodynamic CFD system based upon a set of measured outputs and input data from the system. The system identification method takes a collection of time histories of input and output and fits the parameters of a model structure that will accurately describe the dynamic characteristics and behavior of the actual aerodynamic system. This fitting is undertaken in such a way that the error output is minimized in the process. The success of the system identification technique relies on the choice of the structural analysis data and the quality of the data used for the input signal chosen for the training process of the model. This choice will be discussed in this chapter.

The coupling of the control module into the aeroelastic scheme in the STARS program is described in Chapter 4. For a uniform sampling rate, a closed loop aeroelastic and aeroservoelastic state–space formulation is derived for the determination of the flutter stability condition, using the root locus plot or the structural response of the coupled aeroservoelastic analysis in STARS. Sensor mechanisms are incorporated in the aeroservoelastic analysis. Multisampling rates aeroservoelastic analysis capability is discussed in this chapter.

Chapter 5. An example is presented involving an aeroservoelastic problem of a cantilever wing with control surface. Summaries of all of the necessary data files are also provided. Results are presented for the aeroservoelastic analysis of this cantilever wing with a control surface. The general description of the Hyperx/X43 is shown along with some of the final results of the aeroelastic analysis using STARS.

Chapter 6. Conclusion of the results obtained for the given examples problems using STARS aeroelastic/aeroservoelastic program is summarized in this chapter.

CHAPTER 2

NUMERICAL TECHNIQUES FOR STRUCTURAL VIBRATION ANALYSIS

2.1 Introduction

In this chapter, some of the numerical techniques used to study aeroelastic phenomena in the STARS computer software are introduced. These techniques largely relate to the solution of large–scale vibration and dynamic problems. In the following sections, the theoretical aspects of the structures module in the STARS code will be discussed in detail.

On the subject of the finite element method for free vibration analysis of structures, there are two distinct procedures involved in the analysis process. The first is the continuum discretization process using the finite element procedure, yielding simultaneous algebraic equations. The second is the solution process for the system of equations. The determination of some of the primary natural frequency and modes shapes plays a vital role in the evaluation of the dynamic response, and the structural stability characteristics, under flight conditions.

The solids module in STARS is capable of performing the analysis of static, stability, vibration and dynamics response problems for a wide variety engineering structures, including spinning and objects subjected to mechanical and thermal loading with general and composite material types [16,18,19,20].

2.2 Structural Modeling

A general overview of structural analysis is now presented.

Static analysis

The governing equation of static analysis is of the form

$$\mathbf{Ku} = \mathbf{P} \tag{2.1}$$

where

K = elastic stiffness matrix

$\mathbf{u}$ = nodal displacement vector

$\mathbf{P}$ = mechanical load vector(s), e.g. pressure and thermal loads

This system of linear simultaneous equations is solved using standard numerical procedures. Back substitution is used to obtain the structural displacements.

Elastic Buckling Analysis

This analysis is performed by solving the eigenvalue problem

$$[\mathbf{K}_E + \gamma \mathbf{K}_G]\mathbf{u} = 0 \qquad (2.2)$$

where

$\mathbf{K}_E$ = elastic stiffness

$\mathbf{K}_G$ = geometric stiffness

$\mathbf{u}$ = nodal buckled mode shape vector

γ = buckling load multiplier

The geometric stiffness is obtained when the equation of equilibrium is written in terms of the deformed coordinates and may act to stiffen (add to) or weaken (subtract from) the elastic structural stiffness.

Free Vibration Analysis Formulation

The most general governing equation for the free vibration of a spinning structure with viscous and structural damping is expressed in the form

$$[\mathbf{K}_E(1+i^* g)+\mathbf{K}_G+\mathbf{K}_C]\mathbf{u} \ + \ (\mathbf{C}_c+\mathbf{C}_D)\dot{\mathbf{u}} \ + \ \mathbf{M}\ddot{\mathbf{u}} = 0 \qquad (2.3)$$

where

$\mathbf{K}_C$ = centrifugal force matrix

$\mathbf{C}_c$ = Coriolis matrix

$\mathbf{C}_D$ = viscous damping matrix

$\mathbf{M}$ = inertia matrix

g = structural damping parameter (g=.02)

i^* = imaginary number

From this equation, free vibration in particular cases may be represented as follows:

1. Free vibration, undamped, nonspinning system

$$\mathbf{K}_E\mathbf{u} + \mathbf{M}\ddot{\mathbf{u}} = 0 \tag{2.4}$$

2. Free vibration, damped, nonspinning system

$$[\mathbf{K}_E(1+i^*g)]\mathbf{u} + (\mathbf{C}_D)\dot{\mathbf{u}} + \mathbf{M}\ddot{\mathbf{u}} = 0 \tag{2.5}$$

3. Free vibration, undamped, spinning structure

$$[\mathbf{K}_E + \mathbf{K}_G + \mathbf{K}_C]\mathbf{u} + (\mathbf{C}_c)\dot{\mathbf{u}} + \mathbf{M}\ddot{\mathbf{u}} = 0 \tag{2.6}$$

4. Free vibration, damped, spinning system

$$[\mathbf{K}_E(1+i^*g) + \mathbf{K}_G + \mathbf{K}_C]\mathbf{u} + (\mathbf{C}_c + \mathbf{C}_D)\dot{\mathbf{u}} + \mathbf{M}\ddot{\mathbf{u}} = 0 \tag{2.7}$$

Dynamic response analysis

The dynamic analysis is expressed by the governing differential equation

$$\mathbf{Ku} + \mathbf{C}\dot{\mathbf{u}} + \mathbf{M}\ddot{\mathbf{u}} = \mathbf{F}(t) \tag{2.8}$$

where **F**(t) is the dynamic forcing function, and **K** is the summation of the stiffness coefficients in equation (2.7).

A homogeneous solution is obtained by setting the right hand side of the above equation to zero. The particular solution is then obtained by the modal superposition method. The structural displacements can be computed, along with the stresses for a system subjected to specified dynamic mechanical and thermal loading conditions.

Dynamic element analysis

The equation of motion, expressed in series form in ascending powers of natural frequency ω, takes the form [17,21].

$$[\mathbf{K}_0 - \omega^2(\mathbf{M}_0 - \mathbf{K}_2) - \omega^4(\mathbf{M}_2 - \mathbf{K}_4) - \cdots]\mathbf{q} = 0 \tag{2.9}$$

where **q** is the amplitude of the displacement **u**, and $\mathbf{K}_0$ and $\mathbf{M}_0$ are the static stiffness and mass matrices, respectively. The higher order terms $\mathbf{K}_2, \mathbf{K}_4, \mathbf{M}_2$ constitute the dynamic corrections. The theory of structures is based upon the fundamental assumption that the deflections of a deformed solid element are small and that the governing equilibrium equations are not affected by the deformation. If the equations of equilibrium are expressed in the deformation position for small displacement, the equation of equilibrium will have linear stiffness and mass matrices as a function of the element shape functions. These terms are the dynamic correction terms $\mathbf{K}_2, \mathbf{K}_4, \mathbf{M}_2$. The standard vibration analysis of structures in the undeformed position usually involves the static matrices only and has the familiar form

$$[\mathbf{K}_0 - \omega^2 \mathbf{M}_0]\mathbf{q} = 0 \tag{2.10}$$

However, the inclusion of the higher order quadratic terms into the equation of motion is known to improve the root convergence. Thus equation (2.9) truncated suitably as

$$[\mathbf{A} - \omega^2 \mathbf{B} - \omega^4 \mathbf{C}]\mathbf{q} = 0 \tag{2.11}$$

is termed the dynamic element formulation, with $\mathbf{A} = \mathbf{K}_o$, $\mathbf{B} = \mathbf{M}_o - \mathbf{K}_2$, and $\mathbf{C} = \mathbf{M}_2 - \mathbf{K}_4$.

To effect an efficient and economical eigensolution for large scaled problems, the dynamic equations of motion (equation 2.11) can be rearranged as

$$[\mathbf{E} - \omega^2 \mathbf{I}]\mathbf{y} = 0 \tag{2.12}$$

so as to exploit the matrix sparsity, where

$$\mathbf{E} = \begin{bmatrix} -\mathbf{C}^{-1}\mathbf{B} & \mathbf{C}^{-1}\mathbf{A} \\ \mathbf{I} & \mathbf{0} \end{bmatrix} \qquad y = \begin{bmatrix} \dot{q} \\ q \end{bmatrix} \qquad \dot{q} = \omega^2 q$$

The numerical solutions of the above eigenvalue problem are based on the classical Lanczos and Sturm's sequence methods.

2.3 Numerical Solution of Eigenvalue Problems

A fast and reliable assessment of the natural frequencies and mode shapes is vital in the determination of the stability and dynamic response of a structure subjected to time dependent external excitation. The eigensolvers used in STARS are the inverse iteration/Sturm sequence method and the Lanczos method.

2.3.1 Sturm Sequence Method

The Sturm sequence method is an efficient solution technique [22,23] for a certain broad class of eigenvalue problems that may be expressed in the form

$$\mathbf{A}\ddot{\mathbf{q}} + \mathbf{B}\mathbf{q} = 0 \qquad (2.13)$$

If $\ddot{q} = -\omega^2 q$, substitution into the above equation produces the characteristic eigenvalue problem

$$(\mathbf{B} - \omega^2 \mathbf{A})\mathbf{q} = 0 \qquad (2.14)$$

where **B** is regarded as symmetric, banded and positive definite; **A** is symmetric banded or diagonal; and **q** is the eigenvector of ω. A set of nontrivial solutions to the above equation exists for a set of eigenvalues which can be determined from the requirement that $det(\mathbf{A} - \lambda\mathbf{B}) = 0$, where $\lambda = \frac{1}{\omega^2}$.

Sturm's sequence is useful for vibration analyses, defined by

$det(\mathbf{A} - \lambda\mathbf{B}) = 0 \qquad \lambda = \frac{1}{\omega^2}$ $\qquad \omega$ = natural frequency

or structural stability analyses, defined by

$det(\mathbf{K}_G - \lambda\mathbf{K}_E) = 0 \qquad \lambda = \frac{1}{\mu}$ $\qquad \mu$ = compressive stress factor

$\mathbf{K}_G$ = geometrical stiffness matrix

$\mathbf{K}_E$ = elastic stiffness matrix

or the analysis of vibration of stretched structures, where

$det[\mathbf{M} - \lambda(\mathbf{K}_E + \mathbf{K}_G)] = 0 \qquad \lambda = \frac{1}{\omega^2}$ $\qquad \omega$ = natural frequency

The geometric stiffness is obtained when the equation of equilibrium is expressed in terms of the deformed coordinates. The Sturm sequence procedure can accurately extract all of the roots, or any particular root, directly from the banded **A** and **B** matrices and the associated mode shapes can then be computed by a simple inverse iteration technique. The method first determines the number of roots within a specified range $[\lambda_u, \lambda_l]$. The particular roots are isolated to an accuracy ε by a repeated bisection technique. The bisection technique adopted here simultaneously determines the $[\lambda_u, \lambda_l]$ of all the relevant roots at a particular step. As the bound gets smaller for the associated roots at each step, the root convergence rate becomes faster. The number of changes in sign of consecutive members of the leading principal minors $f_r(\lambda_k)$, starting with $f_0(\lambda) = 1$, is equal to the number of eigenvalues of $(\mathbf{A} - \lambda\mathbf{B})$ smaller than λ_k in algebraic value. The procedure requires a modest working space for an array **D** of magnitude $(m+1)(2m+1)$, where $(2m+1)$ is the full bandwidth of the **A** and **B** matrices. Since **A** and **B** are symmetric, only the upper triangular parts of **A** and **B** are stored. It is important to note that the leading principal minors are obtained during the reduction procedure in which the $(r+1)^{th}$ row is not involved until the $(r)^{th}$ major step. All computation work is done within the array **D**, which slides down the main diagonal after performing the reduction of the $(m+1)^{th}$ row.

Initially, the first $(m+1)$ rows of $(\mathbf{A} - \lambda\mathbf{B})$ are assigned into the **D** array. A number of major operations are then carried out to reduce the subdiagonal elements of **D** to zero. If a typical element of **D** is denoted by $\mathrm{d}_{i,j}$, then the following operations are performed for each value i=1,2,...,r during any typical r^{th} major step:

1. If | $\mathrm{d}_{r+1,i}$| > |$\mathrm{d}_{i,i}$|, interchange $\mathrm{d}_{r+1\,j}$ and $\mathrm{d}_{i,j}$
2. Replace $\mathrm{d}_{r+1,j}$ by $\mathrm{d}_{r+1,j} - \frac{\mathrm{d}_{r+1,i}}{\mathrm{d}_{i,i}} \mathrm{d}_{i,j}$ (j=i,i+1,...,2m+1)

   N is the total number of interchanges that have occurred so far and $\mathrm{d}_{i,i}$ is the current diagonal term of **D**.

   The leading principal minor is given as

   $$f_{r+1}(\lambda) = (-1)^N \quad \mathrm{d}_{1,1}\ \mathrm{d}_{2,2}\ \mathrm{d}_{3,3}\ ,\ldots,\ \mathrm{d}_{r+1,r+1}$$

for r increasing from $(m+1)$ to $(n-1)$ and n being the order of the associated matrices $(\mathbf{A} - \lambda\mathbf{B})$

3. Replace the first row and move each of the next m rows up one row and to the left by one column.

4. Copy the $(r+1)^{th}$ row from $(\mathbf{A}-\lambda\mathbf{B})$ into the $(m+1)^{th}$ row of **D**

$$\mathbf{d}(m+1,j)=\mathbf{a}(r+1,j)-\lambda\mathbf{b}(r+1,j) \qquad (j=1,\cdots,2m+1)$$

For i=1,..., m, the following typical operations are performed:

5. If $|\mathrm{d}_{r+1,j}| > |\mathrm{d}_{i,i}|$, interchange $\mathrm{d}_{r+1,j}$ and $\mathrm{d}_{i,i}$
6. Replace $\mathrm{d}_{r+1,j}$ by $\mathrm{d}_{r+1,j}-\dfrac{\mathrm{d}_{r+1,i}}{\mathrm{d}_{i,i}}\mathrm{d}_{i,j}$ (j=i,i+1,...,2m+1)

   The leading principal minor is given as

   $$f_{r+1}(\lambda)=(-1)^{N}F_1\mathrm{d}_{1,1}\mathrm{d}_{2,2}\cdots,\mathrm{d}_{r+1,r+1}$$

   F_1 stores the values of previous first row diagonal element of **D**

   N is the total number of interchange occurrences so far and di,i is the current diagonal term of **D**.

The individual roots are located by the bisection method on the given upper and lower λ 's range

$$H=\frac{\lambda_u^r+\lambda_l^r}{2} \tag{2.15}$$

It is known that there are p eigenvalues existing in $[\lambda_u^r\ ,H]$ then

a) if p=0, repeat the procedure with $\lambda_u^r=H$

b) if p>0 then $\left|\lambda_u^r-H\right|<\varepsilon$ and p repeated roots occur, each equal to H in numerical value

c) if p>0 and $\left|\lambda_u^r-H\right|>\varepsilon$, then H is the lower bound of λ_i, λ_{i+1}, λ_{i+p-1} and the upper bound for λ_{i-1}, λ_{i-2}, $\cdots$ provided the current λ_u^r is greater than H. Repeating this process will give the bounds of all the isolated roots.

Isolated roots are precisely located using the superlinear convergence technique. If the bounds are such that $f(\lambda_r)=det(\mathbf{A}-\lambda_r\mathbf{B})$ and $f(\lambda_{r+1})=det(\mathbf{A}-\lambda_{r+1}\mathbf{B})$ have opposite signs, then linear interpolation is carried out, giving

$$\lambda_{r+1} = \frac{[\lambda_{r+1} f(\lambda_r) - \lambda_r W_{r+1} f(\lambda_{r+1})]}{f(\lambda_r) - W_{r+1} f(\lambda_{r+1})} \tag{2.16}$$

where $W_{r+1} = 2s$, $s = \frac{1}{2}(p-1)(p-2)$ and p is the number of times λ_r has been used unchanged in the process of interpolation. The new value λ_{r+1} is the old value of λ_r or λ_{r+1} such that $f(\lambda_{r+2})$ and new $f(\lambda_{r+1})$ have opposite signs. The process of weighted interpolation is repeated between λ_{r+2} and λ_{r+1} . Once the eigenvalues are computed by this Sturm sequence procedure the associated eigenvectors can be computed by the inverse iteration scheme

$$(\mathbf{A} - \lambda_r \mathbf{B})\mathbf{q}_r^{i+1} = \mathbf{B}\mathbf{q}^i \tag{2.17}$$

where $\mathbf{q}_r^{i+1}$ tends to converge to the required eigenvector $\mathbf{q}_i$, where $\mathbf{q}_i$ is assumed to be entirely unit elements. Improved solution efficiency can be achieved by omitting the partial pivoting that was described above. This procedure works reasonably well if the system involves positive definite matrices.

If the problem is of the form $det(\mathbf{B} - \omega^2 \mathbf{A}) = 0$ then $\lambda = \omega^2$ and the roots obtained are just inverse of the other forms.

2.3.2 Lanczos Eigensolver

Originally Lanczos[24,25,26] intended his algorithm to be used as a method for extracting a few extreme eigenvalues, with corresponding eigenvectors, for a symmetric matrix[27]. STARS and ANSYS[28] included this algorithm as part of their eigensolution capability. However, the algorithm was employed as a method for reducing a symmetric matrix to tridiagonal form. The Householder method is a more efficient and accurate method for tridiagonalizing a matrix. Since most applications only require a few eigenvalues at one end of the spectrum, and Lanczos algorithm has an advantage that it will isolate desired eigenvalues and eigenvectors at a reasonable accuracy with a low number of iterations. The Lanczos algorithm can be applied to the generalized large symmetric eigenproblem

$$(\mathbf{K} - \lambda\mathbf{M})\mathbf{q} = 0 \qquad \text{where } \mathbf{K} \text{ and } \mathbf{M} \text{ are } n \times n \text{ real matrices}$$

This equation can be rewritten in the standard form and this equation can be rewritten in the standard form

$$(\mathbf{A}-\lambda\mathbf{I})=0 \tag{2.18}$$

The Lanczos Method is a powerful algorithm that can be used to evaluate eigenvalues at both ends of the spectrum of the **A** matrix without solving a full system of equations. It has the great advantage to be gained by a shift and invert procedure. Using a shift factor, and solving for the eigenvectors of $(\mathbf{A}-\sigma\mathbf{I})^{-1}$ instead of **A**, yields the same eigenvalues and eigenvectors. The few eigenvalues, and corresponding eigenvectors, that are close to σ will converge rapidly. The matrices **K** and **M** must be nonsingular. To handle rigid-body modes, the **K** and **M** matrices in STARS must be shifted to maintain numerical stability of the eigenvalue problem $(\mathbf{K}-\lambda^2\mathbf{M})\mathbf{q}=0$. The shift factor σ is defined as

$$\sigma=\frac{\lambda^2}{\max\left[\frac{|\mathbf{K}_{i,i}|}{|\mathbf{M}_{i,i}|}\right]/10^7}+4.$$

where $|\mathbf{K}_{i,i}|$ and $|\mathbf{M}_{i,i}|$ denote the norms of the diagonal elements and the value 10**7 relates to the computational accuracy of the computer.

To obtain the general form of the transformation, one needs to first perform a shift from the origin, $(\mathbf{K}_\sigma-(\lambda-\sigma)\mathbf{M})\mathbf{q}=0$, where $\mathbf{K}_\sigma=\mathbf{K}-\sigma\mathbf{M}$, and then rearrange it into the standard eigenvalue problem of the form $(\mathbf{M}^{-1}\mathbf{K}_\sigma-\hat{\lambda}\mathbf{I})\mathbf{q}=0$. Given a pair of matrices **K**□ and **M**, and a starting vector **r**, these basic methods generate a sequence of Krylov vectors, $\{\mathbf{r},\mathbf{K}_\sigma^{-1}\mathbf{M}\mathbf{r},(\mathbf{K}_\sigma^{-1}\mathbf{M})^2\mathbf{r},\cdots,(\mathbf{K}_\sigma^{-1}\mathbf{M})^j\mathbf{r}\}$ for the *jth* iteration. The sequence converges to the eigenvector corresponding to the eigenvalue, □ that is closest to the shift σ.

To derive the Lanczos algorithm, it will be assumed that the first j Lanczos vectors, $\{\mathbf{q}_1,\mathbf{q}_2,\cdots,\mathbf{q}_j\}$ have been found or assumed initially, and the construction of the j+1 vector will be described. The resulting vectors must be orthogonalized with respect to the mass matrix and satisfy the condition $\mathbf{q}_i^T\mathbf{M}\mathbf{q}_j=\delta_{ij}$. The algorithm contains the following steps:

For j =0,

1. Set $\mathbf{q}_o=0$ and $\mathbf{r}_o=$ random vector

```
    2. $\beta_1 = (\mathbf{r}_o^T \mathbf{M} \mathbf{r}_o)^{1/2}$
    3. $\mathbf{q}_1 = \frac{\mathbf{r}_o}{\beta_1}$   mass orthogonalize the **r** vector to obtain the Lanczos vector **q**
    4. $\mathbf{p}_1 = \mathbf{M}\mathbf{q}_1$
For j =1, 2, 3, ..., repeat:
    1. $\bar{\mathbf{r}}_j = \mathbf{K}_\sigma^{-1} \mathbf{p}_j$
    2. $\hat{\mathbf{r}} = \bar{\mathbf{r}}_j - \mathbf{q}_{j-1}\beta_j$
    3. $\alpha_j = \mathbf{q}_j^T \mathbf{M} \hat{\mathbf{r}}_j = \mathbf{q}_j^T \hat{\mathbf{r}}_j$
    4. $\mathbf{r}_j = \hat{\mathbf{r}}_j - \mathbf{q}_j \alpha_j$
    5. $\bar{\mathbf{p}}_j = \mathbf{M}\mathbf{r}_j$
    6. $\beta_{j+1} = (\mathbf{r}_j^T \mathbf{M} \mathbf{r}_j)^{1/2} = (\bar{\mathbf{p}}_j^T \mathbf{r}_j)^{1/2}$
    7. If enough vectors, then terminate the loop
    8. $\mathbf{q}_{j+1} = \frac{\mathbf{r}_j}{\beta_{j+1}}$
    9. $\mathbf{p}_{j+1} = \frac{\bar{\mathbf{p}}_j}{\beta_{j+1}}$
```

In addition to requiring the storage of the matrices $\mathbf{K}_\sigma$ and **M**, this algorithm requires storage of five vectors of length *n*; one for each of the vectors, $\mathbf{q}_{j-1}$, $\mathbf{q}_j$, $\mathbf{M}\mathbf{r}_j$, $\mathbf{p}_j$, and $\mathbf{r}_j$. The total cost for one step of the algorithm involves a multiplication by **M**, the solution of a system of equations, with $\mathbf{K}_\sigma$ as the coefficient matrix, two inner products and four products of a scalar with a vector.

From the algorithm, $\mathbf{r}_j$ can be written as a three-term relationship

$$\mathbf{r}_j = \mathbf{K}_\sigma^{-1}\mathbf{M}\mathbf{q}_j - \mathbf{q}_j\alpha_j - \mathbf{q}_{j-1}\beta_j \qquad (2.19)$$

where $\alpha_j = \mathbf{q}_j^T \mathbf{M} \mathbf{K}_\sigma^{-1} \mathbf{M} \mathbf{q}_j$ and $\mathbf{r}_j$ is normalized with respect to the mass matrix to obtain $\mathbf{q}_{j+1}$ with normalizing factor $\beta_{j+1} = (\mathbf{r}_j^T \mathbf{M} \mathbf{r}_j)^{1/2}$. After m Lanczos steps all the quantities obtained from the above equation can be rearranged in a global matrix form

$$[\mathbf{K}_\sigma^{-1}\mathbf{M}][\mathbf{Q}_m]-[\mathbf{Q}_m][\mathbf{T}_m]=\mathbf{r}_j e_m^T \tag{2.20}$$

with $e_m^T = <0,0,...,0,1>$. Here, $\mathbf{Q}_m$ is an n □ m matrix with columns $\mathbf{q}_j$, j=1,2,...,m, and $\mathbf{T}_m$ is a tridiagonal matrix of the form

$$\mathbf{T}_m = \begin{bmatrix} \alpha_1 & \beta_2 & & & & \\ \beta_2 & \alpha_2 & \beta_3 & & & \\ & \beta_3 & . & . & & \\ & & . & . & . & \\ & & & . & . & \beta_m \\ & & & & \beta_m & \alpha_m \end{bmatrix} \tag{2.21}$$

From the orthogonality property of the Lanczos vectors, $\mathbf{Q}_m^T\mathbf{M}\mathbf{Q}_m = \mathbf{I}$, the above equation may be expressed as

$$\mathbf{Q}_m^T\mathbf{M}\mathbf{K}_\sigma^{-1}\mathbf{M}\mathbf{Q}_m = \mathbf{T}_m \tag{2.22}$$

The eigenvalues of the tridiagonal matrices converge to the inverses of the eigenvalues of **K** matrix. The eigenvalues of the tridiagonal matrix $\mathbf{T}_m$ converge closer to the eigenvalues of the problem $(\mathbf{A}-\lambda\mathbf{I})=0$ as the total number of Lanczos vectors **q** increases and as the size of the tridiagonal $\mathbf{T}_m$ matrix increases.

2.4 Concluding Remarks

In this section, a detailed formulation of the dynamic equations pertaining to a number of commonly occurring problem types has been presented. This has been followed by details of two important numerical techniques for solving large scale eigenvalue problems. Details of a later development in this connection, involving eigensolution by a progressive simultaneous iteration (PSI) technique, used for analysis of the Hyper-X example problem presented later in this thesis, are given elsewhere [29].

CHAPTER 3

NUMERICAL TECHNIQUES FOR LINEAR AEROELASTIC AND AEROSERVOELASTIC ANALYSIS

3.1 Introduction

The linear aeroelastic and aeroservoelastic modules in STARS have the capability to predict the stability of spacecraft and flight vehicles. Using the results obtained from a solid vibration analysis, STARS can proceed to obtain the flutter and divergence characteristics and perform open– and closed–loop stability analyses for the vehicle.

Reference 30 gives a good history of the development of the linear unsteady aerodynamic analysis method through the years. Thirty years ago, unsteady aerodynamics flutter analysis tools were based mainly on the modified strip theory [31,32]. Doublet–lattice, which allowed the analysis of non–planar aerodynamic surfaces with interference bodies[3,4,33,34], would soon follow. The most important contribution made by the doublet–lattice method to flutter analysis is the provision of a capability for accurately calculating aerodynamic influence coefficients. Rodden later replaced the parabolic approximation of the numerator of the kernel function by a quartic approximation and improved the representation of the kernel integral [35,36]. The complete mathematical description of the doublet–lattice method can be found in the reference 37. Doublet–lattice has proved to be a reliable approximation technique for the subsonic aerodynamic speed range. Other unsteady aerodynamic tools, which have been developed for the subsonic speed range, include the kernel function method [38,39,40]. This method requires knowledge of the pressure modes, which depend on the geometry plan form of the lifting surfaces. As this method has proved to be complicated to use, it is less favored than the doublet–lattice method.

For unsteady supersonic aerodynamic flow, the Mach Box method is the traditional choice for flutter analysis. In this approach, the velocity potential is utilized as the dependent variable [124,125,126]. The method is only applicable for Mach numbers that are greater than 1.414. Other tools, developed for the analysis of unsteady supersonic aerodynamics, include the supersonic doublet–lattice method developed by Giesing and

Kalman [44] and the kernel function method [45,46]. Both these approaches belong to the family of acceleration potential methods. The potential gradient method [5,47,48] developed by Jones and Appa, and known as the Constant Pressure Method (CPM), is preferable. This approach has the ability to model without the need for assuming the pressure modes. Jones and Appa expressed the integral relation between the pressure and the normal velocity in terms of a rearrangement of the exponential term associated with the kernel of the potential gradient. This resulted in the use of the pressure differential as a new variable. The potential gradient in the stream direction is considered as an independent variable and is assumed to be constant over an element [47,49]. The equivalent to the doublet–lattice for the supersonic regime was developed by Brock and Griffin [50]. They employed the subsonic doublet–lattice method with a slightly modified supersonic kernel function, relating the pressure differential across a panel and the normal wash developed by Harder and Rodden[51].

In STARS, unsteady aerodynamic forces in subsonic flow are computed using the Doublet Lattice Method (DLM) [4], whereas the Constant Pressure Method (CPM) is used for supersonic flow. The *k* and *pk* stability solution procedures may be used.

The stiffness and mass, obtained from the solids module of STARS, are expressed in terms of a generalized coordinate system. The DLM or CPM generated aerodynamic forces are also reduced to generalized forces. For aeroservoelastic analysis, aerodynamics and structural data is converted into the Laplace (or *s*) domain and the generalized aerodynamic forces are then curve fitted using Padé and least squares approximations. These give the system of equations in the form of a state space matrix. An open–loop stability analysis may be performed at this point by an eigenvalue analysis, using the state space matrix. Such a system can also be integrated with a control system which includes actuators, sensors, notch or other filters, and analog or digital controllers. From the augmented control system, transfer function frequency response phase and gains can be evaluated. Closed–loop modal damping and frequencies can be computed by solving the eigenvalue problem of the closed–loop augmented state space dynamic matrices.

3.2 Linear Aerodynamics

The aerodynamic influence coefficients (AIC) are important, as an AIC is only a function of the Mach number, the reduced frequency and the plan form. Any number of aeroelastic analyses can be performed, at various altitudes or at different density, stiffness and inertia changes, without having to recompute the AIC matrix. The AICs are independent of aircraft vibration mode shapes and/or static deflection modes and are related to the oscillatory aerodynamic moment and/or forces acting at the specified AIC control points and to the harmonic rotation and deflections of these control points. The AICs may be determined using the doublet lattice method or the constant pressure method, which are both discussed below.

3.2.1 Doublet Lattice Method

In subsonic flow, the unsteady aerodynamic forces can be computed using the doublet lattice method to a high degree of accuracy [4,52]. The normalized down wash velocity of a vibrating structural surface is computed using the equation

$$w(x,y,z) = \frac{1}{8\pi}\iint_{LS} K(x-\xi, y-\eta, z-\varsigma, \omega, M)\delta C_p d\xi d\sigma \qquad (3.1)$$

where

K = kernel

LS = lifting surfaces

δC_p = pressure differential.

η = span wise coordinate

ζ = elevation coordinate

ξ = stream wise coordinate

σ = tangential span wise coordinate

In practice, the integral of the kernel K is approximated by a summation over discrete finite sized lifting elements on the surfaces. The integration of K in the stream wise direction is achieved by simply lumping the effect of a loaded line to a doublet line at the quarter chord position of the element. The normalized dimensional downwash velocity may be expressed as

$$w_r(x,y,z) = \frac{1}{8\pi}\sum_{s=1}^{nb}\delta C_p \delta\xi \int_{Element\ s} K(x-\xi, y-\eta, z-\varsigma, \omega, M) d\sigma \qquad (3.2)$$

where nb is the number of discrete lifting element aero boxes. The downwash w is known to be equal to the summation over the discrete set of structural modal amplitudes, with the condition of zero normal flow at the boundary applied, and δC_p is the unknown pressure component that needs to be computed with K connecting w with δC_p. The above equation can be written, in the form of a set of linear algebraic equations, as

$$\{\mathbf{w}\} = [\mathbf{D}]\{\Delta \mathbf{C}_P\} \tag{3.3}$$

where a typical component of [**D**] is $\mathbf{D}_{rs}$, defined by

$$\mathbf{D}_{rs} = \int_{Element\ s} K(x-\xi_{1/4}, y-\eta, z-\varsigma, \omega, M)\, d\sigma \tag{3.4}$$

with s denoting the sending element, where the doublet is being generated, and r denoting the element that receives the influence of the doublet from s . For each element, the receiving point of the element normal wash boundary condition is located at the center span on the three–quarter chord line of the element as shown in Figure 3.1. The basic idea of the doublet lattice method is to curve fit the numerator of K with a parabola and carry out the integration of K over the element s.

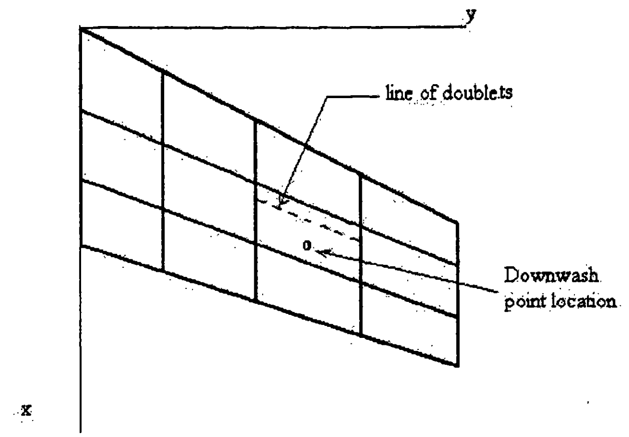

Figure 3.1 Discretization of a wing lifting surface into aero-boxes.

The kernel has the form

$$K = \exp^{-i(x-\xi_{1/4})\frac{\omega}{U_\infty}} (\mathrm{K}_1\mathrm{T}_1 / r^2 + \mathrm{K}_2\mathrm{T}_2^* / r^4) \tag{3.5}$$

where U_∞ is the free stream velocity and K_1 and K_2 are as given in Appendix A of the report by Giesing, Kalman and Rodden[4,38,53]. This kernel represents a semi–infinite line doublet with a strength of the form $\exp(-i(\xi - \xi_{1/4})\frac{\omega}{U_\infty})$. It can be shown that, when the receiving point is down stream of a non–planar sending point of the kernel, the flow field is dominantly being affected by the local strength of the semi–infinite doublet line. It may be noticed that the effect of the planar vortices on the receiving point has a $1/r^2$ relationship and the non–planar effect has a $1/r^4$ relationship. The global and local coordinate systems are related according to

$$
\begin{aligned}
\bar{x} &= x - \xi_c \\
\bar{y} &= (y-\eta_c)\cos\gamma_s + (z-\varsigma_c)\sin\gamma_s \\
\bar{z} &= (z-\varsigma_c)\cos\gamma_s - (y-\eta_c)\sin\gamma_s \\
\bar{\eta} &= (\eta-\eta_c)\cos\gamma_s + (\varsigma-\varsigma_c)\sin\gamma_s \\
\bar{\varsigma} &= (\varsigma-\varsigma_c)\cos\gamma_s - (\eta-\eta_c)\sin\gamma_s
\end{aligned}
\qquad
\begin{aligned}
\bar{\xi} &= \xi - \xi_c \\
\bar{\gamma} &= \gamma_r - \gamma_s \\
x_0 &= x - \xi \\
y_0 &= y - \eta \\
z_0 &= z - \varsigma \\
r &= (y_0^2 + z_0^2)^{1/2}
\end{aligned}
\qquad (3.6)
$$

where ξ_c, η_c, ζ_c denote the coordinates of the center of the quarter–chord vortex line of the sending element and γ_s denotes the dihedral angle of the element, as shown in Figure 3.2

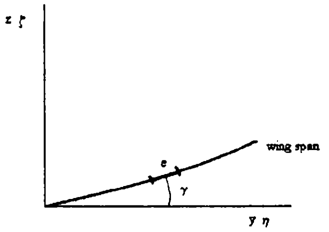

Figure 3.2 The dihedral angle for an element on a lifting surface.

The coefficients in the kernel K of equation (3.5) are of the form[4,53]

$$\begin{aligned}
\mathrm{T}_1 &= \cos(\bar{\gamma}) \\
\mathrm{T}_2^* &= (z_0 \cos\gamma_r - y_0 \sin\gamma_r)(z_0 \cos\gamma_s - y_0 \sin\gamma_s) \\
\mathrm{K}_1 &= I_1 + \frac{Mr}{R}\left[\frac{e^{-ik_1u_1}}{(1+u_1^2)^{1/2}}\right] \qquad (3.7) \\
\mathrm{K}_2 &= -3I_2 - \frac{ik_1M^2r^2}{R^2} - \frac{e^{-ik_1u_1}}{(1+u_1^2)^{1/2}} \\
&\quad - \frac{Mr}{R}\left[(1+u_1^2)\frac{\beta^2r^2}{R^2} + 2 + \frac{Mru_1}{R}\right]\frac{e^{-ik_1u_1}}{(1+u_1^2)^{3/2}}
\end{aligned}$$

where

$$\begin{aligned}
u_1 &= \left(\frac{MR - x_0}{\beta^2 r}\right) \\
r &= (y_0^2 + z_0^2)^{1/2} \\
k_1 &= \frac{\omega r}{U_\infty} \\
\beta &= (1 - M^2)^{1/2} \\
R &= (x_0^2 + \beta^2 r^2)^{1/2} \\
I_1(u_1, k_1) &= \int_{u_1}^{\infty} \frac{e^{ik_1u}}{(1+u^2)^{3/2}}\,du \\
I_2(u_1, k_1) &= \int_{u_1}^{\infty} \frac{e^{ik_1u}}{(1+u^2)^{5/2}}\,du
\end{aligned}$$

Equation (3.5) can be expanded to give

$$\begin{aligned}
K = \mathrm{T}_1\left[\exp^{-i(x-\xi_{1/4})\frac{\omega}{U_\infty}} \mathrm{K}_1 - \mathrm{K}_1^s\right]/r^2 + \mathrm{T}_2^*\left[\exp^{-i(x-\xi_{1/4})\frac{\omega}{U_\infty}} \mathrm{K}_2 - \mathrm{K}_2^s\right]/r^4 \\
+ \left[\mathrm{T}_1\mathrm{K}_1^s/r^2 + \mathrm{T}_2^*\mathrm{K}_2^s/r^4\right] \qquad (3.8)
\end{aligned}$$

with the last term denoting the steady term when ω=0. Equation (3.4) becomes

$$\mathbf{D}_{rs} = \mathbf{D}_{rs}^1 + \mathbf{D}_{rs}^2 + \mathbf{D}_{rs}^s \qquad (3.9)$$

where

$$\mathbf{D}^1_{rs} = \int_{-e}^{e} \frac{A_1\overline{\eta}^2 + B_1\overline{\eta} + C_1}{r^2}\, d\overline{\eta}$$

$$\mathbf{D}^2_{rs} = \int_{-e}^{e} \frac{A_2\overline{\eta}^2 + B_2\overline{\eta} + C_2}{r^4}\, d\overline{\eta}$$

$$\mathbf{D}^s_{rs} = \int_{-e}^{e} \left[T_1 K_1^s / r^2 + T_2^* K_2^s / r^4\right] d\overline{\eta}$$

and with e representing the half-element length and the superscript s denoting the steady state case when $\omega = 0$. The numerators of $\mathbf{D}^1_{rs}$ and $\mathbf{D}^2_{rs}$ of K are very slowly varying functions of $\overline{\eta}$ over the area of an element and can be fitted with a parabolic function and integrated over the element. The third term is integrated analytically.

$$\begin{aligned} T_1\left[\exp^{-i(x-\xi_{1/4})\frac{\omega}{U_\infty}} K_1 - K_1^s\right]/r^2 &= A_1\overline{\eta}^2 + B_1\overline{\eta} + C_1 \\ T_2^*\left[\exp^{-i(x-\xi_{1/4})\frac{\omega}{U_\infty}} K_2 - K_2^s\right]/r^4 &= A_2\overline{\eta}^2 + B_2\overline{\eta} + C_2 \end{aligned} \qquad (3.10)$$

The normal down wash is obtained by summing a series of mode shapes that may be computed using the STARS solid module that was discussed in the last chapter. With w and D being known the aerodynamic force on the aircraft can be computed using the lifting pressure differential, δC_p. The normal down wash for a mode i can be derived from the structural mode shape as

$$\mathbf{w}_i = \frac{d\mathbf{q}_i}{dx} + i\frac{\omega s}{U_\infty}\mathbf{q}_i \qquad (3.12)$$

where s is the semi–span, and $\mathbf{q}_i$ is the *ith* mode shape obtained from the structural vibration analysis.

3.2.2 Constant Pressure Panel Method

The supersonic kernel function relates the pressure differential and the normal velocity based on the potential gradient method. Following a rearrangement of the exponential term in the kernel of the potential gradient, the pressure differential can be derived [5,47]. The constant pressure method starts with the linearized equation of fluid motion

$$\nabla^2\phi' = \frac{1}{a^2}\frac{\mathrm{D}^2\phi'}{\mathrm{D}t^2} \tag{3.13}$$

where ϕ' is the velocity potential, a is the speed of sound and

$$\frac{\mathrm{D}}{\mathrm{D}t}(\ ) = \frac{\partial}{\partial t} + V\frac{\partial}{\partial t} \tag{3.14}$$

We assume a modified velocity potential of the form

$$\Phi = \phi\ \exp(i\tfrac{\mathrm{kMX}}{\beta^2}) \tag{3.15}$$

where l denotes a reference length, $\mathrm{X} = x/l$, $\mathrm{Y} = y/l$, $\mathrm{Z} = z/l$, and $\phi = \phi'/Vl$ is the non–dimensional velocity potential. The solution to equation (3.13) may then be expressed, using the modified velocity potential at a control point (X_0, Y_0, Z_0), as

$$\Phi(\mathrm{X}_0, \mathrm{Y}_0, \mathrm{Z}_0) = \frac{1}{2\pi}\iint K'(\mathrm{X}, \mathrm{Y}, \mathrm{Z})\frac{\partial}{\partial n}\left(\frac{\cos\ \mathrm{k'R}}{\beta^2\mathrm{R}}\right)d\mathrm{A} \tag{3.16}$$

where

$\mathrm{R}^2 = \xi^2 - \beta^2 r^2$

$r^2 = \eta^2 + \xi^2$

$k = \omega\ l / V$

$k' = k\mathrm{M}/\beta^2$

$\mathrm{K'} = \phi_{\mathrm{U}} - \phi_{\mathrm{L}}$ = modified potential doublet

$\dfrac{\partial}{\partial \mathrm{n}} = -l_x\dfrac{\partial}{\partial x} + l_y\dfrac{\partial}{\partial y} + l_z\dfrac{\partial}{\partial z}$

$\xi = \mathrm{X}_0 - \mathrm{X}$

$\eta = \mathrm{Y}_0 - \mathrm{Y}$

$\varsigma = \mathrm{Z}_0 - \mathrm{Z}$

$\beta^2 = \sqrt{M^2 - 1}$

M = Mach number

$(l_x,\ l_y,\ l_z) =$ the direction cosines of the inward drawn normal to the surface

The exponential of equation (3.15) may be rearranged into the product form

$$\exp(ikX\frac{M^2}{\beta^2}) - = -\exp(ikX)\exp(\frac{ik}{\beta^2}X) \tag{3.17}$$

and equation (3.16) can be rewritten in the form

$$\phi(\mathrm{X}_0,\mathrm{Y}_0,\mathrm{Z}_0) = \frac{1}{2\pi}\iint\frac{\partial \mathrm{K}}{\partial \mathrm{X}}\frac{\partial \mathrm{P}}{\partial \mathrm{h}}d\xi d\eta \tag{3.18}$$

so that it may be integrated by parts, where

$$\frac{\partial \mathrm{K}}{\partial \mathrm{X}} = \frac{\partial \Delta\phi}{\partial x} + ik\Delta\phi = -\Delta C_p \tag{3.19}$$

$$\mathrm{P} = \exp(-ik\xi)\int_{\beta r}^{\xi}\exp(ik\xi'/\beta^2)(\frac{\cos k'R'}{R'})d\xi' \tag{3.20}$$

Here ΔC_p is the pressure difference between the upper and lower surfaces. A numerical integration of equation (3.17) is required for a discrete number of panels with the assumption that ΔC_P is a unit pressure distributed over each of the panels. The velocity potential of a panel element will have the form

$$\phi = -\frac{1}{2\pi}\int_{\eta_L}^{\eta_U}\int_{\xi_L}^{\xi_U}\frac{\partial P}{\partial \mathrm{h}}\,d\xi d\eta \tag{3.21}$$

where η_U, η_L, ξ_U and ξ_L are the upper and the lower bounds of η, ξ in a particular discretized element of the lifting surface. At control point i, the normal down wash w_{ij} due to the influence of a unit pressure at the j^{th} element is calculated as

$$w_{ij} = -\frac{1}{2\pi}\int_{\eta_L}^{\eta_U}\int_{\xi_L}^{\xi_U}\frac{\partial}{\partial n_0}\left(\frac{\partial \mathrm{P}}{\partial n}\right)d\xi d\eta \tag{3.22}$$

where

$$\frac{\partial}{\partial n_0} = l_{x0}\frac{\partial}{\partial x_0} + l_{y0}\frac{\partial}{\partial y_0} + l_{z0}\frac{\partial}{\partial z_0}$$

with l_{x_0}, l_{y_0}, l_{z_0} being the directional cosines of the normal at the control point panel. The aerodynamic influence coefficient (AIC) matrix is then simply obtained as

$$[\mathbf{D}] = [w]^{-1} \qquad (3.23)$$

which may be used in the computation of the ΔC_P according to

$$\Delta C_P = [\mathbf{D}]\left\{\frac{D\eta}{DT}\right\}$$

Here $\left\{\frac{D\eta}{DT}\right\}$ is the kinematic non–dimensional down wash due to the *nth* mode. The generalized aerodynamic work influence coefficient in the vibration mode *i* due to the *jth* pressure mode, from the principle of virtual work, is equal to

$$\mathrm{D}_{ij} = ql^3 \iint_S \eta_i \Delta C_{pj} d\xi d\eta$$

where $q = \frac{1}{2}\rho V^2$ is the dynamic pressure and S is the total area of the lifting surfaces.

The new kernel associated with the pressure boundary has a hyperbolic singularity along the forward Mach cone as R approaches zero and a dipole singularity as r approaches zero. The hyperbolic singularity is resolved by performing the first integration in the stream wise direction, which results in an analytic function on the Mach boundary. The dipole singularity is eliminated by using the principal value theorem. A detailed discussion of the structure of the $\frac{\partial P}{\partial n}$ term is discussed in the paper of Jones and Appa[5].

3.3 Linear Aeroelasticity Numerical Solution

The matrix [**D**] obtained from the DLM equation (3.3) or the CPM equation (3.23) is the aerodynamic influence coefficient matrix in the physical coordinate system, which relates the downwash vectors to the pressures on discritized aerodynamic elements. It is of the dimension *nb* by *nb* where the *nb* is number of discrete aerodynamic elements (boxes) as shown in Figure 3.1. It is a square, non-symmetric complex matrix.

By applying the theory of Lagrangian mechanics [54,55], the physical coordinates [**D**] matrix can be transformed into the generalized coordinates, which will have the dimension of *nr* by *nr* generalized modes. This is called a generalized influence coefficient matrix, [**A**], and is used together with the generalized inertia (mass) matrix [**M**] and generalized stiffness matrix [**K**]. These reduced order matrices are then employed, using generalized coordinates (normal modes), for the linear aeroelastic solution.

For a harmonic motion, the equation for the linear flutter problem has the general form

$$\left[[\mathbf{K}]+\frac{V^2}{c}[\mathbf{M}]p^2-\frac{1}{2}V^2\rho[\mathbf{A}(p)]\right]\{\mathbf{q}\}=\mathbf{0} \tag{3.24}$$

where $[\mathbf{K}]$ = defines the generalized elastic stiffness matrix,

$[\mathbf{M}]$ = generalized inertia matrix

$\{\mathbf{q}\}$ = column of generalized nodal displacement vector, $q_i=\overline{q}_i e^{i\omega t}$ for mode i

$[\mathbf{A}(p)]$ = unsteady aerodynamic work influence coefficients matrix

p = differential operator $\frac{c}{V}(\frac{d}{dt})$

V = speed of the air flow

c = reference chord

ρ = free stream density

With the assumption of harmonic motion, the aerodynamic coefficients are functions of the reduced frequencies and the Mach number, and are not dependent on the time derivative. This is a result of the special behavior of $\frac{d(e^{i\omega t})}{dt}=i\omega e^{i\omega t}$.

3.3.1 *p* Method

When the aerodynamic forces can be expressed as a sufficiently simple function of p, the equation of motion becomes a polynomial in p with real coefficients[56]. The non zero **q** solutions to the equation of motion can be determined by setting the determinant formed by the matrix coefficients of the above equation to be equal to zero. At a given value for the airspeed V, the determinant can then be solved directly for p. This leads to complex conjugate roots [56]

$$p=\gamma\, k \pm i^{*}k \tag{3.25}$$

where $k=\omega c/V$ and the rate of decay $\gamma=(1/2\pi)\ln\left(\frac{a_{j+1}}{a_j}\right)$ with a_j and a_{j+1} denoting the amplitudes of successive cycles. The rate of decay (γk) might be interpreted as a modal damping and, when it is plotted against the equivalent airspeed, gives rise to what is commonly known as the v-g plot. Flutter has occurred at the point where the damping first goes to zero on this plot. A plot of the modal frequencies versus airspeed, the $\omega - V$ plot, is also commonly used to identify divergence cases. It should be noted that sub–critical damping values are not reliable for the p or k methods.

3.3.2 *k* Method

In the use of the doublet lattice approach or the supersonic Mach box method, the aerodynamic matrices have the following expression which is valid only for harmonic motion, $p = i^* k$. The equation of flutter is now [56]

$$\left[\frac{1}{V^2}\mathbf{K} - \frac{1}{c^2}\mathbf{M}\ k^2 - \frac{1}{2}\rho\mathbf{A}(i^* k)\right]\{\mathbf{q}\} = 0 \tag{3.26}$$

and, substituting $k = \omega c / V$, the above equation becomes

$$\left[\frac{1}{\omega^2}\mathbf{K} - \mathbf{M} - \frac{\rho c^2}{2k^2}\mathbf{A}(i^* k)\right]\{\mathbf{q}\} = 0 \tag{3.27}$$

At a particular reduced frequency, k, complex roots for $\lambda = \dfrac{1}{\omega^2}$, $\lambda_R + i^* \lambda_I$, are found and interpreted as

$$\lambda_R + i^* \lambda_I = (1/\omega^2)(1 + i^* g) \tag{3.28}$$

where g is the structural damping that is needed to induce the harmonic motion. Note that V no longer appears in the equations but that ρ does. The flutter equation for the k method is represented by the eigenproblem

$$\left[\lambda\mathbf{K}\ \ - (\mathbf{M} + \frac{\rho c^2}{2k^2}\mathbf{A}(i^* k))\right]\ \{\mathbf{q}\} = 0$$

or

$$(\lambda\mathbf{K} - \mathbf{D}_k)\{\mathbf{q}\} = 0 \tag{3.29}$$

where

$$\mathbf{D}_k = (\mathbf{M} + \frac{\rho c^2}{2k^2}\mathbf{A}(i^* k)).$$

This eigenvalue equation can be solved for each specified reduced frequency, k. For each k, an eigenvalue λ_k will be obtained

$$\lambda_k = \lambda_R + i^* \lambda_I \qquad (3.30)$$

where, by definition $\lambda_R = \dfrac{1}{\omega^2}$ $\qquad \omega = \sqrt{\dfrac{1}{\lambda_R}}$

$$k = \frac{\omega c}{V} \qquad V = \frac{\omega c}{k} \qquad (3.31)$$

$$\lambda_I = \frac{g}{\omega^2} \qquad g = \lambda_I \omega^2$$

For each k, a modal frequency, damping and velocity for each mode are computed. The v-g plot can be constructed for tracing the flutter characteristic of each mode shape. This method occasionally produces multiple values of damping at a given velocity.

3.3.3 *p-k* Method

When the flutter equation (3.26) is written in a form showing that the aerodynamic equation is expressed in term of both *p-k*[56], the equation of motion can be written as

$$\left[[\mathbf{K}] + \frac{V^2}{c^2}[\mathbf{M}]p^2 - \frac{1}{2}\rho V^2 [\mathbf{A}(i^* k)] \right] \{\mathbf{q}\} = 0 \qquad (3.32)$$

With an estimated value of k_0, $[A(i^* k)]$ is computed and one can solve the above equation for $p = \gamma k_1 + i^* k_1$. The process is repeated until the solution evaluated at k equals the k value of the aerodynamics matrices $[A(i^* k)]$. In another words, for a given V, one can use a recursive loop to solve the above equation until a solution of p is found that makes the equation equal to zero. From the definition of p, its is seen that

$$p = p_R + i^* p_I = \gamma k + i^* k \qquad (3.33)$$

and this produces the damping

$$\gamma k = p_R \qquad \gamma = \frac{p_R}{k} = \frac{p_R}{p_I} \qquad (3.34)$$

For a constant ρ and Mach number, we then check through the V's to compute modal velocities, damping, and speeds of sound. If a speed of sound and ρ combination lies on the standard atmosphere curve, a 'match point' is obtained. Damping values produced by the *pk* method are considered to be reliable.

3.4 Linear Aeroservoelasticity

Aircraft systems have become more sophisticated, due to the integration of distinct disciplines to achieve simultaneous objectives in the aspects of performance, control, flying and maneuvering techniques, and fuel efficiency for various mission design projects. Aeroservoelastic (ASE) dynamics includes the coupling of structural dynamics, aerodynamics, control dynamics, sensing and actuation. Structural dynamics can be accurately modeled with finite element methods and validated with ground vibration test data. The control dynamics are designed and verified before flying. The aerodynamics can be modeled using the doublet lattice approach or the supersonic constant pressure method.

Extensions to aeroelastic modeling capabilities may be made with control system augmentation of the aero–structural dynamics. The unsteady aerodynamics is curve fitted with Padé approximations to generate a state-space aero–structural dynamics model in the frequency or s domain. The inertial coordinate system for the model is transformed to a local body–axis coordinate system, so that the control system can be augmented into the aero–structural dynamics[57,58].

3.4.1 The State Space Method

The governing equation of motion for the structure that is relevant in an aeroelastic analysis is[57]

$$\left[[\mathbf{M}]\ddot{\mathbf{q}}+[\mathbf{C}]\dot{\mathbf{q}}+[\mathbf{K}]\mathbf{q}-\frac{1}{2}\rho V^2[\mathbf{A}(ik)]\mathbf{q}\right]=\{\mathbf{P}(t)\} \tag{3.35}$$

where

V = free stream airspeed

$[\mathbf{C}]$ = the damping matrix

$[\mathbf{K}]$ = elastic stiffness matrix

$[\mathbf{M}]$ = mass matrix

$\frac{1}{2}\rho V^2$ = the dynamic pressure

$\mathbf{q}$ = the displacement vector

$\mathbf{P}(t)$ = the external force function

k = reduced frequency, $\frac{\omega c}{2V}$, c reference mean chord length

$\mathrm{A}(ik)$ = Aerodynamic work influence coefficient matrices calculated for a given Mach and set of k values

The mode shapes and natural frequencies are computed from the structural free vibration analysis, via the equation

$$[\mathbf{M}]\ddot{\mathbf{q}} + [\mathbf{K}]\mathbf{q} = 0$$

Applying the transformation $\mathbf{q} = \mathbf{\Phi}\boldsymbol{\eta}$ to equation (3.35) and pre–multiplying both sides by $\mathbf{\Phi}^T$ leads to the generalized equation of motion

$$\left[[\hat{\mathbf{M}}]\ddot{\eta} + [\hat{\mathbf{C}}]\dot{\eta} + [\hat{\mathbf{K}}]\eta - \frac{1}{2}\rho V^2[\mathbf{Q}(ik)]\eta\right] = \hat{\mathbf{P}}(t) \tag{3.36}$$

where
$$\hat{\mathbf{M}} = \mathbf{\Phi}^T\mathbf{M}\mathbf{\Phi}$$
$$\hat{\mathbf{C}} = \mathbf{\Phi}^T\mathbf{C}\mathbf{\Phi}$$
$$\hat{\mathbf{K}} = \mathbf{\Phi}^T\mathbf{K}\mathbf{\Phi}$$
$$\mathbf{Q} = \mathbf{\Phi}^T\mathrm{A}(ik)\mathbf{\Phi}$$
$$\hat{\mathbf{P}} = \mathbf{\Phi}^T\mathbf{P}$$

with modal matrix $\mathbf{\Phi} = [\mathbf{\Phi}_r, \mathbf{\Phi}_e, \mathbf{\Phi}_\delta]$ and generalized coordinate matrix $\boldsymbol{\eta} = [\boldsymbol{\eta}_r, \boldsymbol{\eta}_e, \boldsymbol{\eta}_\delta]$; where the rigid body ($r$), elastic ($e$), and control surface ($\delta$) motions make up the generalized displacement vectors. The generalized aerodynamic force matrix **Q**(ik) can be approximated with Padé polynomials in terms of $i^*k = i^*(\omega c/2V) = \frac{sc}{2V}$, where the Laplace variable is $s = i^*\omega$, as

$$\hat{Q}(ik) = A_0 + i^*kA_1 + (i^*k)^2A_2 + \frac{i^*k}{i^*k+\beta_1}A_3 + \frac{i^*k}{i^*k+\beta_2}A_4 + \ldots \tag{3.37}$$

where β_j is the aerodynamic lag term (assume j=1,2) and

$$\frac{i^*k}{i^*k+\beta_1} = \frac{k^2}{k^2+\beta_j^2} + \frac{i^*k\beta_j}{k^2+\beta_j^2}$$

The rigid aerodynamic load coefficients take the form

$$A_0 = \hat{Q}_R(k_1)$$

$$A_I = \frac{\hat{Q}_I(k_1)}{k_1} - \frac{A_3}{\beta_1} - \frac{A_4}{\beta_2}$$

where k_1 is the smallest reduced frequency, which is a value near zero that is used to compute A_j for j= 0, 1, 2, 3, ... Separating the real and imaginary parts in equation (3.37) produces

$$\begin{aligned}\tilde{Q}_R(k) &= \hat{Q}_R(k) - A_0 \\ &= \begin{bmatrix} -k^2 I & \frac{k^2}{k^2+\beta_1^2} I & \frac{k^2}{k^2+\beta_2^2} I \end{bmatrix} \begin{bmatrix} A_2 \\ A_3 \\ A_4 \end{bmatrix} \qquad (3.38) \\ &= S_R(k)\tilde{A}\end{aligned}$$

and

$$\begin{aligned}\tilde{Q}_I(k) &= \frac{\hat{Q}_I(k)}{k} - A_1 \\ &= \begin{bmatrix} 0 & \frac{k^2}{k^2+\beta_1^2} I & \frac{k^2}{k^2+\beta_2^2} I \end{bmatrix} \begin{bmatrix} A_2 \\ A_3 \\ A_4 \end{bmatrix} \qquad (3.39) \\ &= S_I(k)\tilde{A}\end{aligned}$$

The unknown coefficients A_2, A_3 and A_4 can be determined by substituting the previous expressions for A_0, A_1 into equations (3.38) and (3.39). This procedure implies that the resulting solution is sensitive to the choice of β_j when rigid air loads are approximated. In order to uncouple the β_j from the elements of the aerodynamic damping matrix A_1, only the known damping coefficients (the steady aerodynamic derivatives) are used to compute A_1. In this way the solution for the rigid air loads becomes independent of the β_j values. The coefficient A_1 can be estimate as $A_1 = \frac{\hat{Q}_I(k_1)}{k_1}$. For a chosen number ($NF$) of specified values of reduced frequencies k_i, the real and imaginary parts of equation (3.38) and (3.39) can be expressed as

$$\begin{bmatrix} \tilde{Q}_R(k_2) \\ \tilde{Q}_I(k_2) \\ \cdot \\ \cdot \\ \cdot \\ \tilde{Q}_R(k_{NF}) \\ \tilde{Q}_I(k_{NF}) \end{bmatrix} = \begin{bmatrix} \tilde{S}_R(k_2) \\ \tilde{S}_I(k_2) \\ \cdot \\ \cdot \\ \cdot \\ \tilde{S}_R(k_{NF}) \\ \tilde{S}_I(k_{NF}) \end{bmatrix} \begin{bmatrix} A_2 \\ A_3 \\ A_4 \end{bmatrix} \tag{3.40}$$

or

$$\boldsymbol{\hat{Q}} = \boldsymbol{S\tilde{A}}$$

The matrix $\boldsymbol{S}$ is not a square matrix. Pre–multiplying both sides of this equation with $\boldsymbol{S}^T$ implies that

$$\boldsymbol{S}^T\boldsymbol{\hat{Q}} = [\boldsymbol{S}^T\boldsymbol{S}]\boldsymbol{\tilde{A}}$$

Now $\boldsymbol{S}^T\boldsymbol{S}$ can be inverted and the coefficients A_2, A_3, A_4 can be obtained from

$$\boldsymbol{\tilde{A}} = \left[\boldsymbol{S}^T\boldsymbol{S}\right]^{-1}\boldsymbol{S}^T\boldsymbol{\hat{Q}} \tag{3.41}$$

Assuming simple harmonic motion, equation (3.36) can be written as

$$\left[\hat{M}\right]\ddot{\eta} + \left[\hat{C}\right]\dot{\eta} + \left[\hat{K}\right]\eta - \frac{1}{2}\rho V^2\left[A_0\eta + A_1\frac{sc}{2V}\eta + A_2\left(\frac{sc}{2V}\right)^2\eta + A_3\mathbf{x}_1 + A_4\mathbf{x}_2 + \ldots\right] = \boldsymbol{0} \tag{3.42}$$

where

$$\mathbf{x}_j = \frac{s\eta}{s + \dfrac{2V}{c}\beta_j}$$

and

$$\dot{\mathbf{x}}_j + \frac{2V}{c}\beta_j\mathbf{x}_j = \dot{\eta} \tag{3.43}$$

Collecting like terms, this equation may be expressed as

$$(\hat{K}+\bar{q}A_0)\eta+(\hat{C}+\bar{q}\frac{c}{2V}A_1)\dot{\eta}+(\hat{M}+\bar{q}(\frac{c}{2V})^2A_2)\ddot{\eta}+\bar{q}A_3x_1+\bar{q}A_4x_2+\ldots=0$$

or

$$\hat{\hat{K}}\eta+\hat{\hat{C}}\dot{\eta}+\hat{\hat{M}}\ddot{\eta}+\bar{q}A_3x_1+\bar{q}A_4x_2+\ldots=0 \tag{3.44}$$

Equation (3.43) and equation (3.44)) may be combined in the matrix form

$$\begin{bmatrix} I & & & \\ & M & & \\ & & I & \\ & & & I \end{bmatrix}\begin{bmatrix} \dot{\eta} \\ \ddot{\eta} \\ \dot{\mathbf{x}}_1 \\ \dot{\mathbf{x}}_2 \end{bmatrix}=\begin{bmatrix} 0 & I & 0 & 0 \\ -\hat{\hat{K}} & -\hat{\hat{C}} & -\bar{q}A_3 & -\bar{q}A_4 \\ 0 & I & -\frac{2V}{c}\beta_1 I & 0 \\ 0 & I & 0 & -\frac{2V}{c}\beta_2 I \end{bmatrix}\begin{bmatrix} \eta \\ \dot{\eta} \\ \mathbf{x}_1 \\ \mathbf{x}_2 \end{bmatrix} \tag{3.45}$$

or $\quad M'\dot{\mathbf{x}}'=K'\mathbf{x}'$

where $\mathbf{x}'=[(\eta_r \quad \eta_e \quad \eta_\delta \quad \dot{\eta}_r \quad \dot{\eta}_e \quad \dot{\eta}_\delta \quad \mathbf{x}_1 \quad \mathbf{x}_2)]$

and $\quad \dot{\mathbf{x}}'=(M)^{-1}K'\mathbf{x}'$

$\qquad =R\mathbf{x}'$

Now, rearranging the state-space vector $\mathbf{x}'$ as

$$x''=[(\eta_r \quad \eta_e \quad \dot{\eta}_r \quad \dot{\eta}_e \quad \mathbf{x}_1 \quad \mathbf{x}_2)\ (\eta_\delta \quad \dot{\eta}_\delta)]$$

$$=[\hat{\mathbf{x}} \quad u] \tag{3.46}$$

means that equation (3.45) can be partitioned as

$$\begin{bmatrix} \dot{\hat{\mathbf{x}}} \\ \dot{u} \end{bmatrix}=\begin{bmatrix} R_{11} & R_{12} \\ R_{21} & R_{22} \end{bmatrix}\begin{bmatrix} \hat{\mathbf{x}} \\ u \end{bmatrix} \tag{3.47}$$

Here, R_{11} and R_{21} denote the plant dynamics and the R_{12} and R_{22} represent the dynamics of the control modes from the control surfaces. A general form of the state-space equation for the plant dynamics has the expression

$$\dot{\hat{\mathbf{x}}}=\hat{A}\hat{\mathbf{x}}+\hat{B}u \tag{3.48}$$

where

$\hat{A}$ = plant dynamics matrix

$\hat{B}$ = control surface influence matrix

$\hat{\mathbf{x}}$ = generalized coordinates in inertial frame

u = control surface motion input into plant

represent the aircraft dynamics and forcing function terms due to control surface input motions.

The generalized coordinate structural modal displacements are expressed in term of the sensor motion as

$$u_{sen} = T_s \Phi \eta \ = C_0 \mathbf{x} \tag{3.49}$$

where C_0, defined here as $[T_s\Phi \quad 0 \quad 0 \quad 0]$, is the state transformation matrix and T_s is the interpolation matrix that relates the generalized displacements with the actual physical motion reading by the sensor. In a similar way, the sensor velocities and accelerations can be obtained as

$$\begin{bmatrix} \dot{u}_{sen} \\ \ddot{u}_{sen} \end{bmatrix} = \begin{bmatrix} T_s \Phi \dot{\eta} \\ T_s \Phi \ddot{\eta} \end{bmatrix}$$

$$= C_1 \dot{\mathbf{x}}$$

$$= \begin{bmatrix} T_s\Phi & 0 & 0 & 0 \\ 0 & T_s\Phi & 0 & 0 \end{bmatrix} \dot{\mathbf{x}}$$

If $\dot{\mathbf{x}}$ is substituted into this equation, we see that

$$C_1 \dot{\mathbf{x}} = C_1 \hat{A} \mathbf{x} + C_1 \hat{B} u$$

$$= C_2 \mathbf{x} + D_2 u \tag{3.50}$$

The structural nodal displacements, velocity and acceleration for the sensor are obtained by combining equation (3.49) with equation (3.50)

$$y_{sem} = \begin{bmatrix} u_{sen} \\ u_{sen} \\ u_{sen} \end{bmatrix} = \begin{bmatrix} C_0 \\ C_2 \end{bmatrix} \mathbf{x} + \begin{bmatrix} 0 \\ D_2 \end{bmatrix} u$$

$$y_{sen} = \hat{\hat{C}} \mathbf{x} + D u \tag{3.51}$$

which signifies motion at the sensors due to body motion and control surface motions. To integrate the control laws designed for body–axis motion, it is required to convert equation (3.48) from the inertial (Earth) system to the local body coordinate system. Let $\tilde{T}_i$'s to be the coordinate transformation matrices which yield the required state–space equation in the body coordinate system [57]. A transformation of the state space equation into the body coordinates system then gives

$$\dot{\mathbf{x}}_{\mathbf{b}} = \tilde{\boldsymbol{T}}_2^{-1}(\hat{\boldsymbol{A}}\tilde{\boldsymbol{T}}_1 - \tilde{\boldsymbol{T}}_3)\mathbf{x}_{\mathbf{b}} + \tilde{\boldsymbol{T}}_2^{-1}\hat{\boldsymbol{B}}\boldsymbol{u}$$

$$\dot{\mathbf{x}}_b = \boldsymbol{A}\mathbf{x}_b + \boldsymbol{B}\boldsymbol{u} \tag{3.52}$$

$$\mathbf{y}_{sen} = \hat{\hat{\mathbf{C}}}\tilde{\mathbf{T}}_1\mathbf{x}_b + \mathbf{D}\mathbf{u}$$

in which the subscript *b* refers to the body coordinate system.

3.5 Augmentation of Elements and Controller to Plant

Equations (3.49) and (3.52) are the complete state–space formulation of the aircraft integrated structural and aeroelastic characteristics. To construct an aeroservoelastic analysis, the control elements such as actuators, sensors, notch filters and prefilters along with the controller need to be added into the system. We consider the augmentation of an element in series to the plant. The state–space of the element, which is denoted by the subscript *j*, has the form

$$\boldsymbol{x}_j = \boldsymbol{A}_j\boldsymbol{x}_j + \boldsymbol{B}_j\boldsymbol{u}_j \tag{3.35a}$$

$$\boldsymbol{y}_j = \boldsymbol{C}_j\boldsymbol{x}_j + \boldsymbol{D}_j\boldsymbol{u}_j \tag{3.35b}$$

and the state–space of the plant, which is denoted by the subscript *i*, has the form

$$\dot{\boldsymbol{x}}_i = \boldsymbol{A}_i\boldsymbol{x}_i + \boldsymbol{B}_i\boldsymbol{u}_i \tag{3.53c}$$

$$\boldsymbol{y}_i = \boldsymbol{C}_i\boldsymbol{x}_i + \boldsymbol{D}_i\boldsymbol{u}_i \tag{3.35d}$$

It can be observed that the element output $\boldsymbol{y}_j = \boldsymbol{u}_{ic}$, where *c* is the column of the $\boldsymbol{u}$ input matrix of the plant *i*, and substituting the output of control elements for the plant input vector, the state space matrix has the form

$$\begin{bmatrix} \dot{\boldsymbol{x}}_j \\ \dot{\boldsymbol{x}}_i \end{bmatrix} = \begin{bmatrix} \boldsymbol{A}_j & 0 \\ \boldsymbol{B}_{ic}\boldsymbol{C}_j & \boldsymbol{A}_i \end{bmatrix} \begin{bmatrix} \boldsymbol{x}_j \\ \boldsymbol{x}_i \end{bmatrix} + \begin{bmatrix} \boldsymbol{B}_j \\ \boldsymbol{B}_{ic}\boldsymbol{D}_j \end{bmatrix} \boldsymbol{u}_j \tag{3.54}$$

$$\begin{bmatrix} \boldsymbol{y}_j \\ \boldsymbol{y}_i \end{bmatrix} = \begin{bmatrix} \boldsymbol{C}_j & 0 \\ \boldsymbol{D}_{ic}\boldsymbol{C}_j & \boldsymbol{C}_i \end{bmatrix} \begin{bmatrix} \boldsymbol{x}_j \\ \boldsymbol{x}_i \end{bmatrix} + \begin{bmatrix} \boldsymbol{D}_j \\ \boldsymbol{D}_{ic}\boldsymbol{D}_j \end{bmatrix} \boldsymbol{u}_j \tag{3.55}$$

In the case where the element is a gain block $\boldsymbol{G}_j$, the augmentation state–space matrices of a gain to the plant have the form

$$[\dot{x}_i] = [A_i][x_i] + [B_{ic}G_j]u_j \tag{3.56}$$

$$\begin{bmatrix} y_j \\ y_i \end{bmatrix} = \begin{bmatrix} 0 \\ C_i \end{bmatrix}[x_i] + \begin{bmatrix} G_j \\ D_{ic}G_j \end{bmatrix}u_j \tag{3.57}$$

Similarly, the augmentation of a plant in series to an element will give the expression

$$\begin{bmatrix} \dot{x}_i \\ \dot{x}_j \end{bmatrix} = \begin{bmatrix} A_i & 0 \\ B_jC_{ir} & A_j \end{bmatrix}\begin{bmatrix} x_i \\ x_j \end{bmatrix} + \begin{bmatrix} B_i \\ B_jD_{ir} \end{bmatrix}u_i \tag{3.58}$$

$$\begin{bmatrix} y_i \\ y_j \end{bmatrix} = \begin{bmatrix} C_i & 0 \\ D_jC_{ir} & C_j \end{bmatrix}\begin{bmatrix} x_i \\ x_j \end{bmatrix} + \begin{bmatrix} D_i \\ D_jD_{ir} \end{bmatrix}u_i \tag{3.59}$$

where $\mathbf{C}_{ir}$, $\mathbf{D}_{ir}$ are the elements of the r^{th} row of the output of the plant state–space matrix that will be the input of the control element. In the same fashion, the augmentation of a plant to a block gain element will give rise to the state–space matrices

$$[\dot{x}_i] = [A_i][x_i] + [B_i]u_i \tag{3.60}$$

$$\begin{bmatrix} y_i \\ y_j \end{bmatrix} = \begin{bmatrix} C_i \\ G_jC_{ir} \end{bmatrix}[x_i] + \begin{bmatrix} G_i \\ G_jD_{ir} \end{bmatrix}u_i \tag{3.61}$$

To consider signal summation and augmentation into plant, we assume A_{j1}, B_{j1}, C_{j1}, D_{j1} and A_{j2}, B_{j2}, C_{j2}, D_{j2} are two parallel control blocks whose signals will be summed and be the input of the plant with A_i, B_i, C_i, D_i. The procedure requires the block–to–plant augmentation scheme for each of the individual control blocks to use the same input port of the plant and sum the output rows of the plants for each of these blocks.

In the process of closing a control loop with feedback, the final state–space matrices are of the form

$$A_{cl} = \begin{bmatrix} A_i - B_iVD_jC_i & 0 \\ B_jWC_i & A_j - B_jVD_iC_i \end{bmatrix} \qquad B_{cl} = \begin{bmatrix} B_iV \\ B_jWD_i \end{bmatrix} \tag{3.62}$$

$$C_{cl} = \left[WC_i \quad -D_j WC_i \right] \qquad\qquad D_{cl} = \left[D_i V \right] \qquad (3.63)$$

where

$$V = \left[I + D_j D_i \right]^{-1} \qquad\qquad W = \left[I + D_i D_j \right]^{-1}$$

3.5.1 Discretization of Continuous–Time State–Space Equation

Consider the continuous time state equation and output equation

$$\dot{x}(t) = Ax(t) + Bu(t) \qquad (3.64)$$

$$y(t) = Cx(t) + Du(t) \qquad (3.65)$$

For the invariant time case, the zero-order hold (ZOH) discrete–time representation of the above equation has the form[58]

$$x((k+1)T) = G(T)x(kT) + H(T)u(kT) \qquad (3.66)$$

$$y(kT) = C(T)x(kT) + D(T)u(kT) \qquad (3.67)$$

Note here that the matrices $G(T)$ and $H(T)$ are dependent upon the sampling period T. Once the sampling period is fixed, $G(T)$ and $H(T)$ are constant matrices. The matrices $G(T)$ and $H(T)$ can be obtained numerically using the equations

$$G(T) = e^{[A]T} = I + [A]T + \frac{[A]^2}{2!}T^2 + \frac{[A]^3}{3!}T^3 + \ldots \qquad (3.68)$$

$$H(T) = (e^{[A]T} - I)A^{-1}B = ([I]T + \frac{[A]}{2!}T^2 + \frac{[A]^2}{3!}T^3 + \ldots)B \qquad (3.69)$$

The augmentation of the digital blocks and plants follows the same pattern as the analog components. In the case of a hybrid system, the analog control blocks need to be augmented to the system and then the analog state–space system is converted to the digital domain at a given sampling rate. The remaining digital control blocks continue to be augmented to the plant.

3.5.2 State–Space Representation of Dynamic Systems

Consider an nth–order differential system of equation involving derivative terms in the forcing function [16] and expressed in the form

$$y^{(n)} + a_1 y^{(n-1)} + \ldots + a_{n-2}\ddot{y} + a_{n-1}\dot{y} + a_n y = b_0 u^{(n)} + b_1 u^{(n-1)} + b_2 u^{(n-2)} + \ldots + b_{n-1}\dot{u} + b_n u \qquad (3.70)$$

Define a set of n variables, in terms of a set of n state variables, as

$x_1 = y - \beta_0 u$

$x_2 = \dot{y} - \beta_0 \dot{u} - \beta_1 u = \dot{x}_1 - \beta_1 u$

$x_3 = \ddot{y} - \beta_0 \ddot{u} - \beta_1 \dot{u} - \beta_2 \ddot{u} = \dot{x}_2 - \beta_2 u$

.

.

.

$x_n = y^{(n-1)} - \beta_0 u^{(n-1)} - \beta_1 u^{(n-2)} - \ldots - \beta_{n-2} \dot{u} - \beta_{n-1} u = \dot{x}_{n-1} - \beta_{n-1} u$

where

$\beta_0 = b_0$

$\beta_1 = b_1 - a_1 \beta_0$

$\beta_2 = b_2 - a_1 \beta_1 - a_2 \beta_0$

$\beta_3 = b_3 - a_1 \beta_2 - a_2 \beta_1 - a_3 \beta_0$

.

.

.

$\beta_n = b_n - a_1 \beta_{n-1} - \ \ldots \ - a_{n-1} \beta_1 - a_n \beta_0$

With this particular choice of state variables, the uniqueness of the solution of the state equation is guaranteed. Notice that this is not the only choice for a set of state variables for the system. However, for this present choice of state variables, the equation system may be arranged as

$\dot{x}_1 = x_2 - \beta_1 u$

$\dot{x}_2 = x_3 - \beta_2 u$

. (3.71)

.

.

$\dot{x}_{n-1} = x_n - \beta_{n-1} u$

$\dot{x}_n = -a_n x_1 - a_{n-1} x_2 - \ldots - a_1 x_n - \beta_n u$

In matrix form, the above equation and the output equation can be written as

$$\begin{bmatrix} \dot{x}_1 \\ \dot{x}_2 \\ \cdot \\ \cdot \\ \cdot \\ \dot{x}_{n-1} \\ \dot{x}_n \end{bmatrix} = \begin{bmatrix} 0 & 1 & 0 & . & . & . & 0 \\ 0 & 0 & 1 & . & . & . & 0 \\ \cdot & \cdot & \cdot & \cdot & & & \cdot \\ \cdot & \cdot & \cdot & & \cdot & & \cdot \\ \cdot & \cdot & \cdot & & & \cdot & \cdot \\ 0 & 0 & 0 & . & . & . & 1 \\ -a_n & -a_{n-1} & -a_{n-2} & . & . & . & -a_1 \end{bmatrix} \begin{bmatrix} x_1 \\ x_2 \\ \cdot \\ \cdot \\ \cdot \\ x_{n-1} \\ x_n \end{bmatrix} + \begin{bmatrix} \beta_1 \\ \beta_2 \\ \cdot \\ \cdot \\ \cdot \\ \beta_{n-1} \\ \beta_n \end{bmatrix} [u] \quad (3.72)$$

$$y = [1 \quad 0 \quad 0 \quad . \quad . \quad . \quad 0] \begin{bmatrix} x_1 \\ x_2 \\ \cdot \\ \cdot \\ \cdot \\ x_{n-1} \\ x_n \end{bmatrix} + \beta_0 [u] \qquad (3.73)$$

or

$$\dot{\boldsymbol{x}} = \boldsymbol{A}\boldsymbol{x} + \boldsymbol{B}\boldsymbol{u} \qquad (3.74)$$

$$\boldsymbol{y} = \boldsymbol{C}\boldsymbol{x} + \boldsymbol{D}\boldsymbol{u} \qquad (3.75)$$

3.5.3 Transfer Function

Applying the Laplace transformation to equation (3.64) results in the expression

$$s\boldsymbol{x}(s) = \boldsymbol{A}\boldsymbol{x}(s) + \boldsymbol{B}\boldsymbol{u}(s) \qquad (3.76)$$

or

$$\boldsymbol{x}(s) = [s\boldsymbol{I} - \boldsymbol{A}]^{-1} \boldsymbol{B}\boldsymbol{u}(s) \qquad (3.77)$$

Substituting this expression into equation (3.65), we obtain the open–loop frequency response relationship

$$\begin{aligned} \boldsymbol{y}(s) &= [\boldsymbol{C}[s\boldsymbol{I} - \boldsymbol{A}]^{-1} \boldsymbol{B} + \boldsymbol{D}]\boldsymbol{u}(s) \qquad (3.78) \\ &= \boldsymbol{H}(s)\boldsymbol{u}(s) \end{aligned}$$

where $\boldsymbol{H}(s)$ is the equivalent loop (loop gain) transfer function with the analog controller or the loop transfer function without the controller. From $\boldsymbol{H}(s)$, the phase and gain property of the system can be obtained for a range of specified frequencies by constructing a Bodé plot. From the point of view of stability, the damping and modal frequencies for the system may be calculated by solving the eigenvalue problem of the A matrix for various ω_i values and tracking the root changes. The eigenvalues of A are complex conjugate pairs. $-\alpha \pm \beta$. Flutter is indicated by a change of sign of α, and divergence occurs when the frequency β approaches zero. The system instability can be assessed by studying the phase and gain margin characteristics[60].

In the presence of a digital controller, a hybrid approach is adopted for the frequency response solution. Thus A', B', C', D' are the state–space matrices associated with the controller; the related transfer function is simply given by the expression

$$G(z) = [C'[zI - A']^{-1} B' + D'] \qquad (3.79)$$

and the frequency response relationship for the hybrid analog/digital system can be written as

$$\begin{aligned} y(s) &= [G(z)_{[at\ z=e^{sT}]}(\frac{H(s)[ZOH]}{T})\ u(s)] \qquad (3.80) \\ &= H(s)^*\ u(s) \end{aligned}$$

where $H(s)$ is the transfer function for the plant and other analog elements, [ZOH] is the zero order hold complex expression $(e^{-s\tau}(\frac{1-e^{1-sT}}{s}))$, where τ is the time delay, and $H(s)^*$ is the equivalent transfer function of the open–loop hybrid system. For a unity feedback closed loop, the transfer function has the form

$$H(s)^*_{cl} = \frac{H(s)^*}{1 + H(s)^*} \qquad (3.81)$$

With a sensor feedback closed loop, the transfer function has the expression

$$H(s)^*_{cl} = \frac{G_1(z)H(s)^*}{1 + G_1(z)H(s)^*} \qquad (3.82)$$

where $G_1(z)$ is the transfer function of the feedback sensor.

3.6 Concluding Remarks

In this chapter numerical formulations, based on linear unsteady aerodynamics, have been presented for both aeroelastic and aeroservoelastic analysis. Both analog and digital control systems can be accommodated with this formulation. For many practical problems this is a reasonable approximation. A more accurate methodology, employing a nonlinear CFD based formulation, is given in the next chapter.

CHAPTER 4

NUMERICAL TECHNIQUES FOR NONLINEAR AEROELASTICITY AND AEROSERVOELASTICITY

4.1 Introduction

An aeroelasticity/aeroservoelasticity (AE/ASE) analysis requires the successful integration of the individual disciplines of structural dynamics, unsteady aerodynamics and control input/output. The methodology adopted for the analysis of the disciplines may be different, but the components are always the same for an ASE analysis. The most difficult integration task is the numerical coupling to enable the analysis of the fluid–structure interaction.

Several methods have been developed to enable the modeling of the motion and deformation of the structure and fluid boundary. The most common methods are: use of a dynamic mesh, employing some form of remeshing, and the application of the moving boundary condition on a fixed mesh via the surface transpiration method.

A dynamic mesh algorithm [6,9,59,61-63] replaces the network of edges in the mesh with a system of springs, whose stiffness is inversely proportional to the edge length. Every time the body surface is deformed to conform to the applied aerodynamic load, the remainder of the computational domain mesh is moved by solving the static equilibrium equation for the spring system in the x, y and z direction. A deformation for each node in the domain can be computed by an iterative predictor–corrector procedure. This predicts a displacement for the nodes using a linear extrapolation and corrects the predicted value using several Jacobian iteration of the static equilibrium equations. To prevent the appearance of numerical errors that are induced by the motion of the grid, the geometrical conservation law must be satisfied in addition to the standard requirement for conservation of mass, momentum and energy[64,65,66]. Batina[67,68] has undertaken extensive work on this technique, using both structured and unstructured meshes. Initial developments assumed that the fluid mesh moved rigidly or was sheared as the body deformed. This assumption limited the application of the structured dynamic mesh to problems involving rigid body or small amplitude motion. An alternative unstructured grid[69-75] has also been employed to enable the modeling of problems involving complex geometries and flow fields.

The remeshing approach produces a new mesh for the complete computational domain at each time step, in accordance with the structural deformation. This technique requires detailed data keeping for the definitions of the geometry surfaces and the intersection points. This is the most difficult and the most expensive procedure to implement in a general purpose CFD code.

The surface transpiration [76,77] method is based upon the concept of modifying the flow boundary conditions and the definition of the normal at the boundary on the existing CFD grid in accordance with actual structural displacement. The concept was presented originally in a paper by Lighthill in 1958 [76]. With this method, no modifications or remeshing are made to the existing CFD grid, except for a simple change in the flow tangency boundary condition on an element that is subjected to the structural deformation. To maintain the boundary condition of no–flow normal to the surface, the flow solver computes a new normal direction for each surface element as the surface deforms. The accuracy of the method has been demonstrated through the work of Gupta[78],Raj & Harris[79] and Fisher & Arena[80].

In STARS, a finite element technique is used to discretize the solid and the fluid continua. Steady and unsteady aerodynamic solutions are performed by an Euler solver with the additional application of a transpiration boundary method for the unsteady case. As the finite element technique is used in both the solid and fluid regions, the accurate modeling of the interaction between disciplines is achieved. Figure 4.1 shows the number of disciplines that are involved in the multidisciplinary modeling simulation of nonlinear flutter analysis. Some relevant details of finite element formulations, adopted for computational fluid dynamics (CFD) and nonlinear-stability analysis used in the current application, are presented next [17]. An alternative aerodynamic forces computation method implemented into STARS that also utilizes as a perturbation to an already exiting mean steady state flow solution is the Piston Perturbation Method [81] by Arena et al. Piston method [82,83] is a simple technique to use for supersonic flow (Mach >>1). The method computes the pressure on any surface point based on the outward normal vector of the given surface definition [83,84].

In this thesis, a closed loop ASE state-space equation expression will be derived for the systems with uniform sampling rate. The sensor mechanism that computes the physical inputs needed by the control system such as pitch, pitch rate, roll rate, etc. is incorporated into the nonlinear aeroservoelastic analysis. As the control system sometimes is in the body fixed coordinate instead of inertial fixed frame coordinate, the equation of motion from an inertial frame is converted to body fixed reference frame. The aeroservoelasticity can be run for multi sampling rate problems in which the control system has a different sampling rate in comparison to the aeroelastic system.

4.2 Finite Element Computational Fluid Dynamics

The CFD analysis requires two major fundamental solution capabilities. Effective generation of unstructured and solution adaptive domain meshes and finite element analysis techniques for the relevant flow problem. The development of related numerical tools is also necessary for the efficient solution of complex practical problems. These solution capabilities have been appropriately incorporated into the STARS program.

4.2.1 Mesh Generation

The advancing front technique[85] is employed for the automatic generation of unstructured meshes and is suitable for the discretization of complex domains. The algorithm was initially developed for arbitrary, multiconnected, planar domains in which the interior nodes are generated first, then suitably linked to yield the best possible triangulation.

During this process, the mesh generation front is continually updated after each new element is constructed. The technique, initially developed for 2D grids, was further improved and extended for 3D meshes [86,87]. Nodes and triangles then are formed simultaneously for all boundary surfaces. This is done by the generation of tetrahedra by the advancing front approach to fill the entire solution domain. Background grids are used to specify mesh parameters defining node spacing, a stretching parameter and stretching directions. The procedure proves to be flexible with regard to the specification of arbitrary shapes and varying grid density throughout the domain and enables the adaptive mesh generation in accordance with the form of a computed solution.

This 3D automatic unstructured mesh generation scheme has proved to be versatile for modeling practical CFD solution domains around complicated geometrical objects, such as complete aircraft. However, because the advancing front technique involves an extensive search for nodes and faces on the front, the grid generation time tends to be long for complex configurations. A simple modification of the procedure, implemented during the current thesis work, has proven to be efficient and economical. In this method, the technique is first used to generate a coarse grid, whose cells have linear dimensions approximately twice the desired size and then each cell is reduced locally to its desired size [88].

4.2.2 Finite Element Computational Fluid Dynamics Analysis

For a viscous, heat conducting, compressible fluid obeying the laws of conservation of mass, momentum and energy, the dynamic equation of flow can be expressed by the set of partial differential equations,

$$\frac{\partial V}{\partial t}+\frac{\partial \mathbf{F}_{\mathrm{i}}}{\partial \mathrm{x}_{\mathrm{i}}}=\mathbf{f}_{\mathrm{b}},\mathrm{i}=1,2,3 \tag{4.1}$$

where the column vectors, representing the unknowns, the fluxes and the body forces, and the viscous stress tensor are defined as

$$\mathbf{V}=\{\rho\,\rho\mathrm{u}_{\mathrm{j}}\,\rho E\} \tag{4.2}$$

$$\mathbf{F}_{\mathrm{i}}=\left\{\rho\mathrm{u}_{\mathrm{i}}\;\rho\mathrm{u}_{\mathrm{i}}u_{j}+p\delta_{ij}+\sigma_{\mathrm{ij}}\,\mathrm{u}_{\mathrm{i}}(\rho\mathrm{E}+\mathrm{p})+\mathrm{u}_{\mathrm{i}}\sigma_{1i}+\mathrm{k}\frac{\partial\mathrm{T}}{\partial\mathrm{x}_{\mathrm{i}}}\right\} \tag{4.3}$$

$$\mathbf{f}_{b}=\{0\;\;\mathbf{f}_{\mathrm{b}_{\mathrm{j}}}\,\mathrm{u}_{1}\mathbf{f}_{\mathrm{b}_{1}}\} \tag{4.4}$$

$$\sigma_{\mathrm{ij}}=-\frac{2}{3}\mu\frac{\partial\mathrm{u}_{\mathrm{k}}}{\partial x_{k}}\delta_{ij}+\mu\left(\frac{\partial\mathrm{u}_{\mathrm{i}}}{\partial x_{j}}+\frac{\partial\mathrm{u}_{\mathrm{j}}}{\partial x_{i}}\right) \tag{4.5}$$

Here, ρ, p, and E are the density, average pressure intensity and total energy of the fluid respectively; δ_{ij} is the Kronecker delta; u_j is the velocity component in the direction x_j of a Cartesian coordinate system; μ is the viscosity; k is the thermal conductivity and f_b are the body forces. These equations are supplemented by the state equations

$$p=(\gamma-1)\rho\left[E-\frac{1}{2}u_i u_i\right] \tag{4.6}$$

and
$$T=\left[E-\frac{1}{2}u_i u_i\right]c_v \tag{4.7}$$

to complete the equation set, where γ is the ratio of specific heats and c_v is the specific heat at constant volume. This formulation is valid for a perfect gas.

A solution of the inviscid form of equation (4.1) is achieved by first obtaining a Taylor series expansion of **V** in the time domain. The spatial domain, **Ω**, is then discretized by unstructured meshes of 3D tetrahedral elements. Using linear finite element approximations, $\mathbf{V}=\mathbf{a}\hat{\mathbf{V}},\hat{\mathbf{V}}$ being the nodal variable values, and employing a Galerkin weighted residual procedure, a time dependent form of the governing equations can be obtained as[16]:

$$\mathbf{M}\delta\hat{\mathbf{V}}=-\Delta\left[\mathbf{C}\hat{\mathbf{V}}\right]+\mathbf{R} \tag{4.8}$$

where **R** includes all artificial viscosity effects that are essential for capturing shocks and **C** includes a set of symmetric and lumped (diagonal) mass matrices formulated for the artificial dissipation. The solution of equation (4.8) is achieved by advancing this time dependent form until steady conditions are obtained. In the STARS program, this is achieved using an explicit time stepping iterative scheme [86] or an alternative quasi-implicit solution scheme. An accelerated solution procedure, based on the Aitken acceleration technique, has recently been implemented [88,89] and leads to considerable improvement in the solution convergence rate.

4.3 Nonlinear, Computational Fluid Dynamics Based Aeroelastic and Aeroservoelastic Analysis (STARS–CFDASE)

The nonlinear aeroelasticity analysis capability is based on the implementation of the transpiration boundary condition method in the CFD flow solver.

The CPU time required for a CFD based unsteady solution in an aeroelastic simulation can be significant. One research effort of Arena et al. aims to speed up the aerodynamic solution, with the objective of minimizing the CPU time required for the

CFD analysis. For the purpose of accelerating the aerodynamic model solution, an alternative auto regressive moving average model (ARMA) [90-95] based unsteady analysis procedure has been developed. This requires that the nonlinear Euler based CFD analysis is carried out only once at a particular density. The procedure utilizes the system identification technique to obtain a mathematical model of the aerodynamic CFD system, based on a set of measured output and input data from the system. The system identification method uses a collection of time histories of input and output and fits the parameters of a model structure that will accurately describe the dynamic characteristics and behavior of the actual aerodynamic system, such that its error output is minimized in the process. For its success, the system identification technique relies on the choice of the order of the model structure and the quality of the data used for the input signal chosen for the training process of the model. This process will be discussed in more detail in the next section. The system identification method provides the aerodynamic characteristic of the problem in a state-space formulation which is convenient in the derivation of the closed form expression for the aeroservoelastic analysis of uniform sampling rate cases.

4.3.1 Aeroelastic and Aeroservoelastic Analysis

The aeroelastic and aeroservoelastic analysis process, see Figure 4.1, starts with the finite element structural modeling and subsequently computes the natural frequencies, ω and modes, $\mathbf{\Phi}$, that consist of rigid body, elastic and control surface motions, by solving

$$\mathbf{M\ddot{u}} + \mathbf{Ku} = \mathbf{0} \tag{4.9}$$

In this equation, **M** and **K** are the inertial and stiffness matrices respectively and **u** is the displacement vector. This solution is achieved by the use of either a computationally efficient PSI [29](Progressive Simultaneous Iteration) technique or a block Lanczos procedure that fully exploits matrix sparsity. Next, a steady state Euler solution is computed, in which optimum solution convergence is achieved through an explicit or alternative quasi implicit local time stepping solution procedure, that also employs a residual smoothing strategy. The resulting generalized equation of motion for the vehicle may be written as

$$\hat{\mathbf{M}}\ddot{\boldsymbol{q}} + \hat{\mathbf{K}}\boldsymbol{q} + \hat{\mathbf{C}}\dot{\boldsymbol{q}} + \boldsymbol{f}_a(t) + \boldsymbol{f}_I(t) = \mathbf{0} \tag{4.10}$$

where the generalized matrices and vectors are defined as

$\hat{\mathbf{M}}$ = generalized inertia matrix ($=\Phi^T\mathbf{M}\Phi$)

$\hat{\mathbf{K}}, \hat{\mathbf{C}}$ = generalized stiffness ($=\Phi^T\mathbf{K}\Phi$) and damping ($=\Phi^T\mathbf{C}\Phi$) matrices

$\boldsymbol{q}$ = generalized displacement vector ($=\Phi^T\boldsymbol{u}$)

$\dot{\boldsymbol{q}}$ = generalized velocity vector ($=\Phi^T\dot{\boldsymbol{u}}$)

$\ddot{\boldsymbol{q}}$ = generalized acceleration vector ($=\Phi^T\ddot{\boldsymbol{u}}$)

$\boldsymbol{u}$ = structural displacement vector

$\boldsymbol{f}_a(t)$ = generalized aerodynamic (CFD) load vector ($=\Phi_a^T pA$), where p is the Euler pressure, A is the appropriate surface area, and Φ_a is the general displacement modal vector pertaining to the aerodynamic grid points interpolated from relevant general displacement modal structural nodes

$\boldsymbol{f}_I(t)$ = generalized impulse force vector (Figure 4.2) which used to excite the vibrating structure.

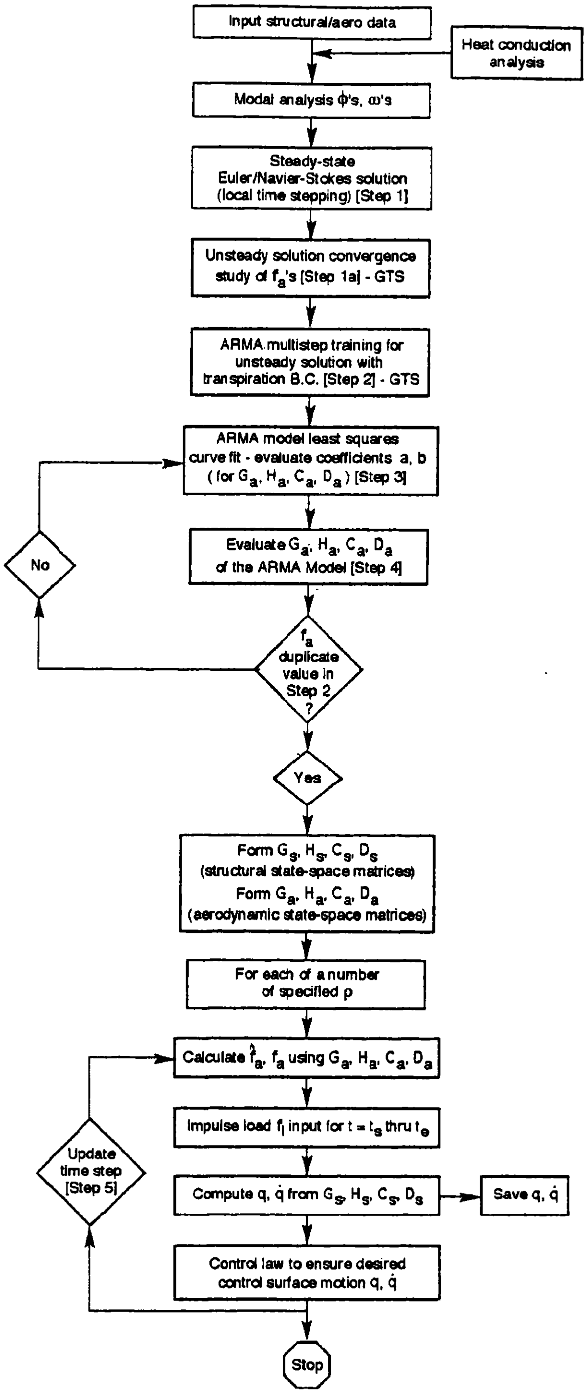
Input structural/aero data
Heat conduction analysis
Modal analysis ϕ's, ω's
Steady-state Euler/Navier-Stokes solution (local time stepping) [Step 1]
Unsteady solution convergence study of f_a's [Step 1a] - GTS
ARMA multistep training for unsteady solution with transpiration B.C. [Step 2] - GTS
ARMA model least squares curve fit - evaluate coefficients a, b (for G_a, H_a, C_a, D_a) [Step 3]
Evaluate G_a, H_a, C_a, D_a of the ARMA Model [Step 4]
No
f_a duplicate value in Step 2 ?
Yes
Form G_s, H_s, C_s, D_s (structural state-space matrices)
Form G_a, H_a, C_a, D_a (aerodynamic state-space matrices)
For each of a number of specified p
Calculate $\hat{f}_a$, f_a using G_a, H_a, C_a, D_a
Impulse load f_i input for $t = t_s$ thru t_e
Update time step [Step 5]
Compute q, $\dot{q}$ from G_s, H_s, C_s, D_s
Save q, $\dot{q}$
Control law to ensure desired control surface motion q, $\dot{q}$
Stop

Figure 4.1. Nonlinear flutter analysis methodology.

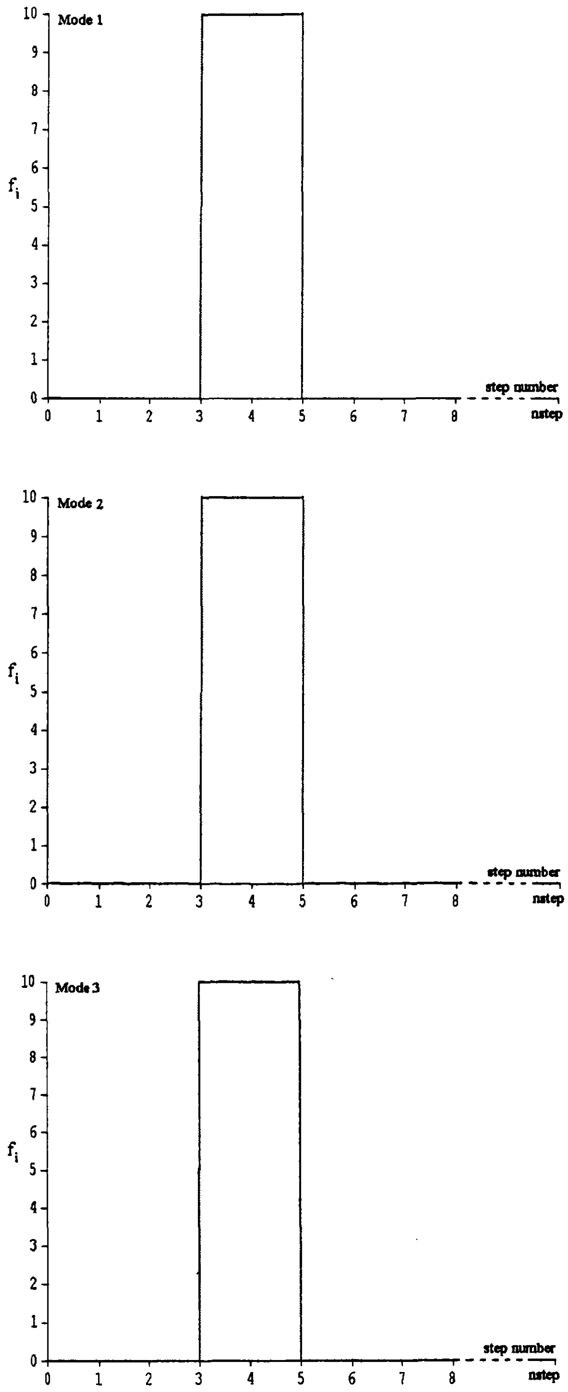

Figure 4.2 The generalized impulse force vector $f_I(k)$.

Equation (4.10) may be formulated next in the state space matrix equation form

$$\dot{\boldsymbol{x}}_s(t) = \mathbf{A}_s \boldsymbol{x}_s(t) + \mathbf{B}_s \boldsymbol{f}(t) \tag{4.11}$$

$$\boldsymbol{y}_s(t) = \mathbf{C}_s \boldsymbol{x}_s(t) + \mathbf{D}_s \boldsymbol{f}(t)$$

where

$$\boldsymbol{x}_s(t) = \begin{bmatrix} q(t) \\ \dot{q}(t) \end{bmatrix} \tag{4.12}$$

$$= \ \boldsymbol{y}_s(t)$$

$$\mathbf{A}_s = \begin{bmatrix} \mathit{0} & \mathbf{I} \\ -\hat{\mathbf{M}}^{-1}\hat{\mathbf{K}} & -\hat{\mathbf{M}}^{-1}\hat{\mathbf{C}} \end{bmatrix} \quad \mathbf{B}_s = \begin{bmatrix} \mathit{0} \\ -\hat{\mathbf{M}}^{-1} \end{bmatrix} \qquad \boldsymbol{f}(t) = \{\boldsymbol{f}_a(t) + \boldsymbol{f}_l(t)\}$$

$$\mathbf{C}_s = [\mathbf{I}] \qquad \mathbf{D}_s = [\mathit{0}]$$

The state-space equations in time domain can then be converted to the discrete time equivalent at the k^{th} step using the zero-order-hold (ZOH) as discussed in Chapter 3 give the following expression

$$\boldsymbol{x}_s(k+1) = \mathbf{G}_s \boldsymbol{x}_s(k) + \mathbf{H}_s \boldsymbol{f}(k) \tag{4.13}$$

$$\boldsymbol{y}_s(k) = \mathbf{C}_s \boldsymbol{x}_s(k) + \mathbf{D}_s \boldsymbol{f}(k) \tag{4.14}$$

in which

$$\mathbf{G}_s = e^{\mathbf{A}_s \Delta t} \qquad \mathbf{H}_s = \left[\int_0^{\Delta t} e^{\mathbf{A}_s \Delta\lambda} d\lambda \right] \mathbf{B}_s = [e^{\mathbf{A}_s \Delta t} - I][\mathbf{A}_s^{-1} \mathbf{B}_s]$$

$$\boldsymbol{f}(k) = \{\boldsymbol{f}_a(k) + \boldsymbol{f}_l(k)\} \tag{4.15}$$

where $\Delta t = t_{n+1} - t_n$ and $\mathbf{C}_s$ and $\mathbf{D}_s$ remain unaltered from equation (4.11). Figure 4.3 depicts a structural model of this form. Data consisting of the $\boldsymbol{q}$ and $\dot{\boldsymbol{q}}$ vectors is then stored for later processing of aeroelastic damping and frequency estimates. To start the unsteady analysis, an impulse signal of magnitude illustrated in Figure 4.2 is input to the $\boldsymbol{f}_l(t)$ vector for a few Δt steps. $\boldsymbol{f}_l(t)$ is the user input that contains a number *nr* of modes of interest for a particular problem.

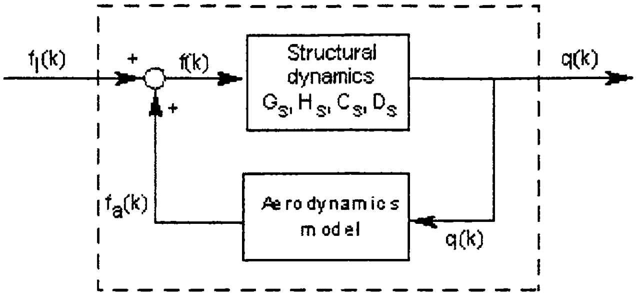

Figure 4.3. Coupled aeroelastic (AE) model

In aeroservoelastic (ASE) analysis, assuming a control law has been designed based upon the linear characteristics of the control derivatives, the control law can be interfaced with the CFD based analysis procedure. Thus, the input to the control law will consist of state variables of the aeroelastic model. Based on the input, the flight control derives the necessary control surface deflections to alleviate the aircraft response.

The desired control surface motion, such as pitch angle to stabilize the structure, can be calculated by using the aeroelastic state output vector as

$$\dot{\boldsymbol{x}}_c(t) = \mathbf{A}_c \boldsymbol{x}_c(t) + \mathbf{B}_c \boldsymbol{u}_c \tag{4.16}$$

$$\boldsymbol{y}_c(t) = \mathbf{C}_c \boldsymbol{x}_c(t) + \mathbf{D}_c \boldsymbol{u}_c \tag{4.17}$$

where $\boldsymbol{u}_c$ is the generalized control input signal vector, defined as

$$\boldsymbol{u}_c = \tilde{\boldsymbol{K}} \boldsymbol{y}_s(t) = \tilde{\boldsymbol{K}} \mathbf{C}_s \boldsymbol{x}_s(t) \tag{4.18}$$

in which typically

$$\boldsymbol{y}_c = [\delta_c^1,\ \delta_c^2, \cdots, \delta_c^{nc}]^T \tag{4.19}$$

Here, nc is the control surfaces indicator; and the constant transition matrix is defined by

$$\widetilde{\mathbf{K}} = \begin{bmatrix} k_1^1 & k_2^1 & \cdots & k_{2NR}^1 \\ \vdots & & & \vdots \\ k_1^{ncb} & k_2^{ncb} & \cdots & k_{2NR}^{ncb} \end{bmatrix} \tag{4.20}$$

assuming *ncb* columns in the $\mathbf{B}_c$ matrix and with the structural state vector

$$x_s(t) = \left[q_1,\ q_2,\ \cdots,\ q_{NE},\ \delta_1,\ \delta_2, \cdots,\ \delta_{NC},\ \dot{q}_1,\ \dot{q}_2, \cdots,\ \dot{q}_{NE},\ \dot{\delta}_1,\ \dot{\delta}_2, \cdots,\ \dot{\delta}_{NC}\right]^T \tag{4.21}$$

NE and *NC* denote the number of elastic and control modes respectively. The deflection of a typical i^{th} control surface can be obtained from the respective $\mathbf{A}_c$, $\mathbf{B}_c$, $\mathbf{C}_c$, and $\mathbf{D}_c$ control state space matrices. For a uniform sampling rate, equation (4.16) is now discretized, to the sampling rate $\Delta t_{CFD} = T_{CFD}$ of the k^{th} CFD time step, to give

$$\boldsymbol{x}_c(k+1) = e^{\mathbf{A}_c \Delta t_{CFD}} \boldsymbol{x}_c(k) + \mathbf{A}_c^{-1}[e^{\mathbf{A}_c \Delta t_{CFD}} \text{ -}\mathbf{I}]\mathbf{B}_c \boldsymbol{u}_c$$

or

$$\boldsymbol{x}_c(k+1) = \mathbf{G}_c \boldsymbol{x}_c(k) + \mathbf{H}_c \boldsymbol{u}_c \tag{4.22}$$

$$\boldsymbol{y}_c(k) = \mathbf{C}_c \boldsymbol{x}_c(k) + \mathbf{D}_c \boldsymbol{u}_c$$

and the current value of $\boldsymbol{y}_c$ can be computed from equation (4.22) and added to the original aeroelastic state vector defined by equation (4.21) in the appropriate modal control location δ_i . This new state space vector is then used for calculating the real nodal displacement $\boldsymbol{u}$ and velocity $\dot{\boldsymbol{u}}$ vectors at every aerodynamic grid point on the deformed structure. Applying the boundary transpiration method, the aerodynamic flow field around the vibrating structure is adjusted accordingly to match the actual deformations on the structure. These aerodynamic flow components are needed for the next Euler solution iteration step, see Figure 4.1. The $\Delta t_{CFD} = T_{CFD}$ should always be less than 1/20 of the highest structural frequency. This mean that in the highest structural mode there is at least 20 sampling points per cycle.

For the case of multisampling rate aeroservoelastic analysis, in which the vehicle's control law system is discretized at $\Delta t_{control}$ a different sampling rate than the Δt_{CFD} of the aeroelastic system, then the control outputs signal $\boldsymbol{y}_c$ in equation (4.22) is only being computed and feedback to the aeroelastic state vector equation (4.21) at only every $\Delta t_{control}$ time steps. The closed loop aeroelastic and other components, such as sensor and actuator which might be analog, analyses are running at every Δt_{CFD} time step, and will receive a control signal from the control law at every $\Delta t_{control}$ time step. Because of the timing of the feedback signal to the aeroelastic loop, it is necessary to set the Δt_{CFD} in such a way that $\Delta t_{control}$ is a multiple of Δt_{CFD}.

This type of an analysis, at a specific Mach number, may then be repeated for a number of altitudes, involving various dynamic pressure values and the instability altitude, signified by a zero damping value, may then be extracted using simple interpolation of each desired state variable. An alternative faster procedure based on a system identification technique, which also provides aerodynamic state space matrices vital in the design of control law is described in the following sections.

4.3.2 Aeroelastic and Aeroservoelastic Analysis With Sensor Mechanism

In the present of sensors, the generalized state space equation of motion (4.11) has the following expression,

$$\dot{x}_s(t) = \mathbf{A}_s x_s(t) + \mathbf{B}_s f(t) \tag{4.23}$$

$$y_s(t) = \begin{Bmatrix} q_s \\ \dot{q}_s \\ u_{\text{sen}} \\ \dot{u}_{\text{sen}} \\ \ddot{u}_{\text{sen}} \end{Bmatrix} = \begin{bmatrix} \mathbf{I} & \mathbf{0} \\ \mathbf{0} & \mathbf{I} \\ \mathbf{T}_s\mathbf{\Phi} & \mathbf{0} \\ \mathbf{0} & \mathbf{T}_s\mathbf{\Phi} \\ \mathbf{T}_s\mathbf{\Phi}(-\hat{\mathbf{M}}^{-1}\hat{\mathbf{K}}) & \mathbf{T}_s\mathbf{\Phi}(-\hat{\mathbf{M}}^{-1}\hat{\mathbf{C}}) \end{bmatrix} \begin{Bmatrix} q_s(t) \\ \dot{q}_s(t) \end{Bmatrix} + \begin{bmatrix} \mathbf{0} \\ \mathbf{0} \\ \mathbf{0} \\ \mathbf{0} \\ -\mathbf{T}_s\mathbf{\Phi}\hat{\mathbf{M}}^{-1} \end{bmatrix} f(t)$$

or

$$y_s(t) = \mathbf{C}_{ss} x_s(t) + \mathbf{D}_{ss} f(t)$$

u_{sen}, $\dot{u}_{sen}$ and $\ddot{u}_{sen}$are the physical sensor's displacement, velocity and acceleration vectors that were mention previously in Equation (3.51). $\mathbf{T}_s$ is the interpolation matrix that relates the generalized motion to the actual physical sensors motions.

In order to incorporate the control laws to body fixed frame coordinate system, it is necessary to transfer the equation of motion (4.23) from an inertial frame to a body fixed. The above equation will have the following transformation as mentioned in chapter 3

$$\dot{\boldsymbol{x}}_s(t) = \mathbf{T}_2^{-1}(\mathbf{A}_s\tilde{\mathbf{T}}_1 - \tilde{\mathbf{T}}_3)\boldsymbol{x}_s(t) + \mathbf{T}_2^{-1}\boldsymbol{f}(t) \tag{4.24}$$

$$\boldsymbol{y}_s(t) = \mathbf{C}_{ss}\tilde{\mathbf{T}}_1\boldsymbol{x}_s(t) + \mathbf{D}_{ss}\boldsymbol{f}(t)$$

$\tilde{\boldsymbol{T}}_i's$ are the coordinate transformation matrices which tranform the required state–space equation in the body coordinate system, which is defined in the Reference 57. The Equation (4.24) is discretized to Δt_{CFD} using ZOH to obtain

$$\boldsymbol{x}_s(k+1) = \mathbf{G}_s\boldsymbol{x}_s(k) + \mathbf{H}_s\boldsymbol{f}(k)$$

$$\boldsymbol{y}_s(k) = \begin{Bmatrix} \boldsymbol{q}_s(k) \\ \dot{\boldsymbol{q}}_s(k) \\ \boldsymbol{u}_{\text{sen}}(k) \\ \dot{\boldsymbol{u}}_{\text{sen}}(k) \\ \ddot{\boldsymbol{u}}_{\text{sen}}(k) \end{Bmatrix} = \begin{bmatrix} \mathbf{I} & \mathbf{0} \\ \mathbf{0} & \mathbf{I} \\ \mathbf{T}_s\boldsymbol{\Phi} & \mathbf{0} \\ \mathbf{0} & \mathbf{T}_s\boldsymbol{\Phi} \\ \mathbf{T}_s\boldsymbol{\Phi}(-\hat{\mathbf{M}}^{-1}\hat{\mathbf{K}}) & \mathbf{T}_s\boldsymbol{\Phi}(-\hat{\mathbf{M}}^{-1}\hat{\mathbf{C}}) \end{bmatrix} \tilde{\mathbf{T}}_1 \begin{Bmatrix} \boldsymbol{q}_s(k) \\ \dot{\boldsymbol{q}}_s(k) \end{Bmatrix} + \begin{bmatrix} \mathbf{0} \\ \mathbf{0} \\ \mathbf{0} \\ \mathbf{0} \\ -\mathbf{T}_s\boldsymbol{\Phi}\hat{\mathbf{M}}^{-1} \end{bmatrix} \boldsymbol{f}(k) \tag{3.25}$$

The sensor signals are input to the control system and the control output will be fed back at the appropriate time to complete the aeroservoelastic analysis loop.

4.3.3 ARMA Model in Aeroelastic and Aeroservoelastic Analysis

The model structure used in the system identification technique is the auto regressive moving average model (ARMA) [90-95]. The technique describes the modal response force at time k of a system as a summation of scaled previous outputs and scaled values of modal displacement input to the system, as shown in equation (4.26). The ARMA model makes the assumptions that most aeroelastic systems can be treated as dynamically linear[17,97] i.e. the aerodynamics responds linearly for small perturbations about a potential nonlinear steady state mean flow.

The basic autoregressive moving average (ARMA) model of Figure 4.4, at time k, may be written as

$$\boldsymbol{f}_a(k) = \sum_{i=1}^{na}[A_i]\boldsymbol{f}_a(k-i) + \sum_{m=0}^{nb-1}[\boldsymbol{B}_m]\boldsymbol{q}(k-m) \tag{4.26}$$

in which the $A_i's$ and $\boldsymbol{B}_m's$ are unknowns to be determined from excitation of the structure through a prescribed motion containing the spectrum of calculated structural eigenmodes. In addition, na and nb are the orders of the coefficients $A_i's$ and $\boldsymbol{B}_m's$ that are used to approximate the generalized aerodynamic forces. It may be noted that the generalized forces can be scaled by the training density, $\hat{\rho}$, and that further scaling the generalized forces on the right hand side results in the scaled $\hat{\boldsymbol{f}}_a$ aerodynamic force vector,

$$\hat{\boldsymbol{f}}_a(k)=\frac{\boldsymbol{f}_a(k)}{\hat{\rho}}=\sum_{i=1}^{na}[A_i]\hat{\boldsymbol{f}}_a(k-i)+\frac{1}{\hat{\rho}}\sum_{m=0}^{nb-1}[\boldsymbol{B}_m]\boldsymbol{q}(k-m) \tag{4.27}$$

q(k)
ARMA Model
f_a(k)

Figure 4.4. Aerodynamic model.

Next, a state vector, $\boldsymbol{x}_a$, is defined for the scaled aerodynamic system which contains a total of *(na+nb-1)nr* states, as

$$\boldsymbol{x}_a(k)=\begin{bmatrix}\hat{\boldsymbol{f}}_a(k-1)\\ \vdots\\ \hat{\boldsymbol{f}}_a(k-na)\\ \boldsymbol{q}(k)\\ \vdots\\ \boldsymbol{q}(k-nb+1)\end{bmatrix} \tag{4.28}$$

The state space form for the scaled aerodynamic model can now be written as

$$\boldsymbol{x}_a(k+1)=\mathbf{G}_a\boldsymbol{x}_a(k)+\mathbf{H}_a\boldsymbol{q}(k) \tag{4.29}$$

$$\hat{\boldsymbol{f}}_a(k)=\mathbf{C}_a\boldsymbol{x}_a(k)+\mathbf{D}_a\boldsymbol{q}(k)+\hat{\boldsymbol{f}}_o \tag{4.30}$$

in which

$$
\mathbf{G}_a = \begin{bmatrix}
A_1 & A_2 & \cdots & A_{na-1} & A_{na} & \frac{1}{\hat{\rho}}B_1 & \frac{1}{\hat{\rho}}B_2 & \cdots & \frac{1}{\hat{\rho}}B_{nb-2} & \frac{1}{\hat{\rho}}B_{nb-1} \\
I & 0 & \cdots & 0 & 0 & 0 & 0 & \cdots & 0 & 0 \\
0 & I & \cdots & 0 & 0 & 0 & 0 & \cdots & 0 & 0 \\
\vdots & \vdots & \ddots & \vdots & \vdots & \vdots & \vdots & \ddots & \vdots & \vdots \\
0 & 0 & & I & 0 & 0 & 0 & \cdots & 0 & 0 \\
0 & 0 & \cdots & 0 & 0 & 0 & 0 & \cdots & 0 & 0 \\
0 & 0 & \cdots & 0 & 0 & I & 0 & \cdots & 0 & 0 \\
0 & 0 & \cdots & 0 & 0 & 0 & I & \cdots & 0 & 0 \\
\vdots & \vdots & \ddots & \vdots & \vdots & \vdots & \vdots & \ddots & \vdots & \vdots \\
0 & 0 & \cdots & 0 & 0 & 0 & 0 & \cdots & I & 0
\end{bmatrix}
\qquad
\mathbf{H}_a = \begin{bmatrix}
\frac{1}{\hat{\rho}}B_o \\ 0 \\ 0 \\ \vdots \\ 0 \\ I \\ 0 \\ 0 \\ \vdots \\ 0
\end{bmatrix}
$$

$$
\mathbf{C}_a = \begin{bmatrix} A_1 & A_2 & \cdots & A_{na-1} & A_{na} & \frac{1}{\hat{\rho}}B_1 & \frac{1}{\hat{\rho}}B_2 & \cdots & \frac{1}{\hat{\rho}}B_{nb-2} & \frac{1}{\hat{\rho}}B_{nb-1} \end{bmatrix}
\qquad
\mathbf{D}_a = \begin{bmatrix} \frac{1}{\hat{\rho}}B_o \end{bmatrix}
\tag{4.31}
$$

It should be noted that the output equation for the scaled aerodynamic model may include a known vector of static offsets, $\hat{f}_o = f_o / \hat{\rho}$. The static offsets are subtracted from the time history data in the derivation of the aerodynamic model, since the ARMA model structure only models the dynamics of the system. The generalized force vector $f_a = \hat{f}_a \times \rho$ is then fed back into the structural state space matrix equations (4.13) and (4.14) in the next solution iteration, as shown in Figure 4.5.

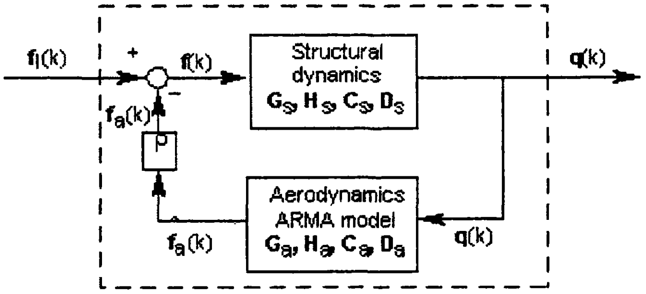

Figure 4.5. Coupled ARMA aeroelastic (AE) model.

For the coupled aeroelastic model, a combined structural and aerodynamic state space matrix formulation is derived which enables depiction of aeroelastic root locus plots. These assist in the control law design, as shown in Figure 4.6. As the density increases, the roots become unstable and flutter occurs.

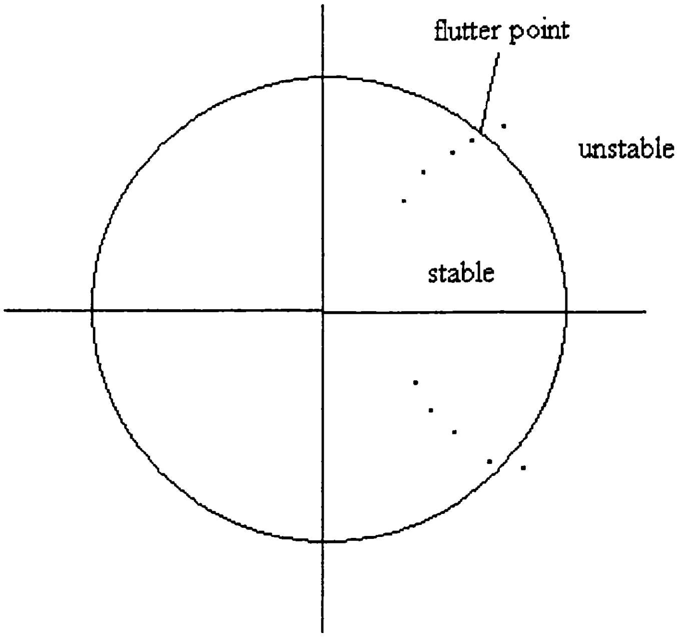

Figure 4.6 An example of the root locus plot.

Thus the input to the aerodynamic state space equation can be expressed in terms of the structural output as

$$\boldsymbol{x}_a(k+1) = \mathbf{G}_a \boldsymbol{x}_a(k) + \mathbf{H}_a \mathbf{C}_s \boldsymbol{x}_s(k) \tag{4.32}$$

$$\boldsymbol{f}_a(k) = \rho \mathbf{C}_a \boldsymbol{x}_a(k) + \rho \mathbf{D}_a \mathbf{C}_s \boldsymbol{x}_s(k) + \rho \hat{\boldsymbol{f}}_o \tag{4.33}$$

From Figure 4.4, $\boldsymbol{f}_a$ can be obtained as

$$\boldsymbol{f}(k) = \boldsymbol{f}_l(k) + \boldsymbol{f}_a(k) \tag{4.34}$$

in which $\boldsymbol{f}_l(k)$ is the user's input generalized impulse force vector. Substituting equations (4.33) and (4.34) into equations (4.13) and (4.14) gives

$$\boldsymbol{x}_s(k+1) = (\mathbf{G}_s + \mathbf{H}_s \rho \mathbf{D}_a \mathbf{C}_s)\boldsymbol{x}_s(k) + \mathbf{H}_s \rho \mathbf{C}_a \boldsymbol{x}_a + \mathbf{H}_s \boldsymbol{f}_l + \mathbf{H}_s \rho \hat{\boldsymbol{f}}_o \tag{4.35}$$

$$\boldsymbol{y}_s(k) = \begin{Bmatrix} q(k) \\ \dot{q}(k) \end{Bmatrix} = \mathbf{C}_s \boldsymbol{x}_s(k) \tag{4.36}$$

and the combined aeroelastic state space matrix may be written as

$$\begin{Bmatrix} x_s(k+1) \\ x_a(k+1) \end{Bmatrix} = \begin{bmatrix} \mathbf{G}_s + \rho\mathbf{H}_s\mathbf{D}_a\mathbf{C}_s & \rho\mathbf{H}_s\mathbf{C}_a \\ \mathbf{H}_a\mathbf{C}_s & \mathbf{G}_a \end{bmatrix} \begin{Bmatrix} x_s(k) \\ x_a(k) \end{Bmatrix} + \begin{bmatrix} \mathbf{H}_s \\ 0 \end{bmatrix} f_l(k) + \begin{bmatrix} \rho H_s \hat{f}_o \\ 0 \end{bmatrix} \tag{4.37}$$

$$\begin{bmatrix} q(k) \\ \dot{q}(k) \end{bmatrix} = \begin{bmatrix} \mathbf{C}_s & 0 \end{bmatrix} \begin{Bmatrix} x_s(k) \\ x_a(k) \end{Bmatrix} \tag{4.38}$$

or

$$x_{sa}(k+1) = \mathbf{G}_{sa} x_{sa}(k) + \mathbf{H}_{sa1} f_l(k) + \mathbf{H}_{sa2} \tag{4.39}$$

The relevant root locus plot, derived from the $\mathbf{G}_{sa}$ matrix, shows the location of the roots as a function of density, which is analogous to the plotting of q and $\dot{q}$ contained in $\mathbf{x}_s$, equation (4.12). This matrix $\mathbf{G}_{sa}$ can be used in a control law design process to obtain the control state space matrices.

Thus, once the control law is designed, we may obtain the aeroservoelastic response for the system with a uniform sampling rate, as shown in Figure 4.7. Starting with the assumption that $\mathbf{q}(k)$ is zero, the vector $\hat{f}_a(k)$ is calculated from equation (4.27), so that $f_a(k)$ is simply obtained as $f_a(k) = \rho_{inf} \times \hat{f}_a(k)$. Then, for each succeeding step, $f(k)$ is computed first, equation (4.15), and $\mathbf{y}_s$ is calculated using equation (4.14) and saved in the file xn.dat. Using the calculated structural output $\mathbf{y}_s$, the control surface motion, δ_c^i, is computed from equation (4.17) for the *NC* control surfaces. The control surface deflections vector $\mathbf{y}_c$ is then summed with the feedback structural $\mathbf{y}_s$ signal to obtain the $\mathbf{q}(k)$, equation (4.20), and the analysis continues with the next time step.

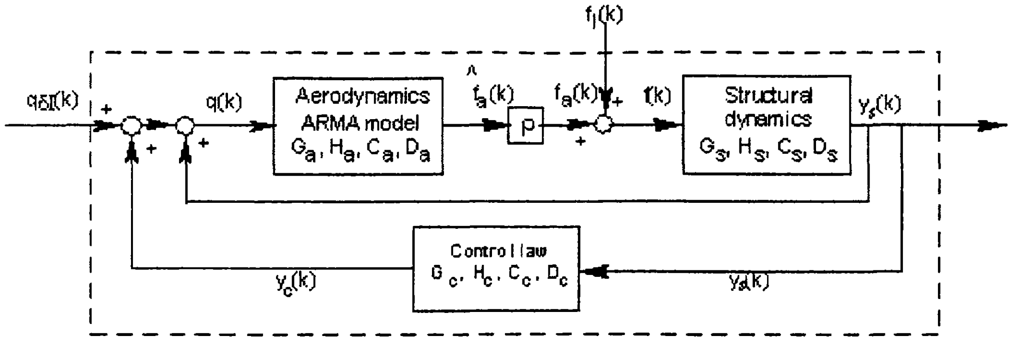

Figure 4.7. Coupled ARMA aeroservoelastic (ASE) model.

A closed form of the coupled aeroservoelastic model consisting of the structural, aerodynamic and control state space matrix formulations can also be derived. This enables depiction of aeroservoelastic root locus plots, which assist in the control law design[96]. The control module will have the state space equation

$$\boldsymbol{x}_c(k+1) = \mathbf{G}_c \boldsymbol{x}_c(k) + \mathbf{H}_c \boldsymbol{u}_c \tag{4.40}$$

$$\boldsymbol{y}_c(k) = \mathbf{C}_c \boldsymbol{x}_c(k) + \mathbf{D}_c \boldsymbol{u}_c \tag{4.41}$$

with

$$\boldsymbol{u}_c = \widetilde{\boldsymbol{K}} \boldsymbol{y}_s(k) = \widetilde{\boldsymbol{K}} \mathbf{C}_s \boldsymbol{x}_s(k) \tag{4.42}$$

$$\boldsymbol{x}_c(k+1) = \mathbf{G}_c \boldsymbol{x}_c(k) + \mathbf{H}_c \widetilde{\boldsymbol{K}} \mathbf{C}_s \boldsymbol{x}_s(k) \tag{4.43}$$

$$\boldsymbol{y}_c(k) = \mathbf{C}_c \boldsymbol{x}_c(k) + \mathbf{D}_c \widetilde{\boldsymbol{K}} \mathbf{C}_s \boldsymbol{x}_s(k) \tag{4.44}$$

Figure 4.7 shows that the feedback $\boldsymbol{q}(k)$ signal is the summation of components as

$$\boldsymbol{q}(k) = \boldsymbol{q}_{\delta I}(k) + \boldsymbol{y}_c(k) + \boldsymbol{y}_s(k) \tag{4.45}$$

in which $q_{\delta I}(k)$ is the pilot/external input. Substituting equations (4.14), (4.44) and (4.45) into equations (4.29) and (4.30), it can be seen that the aerodynamic equation can be written as

$$\mathbf{x}_a(k+1) = \mathbf{G}_a\mathbf{x}_a(k) + \mathbf{H}_a q_{\delta I}(k) + \mathbf{H}_a C_c x_c(k) + \mathbf{H}_a\mathbf{D}_c\tilde{K}\mathbf{C}_s x_s(k) + \mathbf{H}_a\mathbf{C}_s x_s(k) \quad (4.46)$$

$$f_a(k) = \rho\mathbf{C}_a x_a(k) + \rho\mathbf{D}_a(\mathbf{C}_s + \mathbf{D}_c\tilde{K}\mathbf{C}_s)x_s(k) + \rho D_a\mathbf{C}_c x_c(k) + \rho\mathbf{D}_a q_{\delta I}(k) + \rho\hat{f}_o \quad (4.47)$$

Figure 4.6 shows that the signal $f(k)$ can be obtained from

$$f(k) = f_I(k) + f_a(k) \quad (4.48)$$

Substituting equation (4.47) and equation (4.48) into equation (4.13) and (4.14) will give the structural state space matrices with the form

$$x_s(k+1) = \mathbf{H}_s\rho\mathbf{C}_a x_a + (\mathbf{G}_s + \mathbf{H}_s\rho\mathbf{D}_a(\mathbf{C}_s + \mathbf{D}_c\tilde{K}\mathbf{C}_s))x_s(k) + \mathbf{H}_s\rho\mathbf{D}_a\mathbf{C}_c x_c(k)$$

$$+ \mathbf{H}_s\rho\mathbf{D}_a q_{\delta I}(k) + \mathbf{H}_s\rho\hat{f}_o + \mathbf{H}_s f_I \quad (4.49)$$

$$y_s(k) = \mathbf{C}_s x_s(k) \quad (4.50)$$

The state space matrix equation of the acroservoelastic analysis with a uniform sampling rate may be written as

$$\begin{Bmatrix} x_s(k+1) \\ x_a(k+1) \\ x_c(k+1) \end{Bmatrix} = \begin{bmatrix} \mathbf{G}_s + \mathbf{H}_s\rho\mathbf{D}_a(\mathbf{C}_s + \mathbf{D}_c\tilde{\mathbf{K}}\mathbf{C}_s) & \mathbf{H}_s\rho\mathbf{C}_a & \mathbf{H}_s\rho\mathbf{D}_a\mathbf{C}_c \\ \mathbf{H}_a(\mathbf{C}_s + \mathbf{D}_c\tilde{\mathbf{K}}\mathbf{C}_s) & \mathbf{G}_a & \mathbf{H}_a\mathbf{C}_c \\ \mathbf{H}_c\tilde{\mathbf{K}}\mathbf{C}_s & 0 & \mathbf{G}_c \end{bmatrix} \begin{Bmatrix} x_s(k) \\ x_a(k) \\ x_c(k) \end{Bmatrix}$$

$$+ \begin{bmatrix} \mathbf{H}_s \\ 0 \\ 0 \end{bmatrix} f_I(k) + \begin{bmatrix} \mathbf{H}_s\rho\mathbf{D}_a \\ \mathbf{H}_a \\ 0 \end{bmatrix} q_{\delta I}(k) + \begin{bmatrix} \mathbf{H}_s\rho\hat{f}_o \\ 0 \\ 0 \end{bmatrix} \quad (4.51)$$

$$\begin{bmatrix} q(k) \\ \dot{q}(k) \end{bmatrix} = [\mathbf{C}_s \quad 0 \quad 0] \begin{Bmatrix} x_s \\ x_a \\ x_c \end{Bmatrix} \quad (4.52)$$

or

$$\begin{aligned}\mathbf{x}_{sac}(k+1) &= \mathbf{G}_{sac}\mathbf{x}_{sac}(k) + \mathbf{H}_{sac1} f_l(k) + \mathbf{H}_{sac2} q_{\delta l}(k) + \mathbf{H}_{sac3} \\ \mathbf{y}_{sac}(k) &= \mathbf{C}_{sac}\mathbf{x}_{sac}(k)\end{aligned} \tag{4.53}$$

The relevant root locus plot, derived from the $\mathbf{G}_{sac}$ matrix, shows the location of roots as a function of density, which is analog to the plotting of q and $\dot{q}$ contained in y_s, equation (4.12). For a uniform sampling rate closed loop control feedback system, the response can be computed using equations (4.51) and (4.52).

4.3.3.1 Model Identification

As discussed in the previous section, the aerodynamic model is based on the ARMA [90-95,97] structure of equation (4.23). This model structure describes the dynamic response of any multi input multi output (MIMO) system as a linear combination of scaled outputs and scaled inputs for the system. The discrete time model procedure utilizes this model structure to develop a simple algebraic model, which is equivalent to the unsteady CFD solution for a given Mach number and structural geometry. The procedure for determining the unknown coefficient matrices in the ARMA model, A_i and B_i, involves three steps:

1. Prescribe a known displacement time history, or input signal, through the unsteady CFD solution and record the aerodynamic response, or output signal.
2. Select a model size, na and nb in equation (4.24) and identify the ARMA coefficients which match the input output data recorded in step 1.
3. Implement the computed aerodynamic model, equations (4.29) and (4.30) from step 2 for the input signal used in step 1, and compare the model output to the actual system output.

The system identification procedure described above is an iterative procedure. If the comparison in step 3 shows that the model does not match the actual CFD solution, step 2 is repeated for a different choice of na and nb. The coefficient identification mentioned in step 2 is accomplished by minimizing the error between the model output and the unsteady CFD output, using a least squares fit. Since this will result in an over determined system of equations, STARS uses an implementation of singular value decomposition (SVD) to extract the ARMA coefficient matrices from a matrix of system equations assembled from the training data.

The success of this identification procedure is highly dependent on the amount and quality of training data available in step 2. Hence an "optimum" input signal should be used in step 1, which will excite a broad response spectrum in the unsteady CFD solution. Once an accurate model is identified, it can then be used in place of the CFD solution in the coupled aeroelastic or aero simulation, Figure 4.5.

4.3.3.2 Input Optimization

The input of the ARMA[97] model for the unsteady CFD solver is the generalized displacement of the structure in the flow field. However, the Euler CFD solver in the STARS program also requires the velocity of the structure to satisfy its boundary condition requirements. Therefore, any prescribed input signal for structural displacement must be uniquely differentiable in order to obtain the physical velocity of the structure for input to the CFD solver. Alternatively, a velocity may be specified, which can then be integrated to obtain the consistent structural displacement. In either case, the input must be selected which excites a wide range of dynamic frequencies in the flow field in order identify a practically useful model.

In the STARS program, a 753211 variable amplitude multistep input, see Figure 4.8, is implemented on the velocity boundary condition for the training process of the system. The 753211 variable multistep input is widely used by the flight test community because of its ease of implementation and excellent frequency content. A velocity signal 753211, with the magnitude as shown in Figure 4.8, is input in sequence for each of the $\dot{q}$ modes. The aerodynamics output computed for the particular modal displacement and velocity is collected for future model training. Once the 753211 signal input to the $\dot{q}_1$ mode is about to finish, a 2nd 753211 signal input to the $\dot{q}_2$ mode will start and this will continue for *nr* modes. The purpose of inputting the signal one mode at a time is to study its influence on the coupling behavior of the structure's generalized aerodynamic forces. As mentioned previously, the prescribed velocity function is then integrated numerically to compute the displacement boundary condition, which also becomes the training input for the ARMA model.

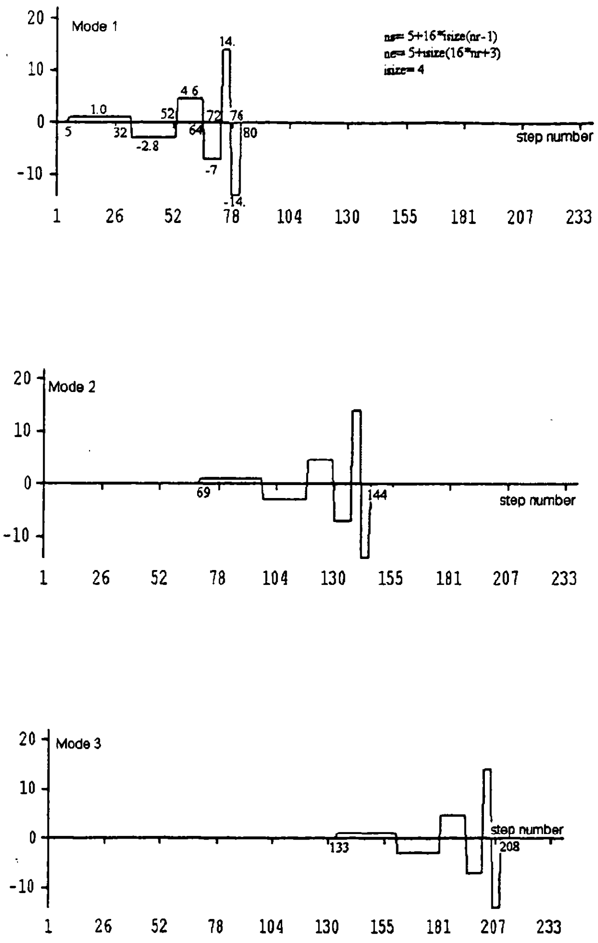

Figure 4.8. 573211 variable amplitude multistep velocity input signal for several modes.

Most aeroelastic problems are formulated with multiple structural modes and, hence, will require a separate multistep input signal for each mode. Intuitively, it is obvious that all modes may not be run simultaneously or the ARMA model will fail to discriminate between the effects of the different mode shapes. Furthermore, it will take a large amount of computational effort if the input signal for each mode is run independently. In order to save time, and still guarantee a unique solution, the multistep input signal for each mode is applied in a staggered fashion, such that they slightly overlap but are still out of phase, as shown in Figure 4.8.

4.4 Concluding Remarks

In this section a description of the CFD solution technique has been given. This has been followed by a detailed formulation for CFD based aeroelastic and aeroservoelastic analysis. A closed form expression of the aeroelastic and aeroservoelastic analyses were incorporated into STARS for the uniform sampling rate case along with the sensor mechanism. The ARMA procedure has also been explained along with the implementation of control laws.

CHAPTER 5

NUMERICAL EXAMPLE (STARS-CFDASE)

5.1 Introduction

A large number of CFD-based aeroelastic analyses has been performed in support of NASA projects such as Pegasus®, the SR-71 airplane, SR-71/Hypersonic Launch Vehicle, High Speed Civil Transport (HSCT), National Aerospace Plane (NASP), and Generic Hypersonic Vehicle (GHV) projects, among others. Some analysis results have been correlated with those obtained from flight testing. In the area of aeroelasticity, the associated solution module has been checked out by comparing results with those obtained from tests as well as other analysis methods. The aeroelastic analysis for the X43 Hyper-X was performed. The results are shown in the following section. This is a typical example problem of a detailed, CFD-based, aeroelastic and aeroservoelastic analysis.

Figure 5.1 shows the global analysis flow chart for nonlinear AE and ASE analyses using the usual Euler or the ARMA approach. This module is activated by typing the command 'cfdaserun'. Thus, a steady-state solution of the flow is first implemented that requires input data[98,88] for two-dimensional surface and three-dimensional volume generation involving triangular and tetrahedral elements, respectively. For surface and volume grid generation, two input files having background (job.bac) and surface (job.sur) definitions are generated; plots of these surfaces are produced by the GLPLOT program. The input data file[98], job.bco, is used to set up boundary conditions, and the file job.cons is the required input file for steady-state flow analysis. An alternative procedure for steady-state flow analysis only can also be performed in double precision by using the STEADYDP solution module Figure 5.1.

The data files needed for subsequent CFD-based aeroelastic analysis relate to structural vibration analysis. The data files solids.dat, (the term 'solids' is a generic identifier that can be set to any name).

For subsequent unsteady flow analysis, related input data[98] is represented by the file job.scalars. The unsteady parameter input data file, job.conu, contains parameters that dictate the pattern of solution convergence. In all these data sets, the term 'job' is generic and signifies the problem under consideration. Additional comment lines may be inserted at appropriate places with 'c' or 'C' in the first column.

Detailed, color graphic plots of solution results are conveniently obtained by using the POSTPLOTF submodule of the STARS program. The unsteady generalized displacements can also be plotted by employing the QUICKPLOT program (activated by typing 'qp'), and black-and-white contour plots of solution results are achieved by the XPLT [98] program, which is part of POSTPLOTF.

5.2 Cantilever Wing Nonlinear Aeroelastic Analysis

A cantilever wing with a NACA 0012 airfoil was use to demonstrate the integration of the control discipline in with the aeroelasticity analysis capability. The results for the aeroelastic analysis and aeroservoelastic analysis for the cantilever wing will be shown. . Figure 5.2 shows the form of the background mesh that was employed in the 3-D meshing of the computational solution domain surrounding the cantilever wing. Figure 5.3 shows a cantilever wing, with a NACA 0012 airfoil cross section, and the solution domain. The figure also shows the edges and surfaces, marked appropriately for the description of the CFD model.

The basic input data parameters were:

Wing span	=	2.0178 m
Wing chord length	=	1.0089 m
Mach number	=	2.0
Angle of attack	=	0°
Speed of sound at infinity	=	340.29 m/s^2

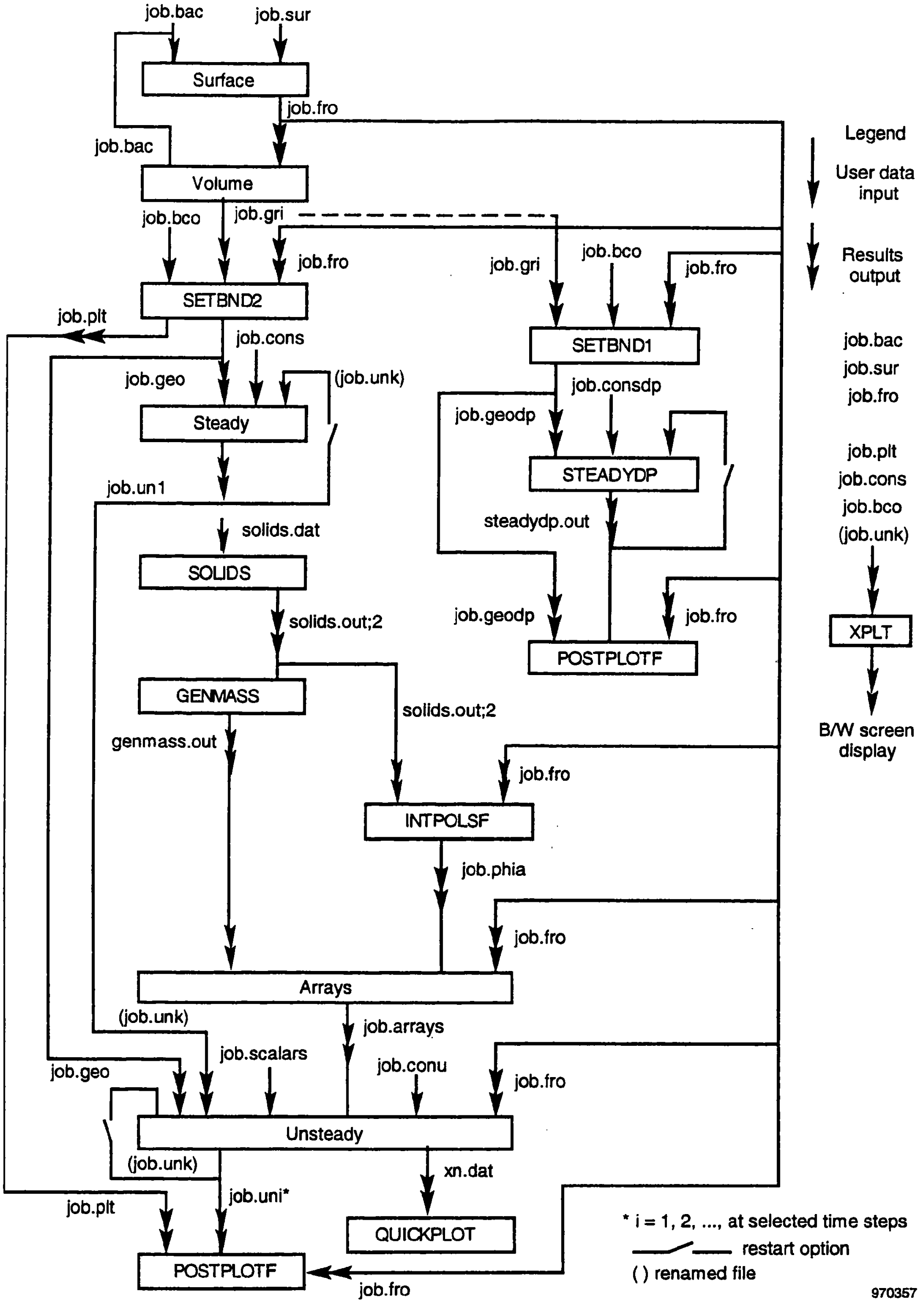

Figure 5.1. Flowchart for CFD-based aeroelastic analysis.

Structural data

Young's modulus	=	6.8947E+10
Poisson's ratio	=	0.3
Density	=	2764.925 kg/m^3

The meshes employed for the analysis were such that

Number of fluid nodes	=	65,745
Number of fluid elements	=	351,932
Number of structural nodes	=	486
Number of structural elements	=	1,549

Detailed data such as the finite element structural model, CFD model and control modul files are documented in the Appendix A, Appendix B and Appendix C.

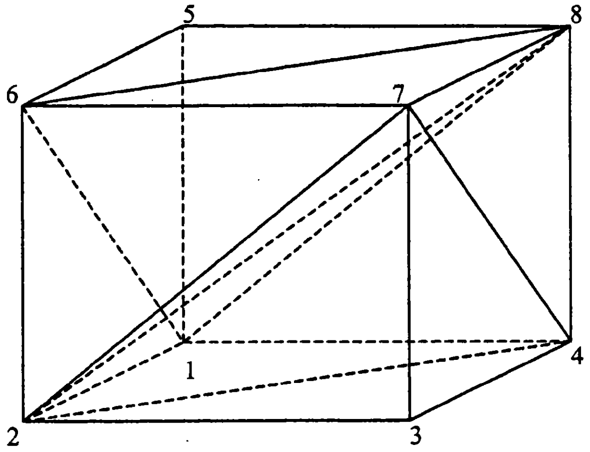

Figure 5.2. Background domain for aeroelastic analysis.

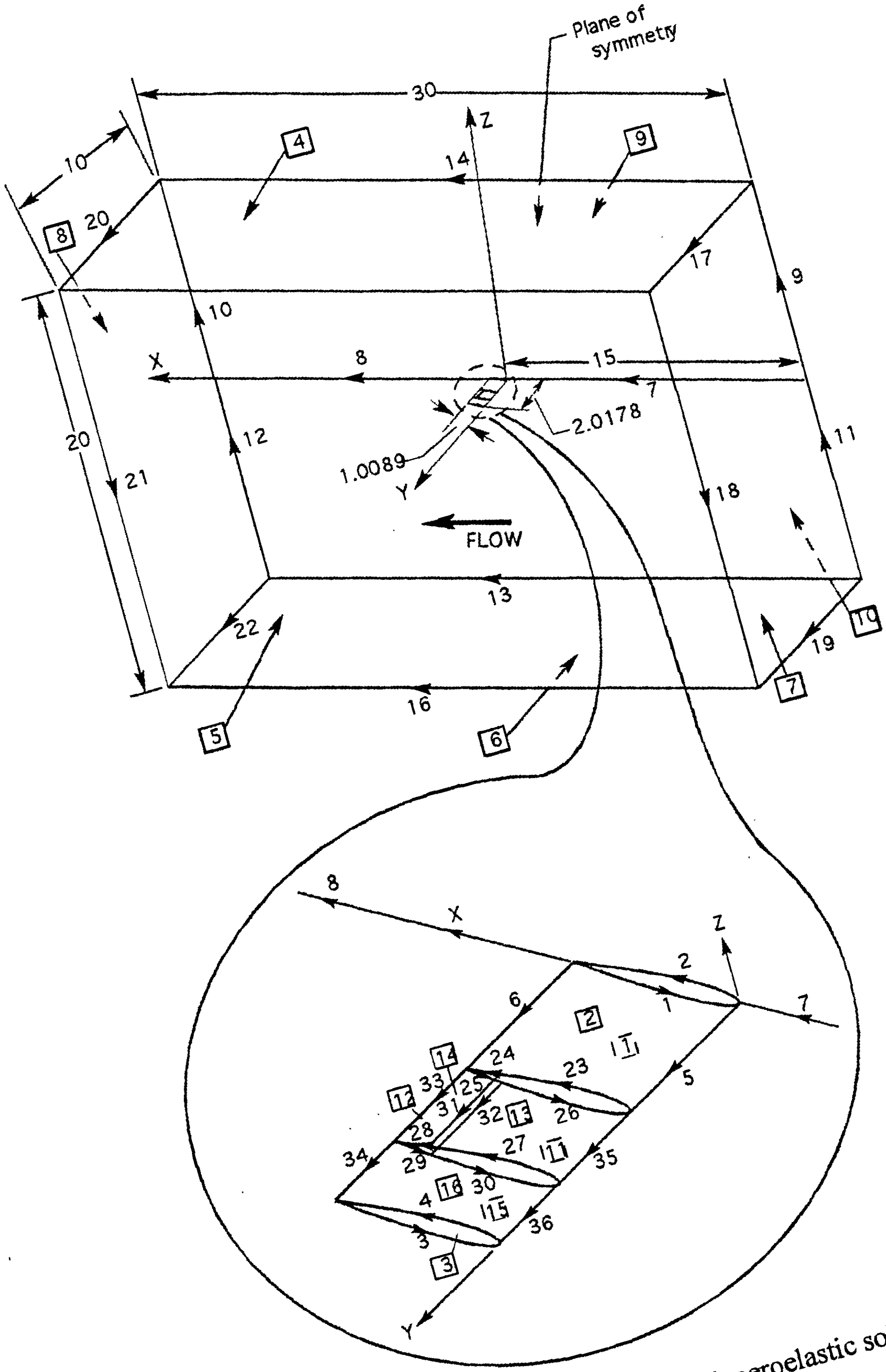

Figure 5.3. Cantilever wing with aeroelastic solution domain.

5.2.1 Analysis Results

Figure 5.4(a) shows the view of the surface grid on the wing and a detail of the grid on the symmetry plane for the aerodynamic analysis. A view of the surface grid on the wing for the structural analysis is shown in Figure 5.4(b). Figure 5.5 shows the distribution of Mach number and pressure on the wing at a converged steady–state. The first eight structural vibration modes are illustrated in Figure 5.6. The first bending, first torsion and control surface mode (mode number 7) are used for this aeroelastic and aeroservoelastic example study. For this particular example the first bending and first torsion modes will couple with each other to cause flutter. For the stability analysis, a series of aeroelastic analyses were run for a range of densities and at each density the damping values was calculated from the generalized displacements such as the one obtained in Figure 5.7(a), which was run for the density at $.97\frac{kg}{m^3}$. The generalized displacement in Figure 5.7(a) showed that at this density or altitude the wing displacement would grow and flutter. Figure 5.7(b) shows the open–loop aeroelasticity root locus plot of all the eigen roots motion computed for a range of densities. Whenever any of the roots has crossed outside the unit circle the wing has become unstable and flutters. According to Figure 5.7(b), the wing flutter occurs at a density equal to $.955\frac{kg}{m^3}$. Figure 5.8 plots the calculated generalized displacement response damping verses density at which the runs were made for a number of densities. As density increases the damping value decreases, and at the point where damping is less than zero then flutter occurs. The zero damping value is located at a density equal to $0.955\frac{kg}{m^3}$ in Figure 5.8. The augmented stable solution, with application of control surface motion applied at time = 1 second for an unstable aeroelastic solution at density = $1.3709\frac{kg}{m^3}$, is displayed in Figure 5.9.

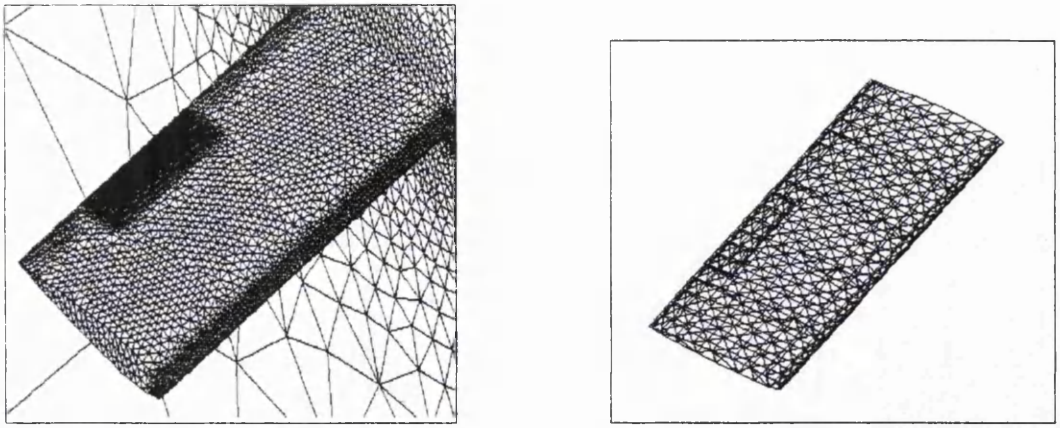

(a) mesh employed for the aerodynamics (b) mesh employed for structural mechanics

Figure 5.4. View of meshes employed for the analysis of the cantilever wing.

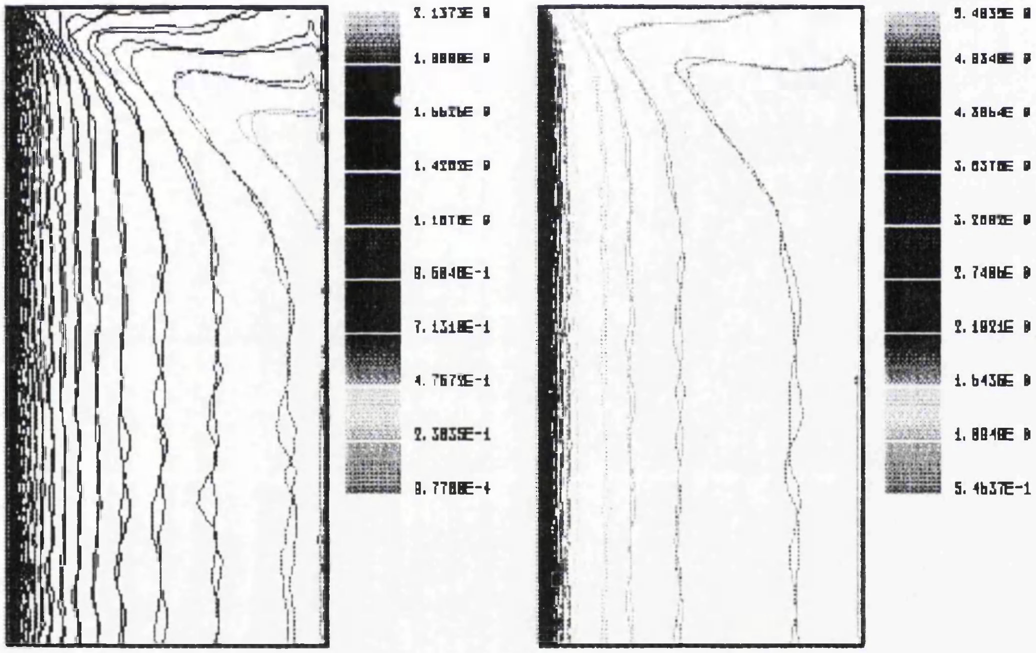

(a) Mach distribution. (b) Pressure distribution.

Figure 5.5. Cantilever wing steady–state Mach number and pressure distributions.

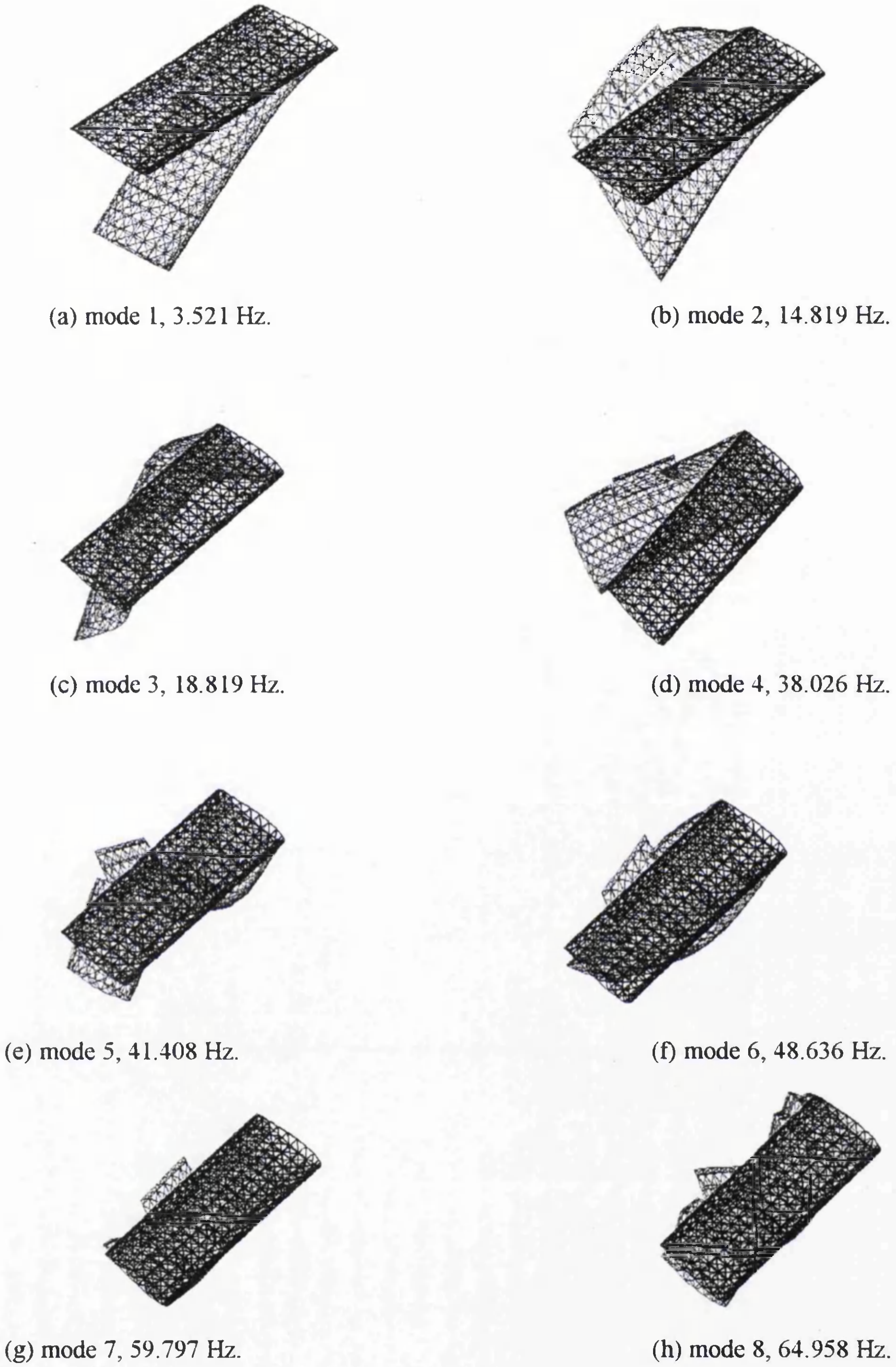

(a) mode 1, 3.521 Hz.

(b) mode 2, 14.819 Hz.

(c) mode 3, 18.819 Hz.

(d) mode 4, 38.026 Hz.

(e) mode 5, 41.408 Hz.

(f) mode 6, 48.636 Hz.

(g) mode 7, 59.797 Hz.

(h) mode 8, 64.958 Hz.

Figure 5.6. Illustration of the structural modes of the cantilever wing.

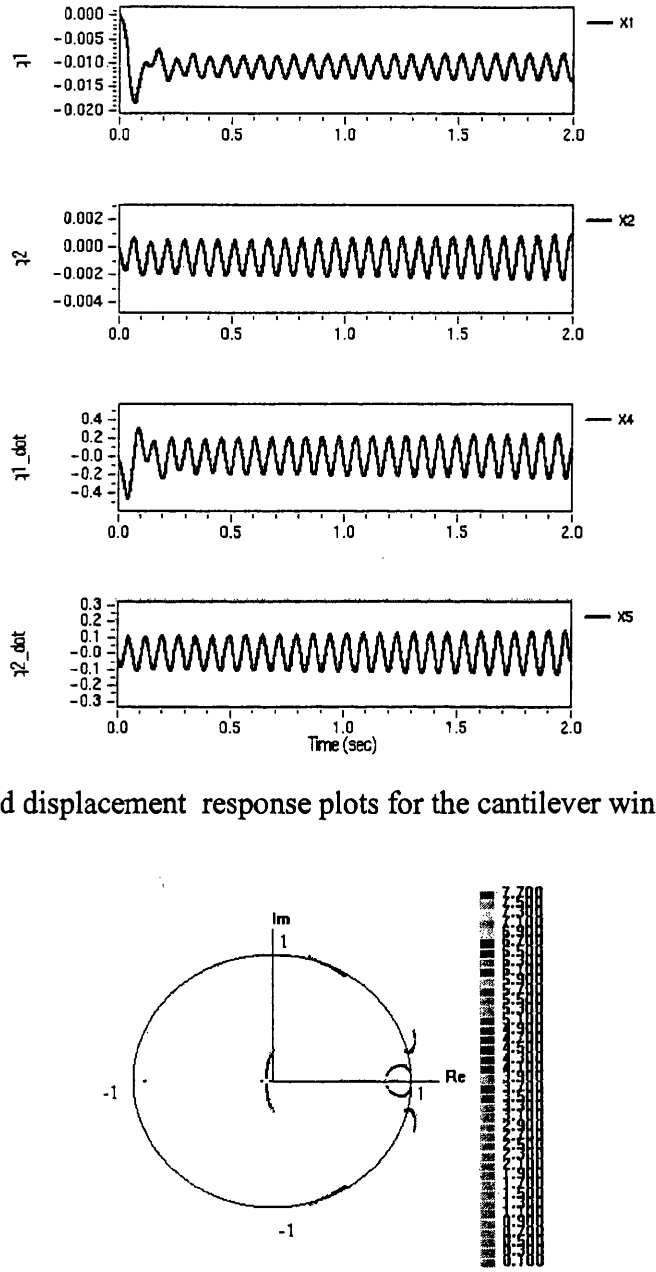

(a) Generalized displacement response plots for the cantilever wing at density = 0.97 kg/m^3.

(b) Open–loop root locus plots of the cantilever wing, flutter at density = 0.955kg/m^3.

Figure 5.7 Stability response analysis of the cantilever wing.

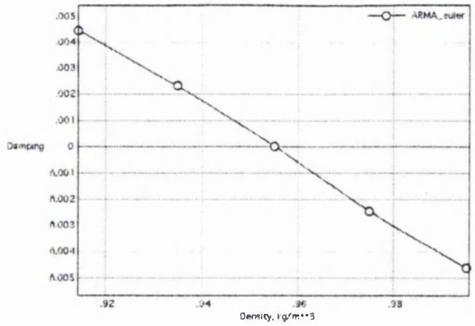

Figure 5.8. Aeroelastic stability plot for cantilever wing.

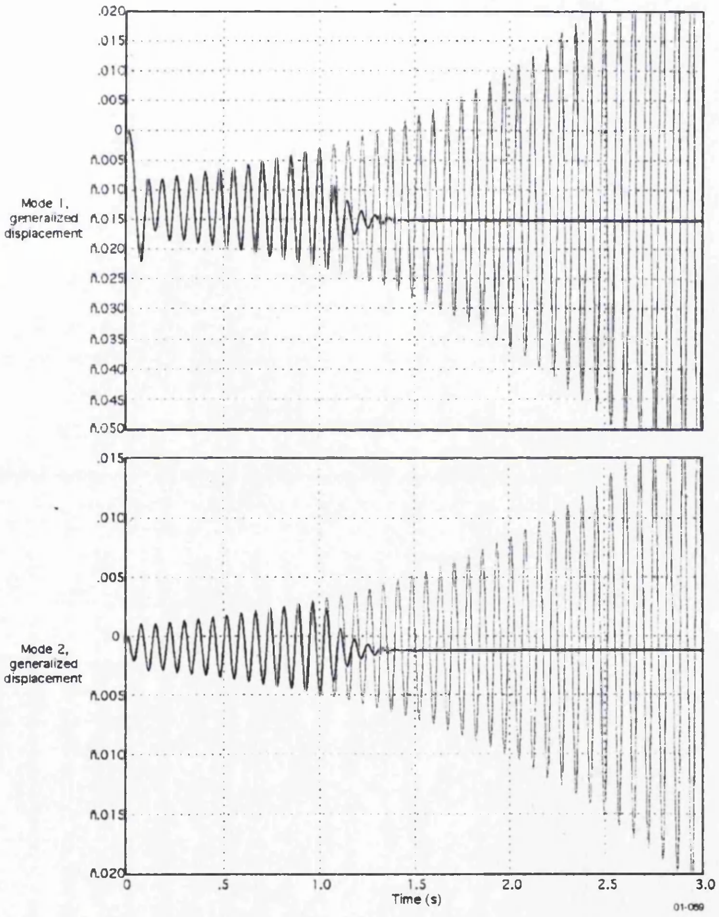

Figure 5.9 Generalized displacement of the cantilever wing, with and without control application, at time 1 sec, for density =1.3709 kg/m^3.

5.3 HyperX X-43 Nonlinear Aeroelastic Analysis

Hyper-X is an experimental flight research vehicle that is used to demonstrate airframe–integrated, scramjet powered engine (supersonic–combustion ramjet) technologies that are capable of hypersonic speed (faster than Mach 5) and reusable space launchers. Scramjets are ramjet engines in which the airflow through the engine remains supersonic. This experimental research vehicle should be capable of expanding the speed boundaries of air breathing propulsion. Figure 5.10 provides a view of the geometry of the NASA HyperX vehicle and gives details of the flight trajectory. The Hyper-X[99,100] launch vehicle stack is carried under the wing of NASA's B-52 up to the altitude of 19,000 ft over the Pacific Ocean. The X-43A (free-flyer) vehicle, the adapter and the booster rocket Pegasus is called the Hyper-X launch vehicle stack. Once separated from the B-52, the research vehicle will be powered by the Pegasus solid rocket booster to the scramjet engine test points condition and separation will occur at approximately 95,000 ft altitude. At the designated altitude, the X-43A vehicle will separate from the booster launch vehicle to a safe distance where the Hyper-X launch vehicle's scramjet propulsion engine test will be conducted at Mach 7.0. In this study the aeroelastic analysis is carried out for the free-flyer at Mach 7.0 case.

Figure 5.11 presents a view of the finite element mesh used for the structural vibration analysis model. The structural vibration frequencies computed by STARS are compared in Table 5.1 with the values computed by NASTRAN and with the results of ground vibration tests performed on the Hyper-X vehicle. Figure 5.12 illustrates the surface mesh employed for the aerodynamics simulation model used in the aeroelastic stability analysis. A view of the computational domain employed for the aerodynamics simulation of the HyperX/X–43[101,102] is given in Figure 5.13. Figure 5.14 shows the top and bottom views of the steady state Mach distribution of the Hyper-X free flyer at free stream Mach 7.0. The flutter results, obtained using STARS ARMA–CFD analysis modules, for a free stream Mach number of 7.0 is shown in Figure 5.15. In Figure 5.15, the flutter points were collected for ARMA-pertubation Piston, perturbation Piston and ARMA-Euler aeroelastic solution analysis. The perturbation Piston and ARMA-perturbation Piston show flutter is occuring at approximately at 28,500 ft altitude, and the

ARMA-Euler solution shows that the flutter point is at 34,000 ft altitude. Figure 5.16 depicts the predicted conservative flutter point of the ARMA-Euler solution for the free flyer at Mach 7.0, which means that at Mach 7.0 the flyer is stable at any altitude above 34,000 ft. A summary of the CPU requirements for different aeroelastic analysis schemes is given in Table 5.2.

For the solid mechanics,

NN = number of structural nodes = 11686 (70,116 dof)
NEL = number of structural elements = 11,245
Element types : line, shell, solids
Material types : Isotropic, orthotropic
NR = number of roots = 30
CPU = 3 min (IBM 6000-370 / PC 1G HZ)

For the finite element ARMA –CFD model:

Mach = 7.0
NN = number of nodes = 229,149
NEL = number of elements = 1,243,804

5.4 Concluding Remarks

In this chapter a number of numerical examples are presented that pertain to practical problems of current interest. In particular it has been demonstrated that suitable control law design will effect suppression of flutter for the cantilever wing example with uniform sampling rate. The sensor and multisampling rate formulations are being run for a current project, however I do not have permission to release the data at this point. Also, it has been emphasized that PC's may be used to solve real world problems such as the X-43, using an ARMA technique.

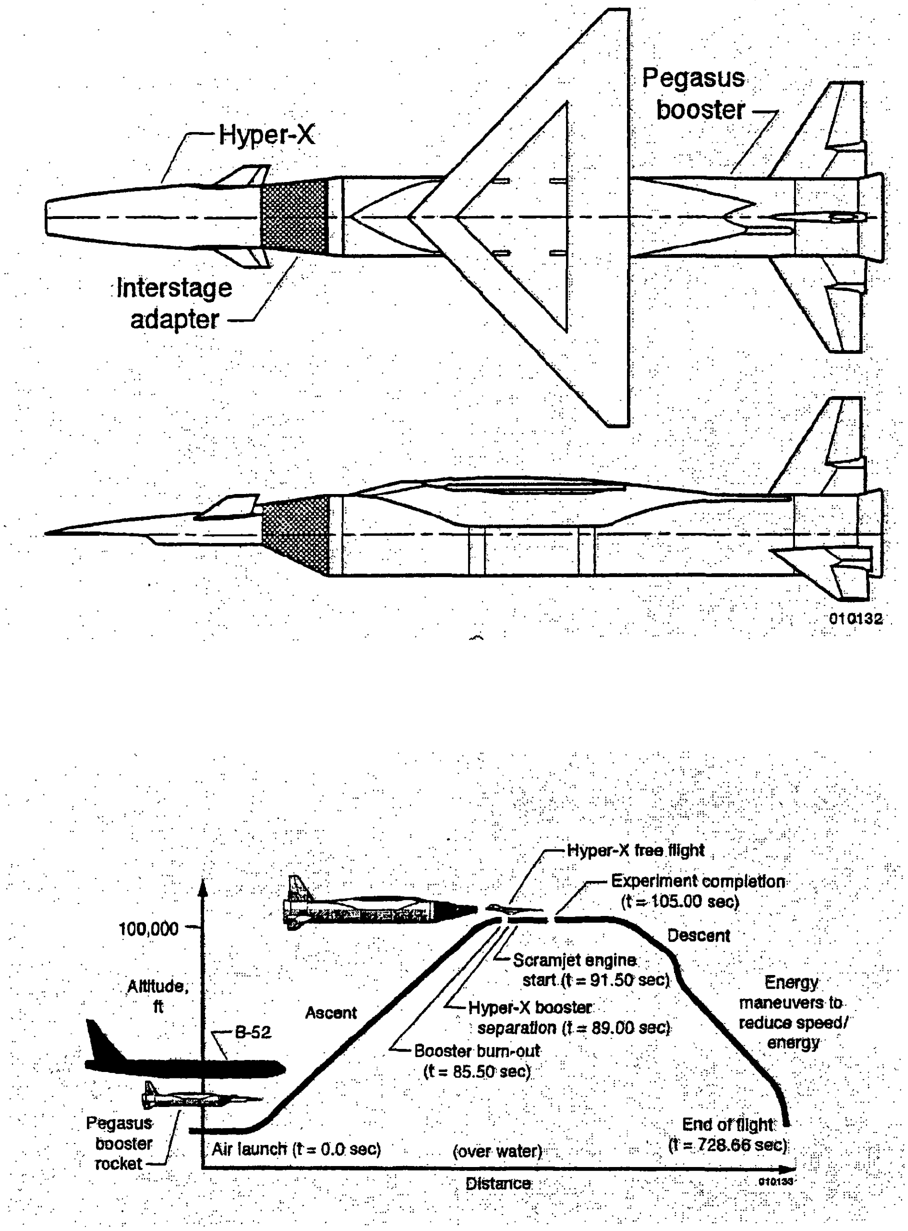
Hyper-X
Pegasus booster
Interstage adapter
010132
Hyper-X free flight
Experiment completion (t = 105.00 sec)
100,000
Altitude, ft
Descent
Scramjet engine start (t = 91.50 sec)
Energy maneuvers to reduce speed/ energy
Ascent
Hyper-X booster separation (t = 89.00 sec)
B-52
Booster burn-out (t = 85.50 sec)
Pegasus booster rocket
End of flight (t = 728.66 sec)
Air launch (t = 0.0 sec)
(over water)
Distance
010133

Figure 5.10 Hyper-X research vehicle, showing the geometry and the proposed trajectory.

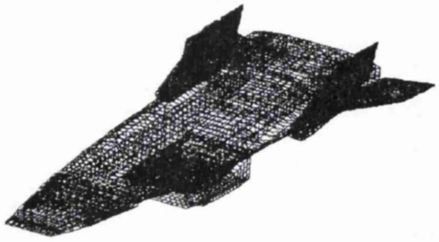

Figure 5.11. Structural representation of the HyperX Free–Flyer

Table 5.1 STARS modal analysis of the X-43 Free-Flyer.

Mode	STARS	GVT	NASTRAN	Mode Shape
#	Frequency (Hz)	Frequency (Hz)	Frequency (Hz)	
1-6	0.0	0.0	0.0	Rigid Body
8	39.81	40.03	37.54	HT pitch – S
9	40.98	41.90	38.54	HT pitch – A
10	45.65	46.62	44.14	Fuselage 1st bend – S, HT pitch
11	82.76		76.87	HT yaw – A
12	88.82		79.22	HT yaw – S
13	89.15	77.29	82.45	Fuselage 1st torsion – A, HT bend
14	98.02	95.64	92.54	Fuselage 2nd bend – S, some HT bend/pitch
15	110.51	107.91	105.07	Fuselage 1st bend – A, rudder pitch
16	117.40		108.94	Rudder pitch – S, some outward bend
17	120.71		113.24	Rudder pitch – A, some fuse 1st bend – A
18	141.34		148.63	Fuselage 2nd torsion – A, rudder pitch, HT
19	146.87		119.36	HT bend – S, some F2B, some panel motion
20	148.44		146.82	Upper mid panel – S
21	153.16		151.30	Upper & lower forward/mid panel – S
22	160.67		159.13	Upper rear inbd panel - S

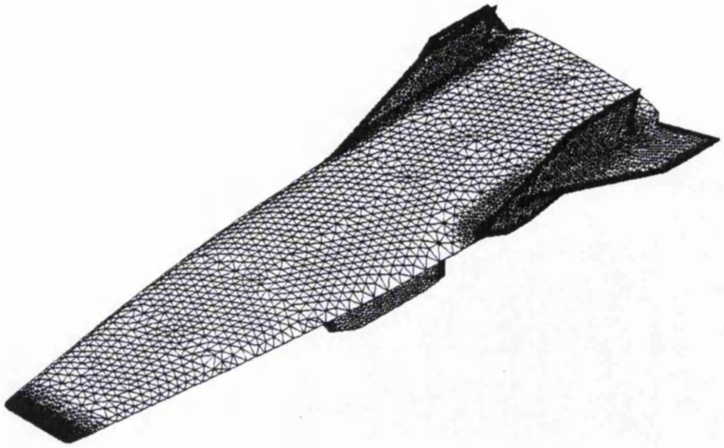

Figure 5.12 Surface mesh for the aerodynamic analysis of the HyperX Free-Flyer

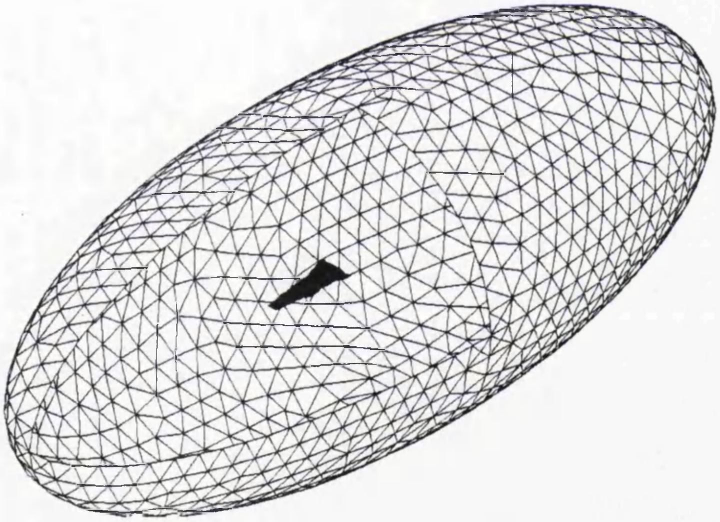

Figure 5.13 Computational domain for the analysis of the HyperX Free-Flyer

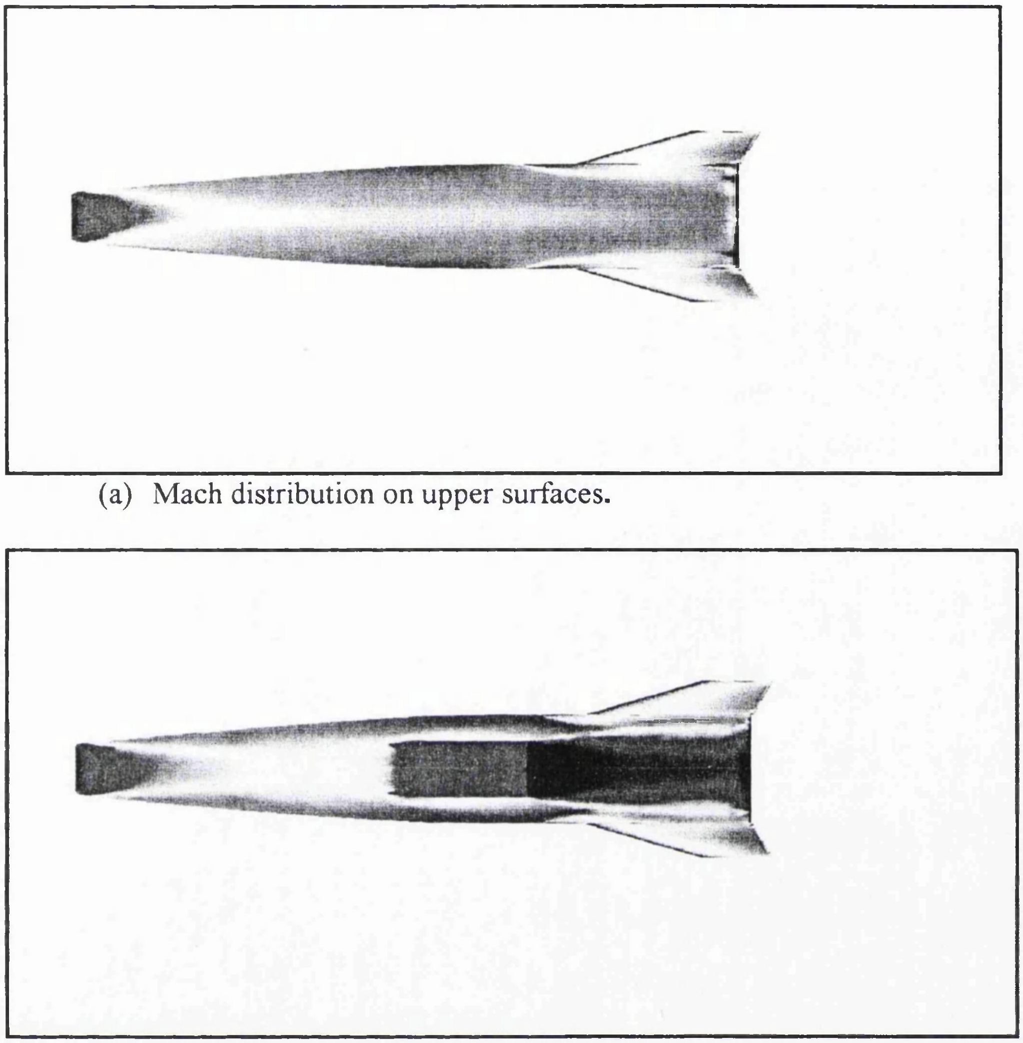

(a) Mach distribution on upper surfaces.

(b) Mach distribution on lower surfaces

Figure 5.14. X-43 CFD steady-state solution results for Mach 7.0.

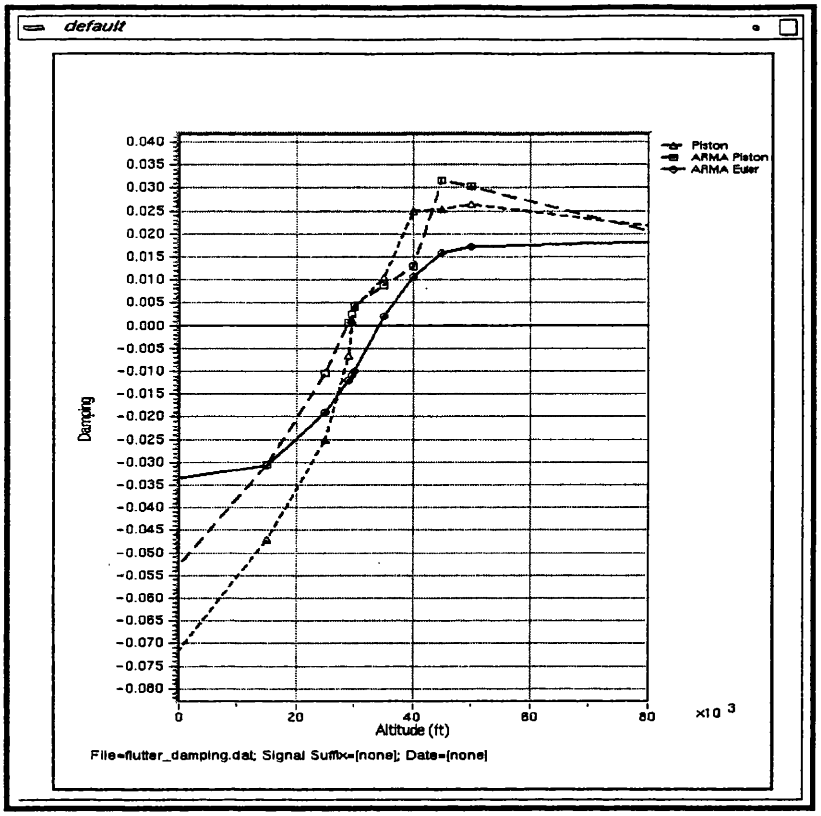

File=flutter_damping.dat; Signal Suffix=[none]; Date=[none]

Figure 5.15 ARMA-CFD aeroelastic flutter prediction for the HyperX/X-43 vehicle at Mach 7.0.

Table 5.2 ARMA Solution CPU time (PC 600M HZ) for the HyperX analysis at Mach7.0

	Step 1	Step 1A	Step 2	Step 3	Step 4	Step 5	Total time
ARMA-Euler	128 hr.	89 hr.	40 hr.	10 sec.	10 sec.	2 min	260 hr.
ARMA-Piston Perturbation	128 hr.	1 min	40 sec.	10 sec.	10 sec.	2 min	128 hr.
Piston Perturbation	128 hr.	--	--	--	--	15 min.	128hr.

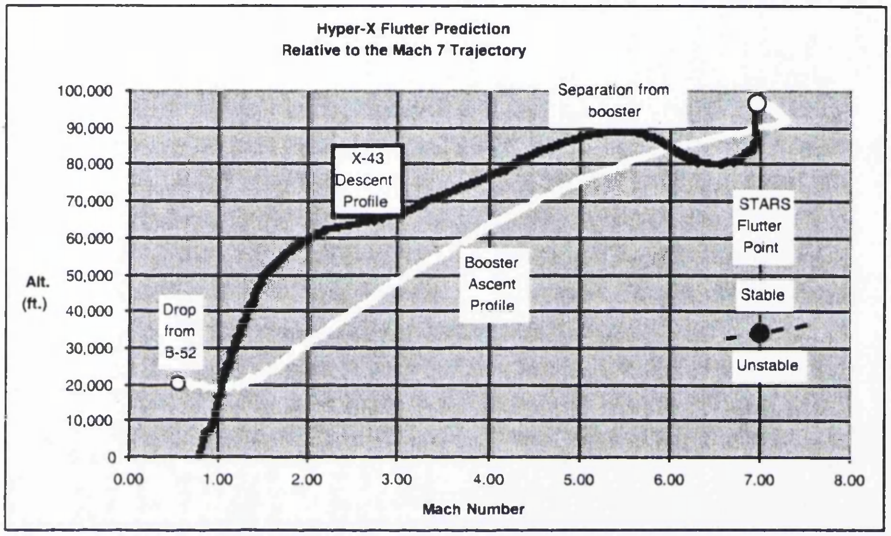

Figure 5.16 Predicted flutter point and Mach 7.0 flight trajectory of the X-43.

CHAPTER 6

CONCLUSION

6.1 Summary

The integration of the control disciplines into the multidisciplinary aeroelastic computer program STARS in a generalized form has been described in this thesis work. The adoption of the finite element procedure for both the structural and fluid discretization ensures accurate modeling of the interaction between the two disciplines of solid and fluid mechanics. In addition, use of CFD modeling of the fluid ensures accurate flow simulation around complex geometries.

A study of alternative methods of computing the aerodynamic components has been demonstrated by the implementation of both Euler methods and the Piston Perturbation technique within the CFD code. A more efficient use of CPU time was ensured, by employing the method of system identification to approximate the aerodynamics, within a state–space matrix formulation called ARMA. With the ARMA formulation, the aerodynamic forces can be computed at a faster rate than can be achieved by employing traditional CFD methods. The ARMA model has proven its inherent efficiency in the overall ASE analysis including the control design integration task. With ARMA, the aerodynamic characteristics of the structure are expressed in terms of state–space matrices and the control engineer can utilize these aeroelastic matrices to design an appropriate control law for the structure, to prevent undesirable flutter. General flutter stability characteristics can be determined within a shorter time period for aeroservoelastic analysis, compared to the time required when an Euler based CFD approach is adopted. A closed loop state–space expression for the full nonlinear aeroservoelastic control has been formulated for STARS.

The integration of the control laws into the aeroelastic system has been verified by utilizing the MATLAB μ control toolbox to simulate the aeroservoelastic running scheme. The signal result output was found to be the same for both the STARS and the MATLAB simulations. This validates the aeroservoelasticity numerical integration methodology that is employed.

The example of a cantilever wing with a control surface, that has been included in this thesis, demonstrates both the aeroelastic and aeroservoelastic analysis capability of STARS. The results obtained demonstrated that the ARMA Piston perturbation is as accurate as the pure Euler and Piston perturbation methods. It was shown how the integrated control law helped to stablise the wing at a density at which it would normally be expected to flutter. In related work, which is not included here, a model of the BACT wing from NASA Langley has been analysed using the aeroelastic and aeroservoelastic capabilities of STARS that have been developed in this thesis. The results obtained have been compared to those produced by Stephens [96]. When the control loop is not closed, STARS will give the aeroelastic results and when it is closed then the full aeroservoelastic analysis can be carried out.

The application of the procedures that have been developed to the aeroelastic analysis of flight vehicles HyperX/X-43 has also been included. Again, the calculations demonstrated that results obtained using the ARMA Piston perturbation are as accurate as those produced when pure Euler and Piston perturbation methods are employed. The flutter point for the HyperX/X-43 at a Mach number of 7 was determined. Boeing has produced results of a flutter analysis for this vehicle using the panel method. However, their solution was not a match point type of solution, so that their results cannot correctly be compared with the match point solutions of STARS. Both solutions do, however, indicate that the vehicle is over designed and very stable. From experience the flutter point obtained from the panel method, or linear aeroelasticity analysis, has a safety margin of about 20 percent. The flutter point obtained from nonlinear aeroelasticity has a much smaller safety margin. For a supersonic flow, panel approximations do not have the capability of the CFD approach to compute the shock wave that is present in the real physical flow solution. This is the primary motivation for research in the field of nonlinear aeroservoelasticity. Much recent emphasis has been placed on modeling of multiphysics[103,104] phenomenon that includes a variety of topics such as aeroelasticity.

The results that have been computed for this thesis have been obtained using a single CPU machine. The flutter solution time, for the Mach 7.0 analysis for the HyperX/X-43 using the ARMA model, was around 225 hours of CPU time on a 1 GHz PC.

Work on the STARS program is continuing and the capabilities of the program are currently being enhanced in areas such as combustion chemistry and a nonlinear control laws integration.

6.2 Concluding Remarks

The development and implementation work that has been described in this thesis has demonstrated that the techniques that have been employed can be routinely used for solution of large complex, practical problems.

APPENDIX A

Control Law Data Verification of STARS

Matlab model of the aeroservoelastic problem of the wing in can.m file.

```
gc  =[     1.4554    -0.6082    -0.3573    -0.0816    -0.1207
    1.         0          0          0          0
    0          0     0.5179     0.4651    -0.2160
    0          0    -0.4492     0.8606     0.0859
    0          0    -0.2170    -0.0726     0.6776];


hc  =[ 0          0          0
       0          0          0
       0.6303    -0.3140    -0.0427
      -0.1496     0.1331     0.0058
       0.1913    -0.1502    -0.0148];

cc  =[ 0 0 0 0 0
       0 0 0 0 0
       0.1688     0.1429         0          0          0];

dc  =[ 0      0      0
       0      0      0
       0      0      0];


aero_wing
soli_wing

nstep = 900;
dt = .268570E-02;
fo=[.204124E+03;  .544244E+02; -.110690E+02]/.122500E+01;
rho = 1.3709;


% Assume that you have (gc,hc,cc,dc)
GM = pck(gc,hc,cc,dc);

% Assume that you have (gs,hs,cs,ds)
SD = pck(gs,hs,cs,ds);

% Assume that you have (ga,ha,ca,da)
AD = pck(ga,ha,ca,da);

% Assume that you have F0
```

```
F0 = fo;

% Assume that you have rho
rho = 1.3709*eye(3);


systemnames = 'GM SD AD rho F0';
inputvar = '[fi(3);fo]';
outputvar = '[SD]';
input_to_AD = '[SD+GM]';
input_to_SD = '[fi+rho]';
input_to_GM = '[SD]';
input_to_F0 = '[fo]';
input_to_rho = '[AD+F0]';
sysoutname = 'P';
sysic;

fi = zeros(nstep,3);
fi(3,:) = [10 10 10];

fo = ones(nstep,1);

input = [fi fo];
input = vpck(input,[dt:dt:dt*nstep]);
input = vtp(input);

output = dtrsp(P,input,dt,dt*nstep);

q1 = sel(output,1,1);
q2 = sel(output,2,1);
q3 = sel(output,3,1);

%vplot(q1);


xnc_1p3709;
TIME = xn(:,1);
Q1 = xn(:,2);
Q = vpck(Q1,TIME);

vplot(q1,Q,'r');
legend('new','old');
```

This is the aerodynamic state-space matrices in aero_wing.m file

```
ga=[ -.991061E+00  .000000E+00  .000000E+00 -.205194E+06 -.262871E+06 -
.944439E+04 -.986498E+03 -.235387E+04 -.159922E+04
  .000000E+00 -.926970E+00  .000000E+00 -.282305E+05 -.557178E+05
.782857E+04  .150087E+04  .274492E+04  .118194E+04
  .000000E+00  .000000E+00 -.858700E-01 -.101491E+04 -.319707E+03 -
.134413E+04  .297272E+03  .171144E+03  .446051E+03
  .000000E+00  .000000E+00  .000000E+00  .000000E+00  .000000E+00
.000000E+00  .000000E+00  .000000E+00  .000000E+00
  .000000E+00  .000000E+00  .000000E+00  .000000E+00  .000000E+00
.000000E+00  .000000E+00  .000000E+00  .000000E+00
```

```
  .000000E+00  .000000E+00  .000000E+00  .000000E+00  .000000E+00
.000000E+00  .000000E+00  .000000E+00  .000000E+00
  .000000E+00  .000000E+00  .000000E+00  .100000E+01  .000000E+00
.000000E+00  .000000E+00  .000000E+00  .000000E+00
  .000000E+00  .000000E+00  .000000E+00  .000000E+00  .100000E+01
.000000E+00  .000000E+00  .000000E+00  .000000E+00
  .000000E+00  .000000E+00  .000000E+00  .000000E+00  .000000E+00
.100000E+01  .000000E+00  .000000E+00  .000000E+00]
ha=[  .247315E+06 -.215598E+06 -.112413E+05
  .295572E+05  .448691E+05  .114084E+05
  .778613E+03  .356820E+03  .298628E+04
  .100000E+01  .000000E+00  .000000E+00
  .000000E+00  .100000E+01  .000000E+00
  .000000E+00  .000000E+00  .100000E+01
  .000000E+00  .000000E+00  .000000E+00
  .000000E+00  .000000E+00  .000000E+00
  .000000E+00  .000000E+00  .000000E+00]
ca=[ -.991061E+00  .000000E+00  .000000E+00 -.205194E+06 -.262871E+06 -
.944439E+04 -.986498E+03 -.235387E+04 -.159922E+04
  .000000E+00 -.926970E+00  .000000E+00 -.282305E+05 -.557178E+05
.782857E+04  .150087E+04  .274492E+04  .118194E+04
  .000000E+00  .000000E+00 -.858700E-01 -.101491E+04 -.319707E+03 -
.134413E+04  .297272E+03  .171144E+03  .446051E+03]
da=[  .247315E+06 -.215598E+06 -.112413E+05
  .295572E+05  .448691E+05  .114084E+05
  .778613E+03  .356820E+03  .298628E+04]
Ga=ga;
Ha=ha;
Ca=ca;
Da=da;
```

This is the structural state-space matrices in the soli_wing.m file

```
gs=[  .995864E+00  .690952E-12 -.401843E-10 -.131238E+01  .513219E-09 -
.277335E-07
  .282288E-11  .959155E+00 -.384297E-10  .208874E-08 -.229246E+02 -
.263249E-07
 -.537965E-08 -.125927E-08  .505652E+00 -.363673E-05 -.848386E-06 -
.311618E+03
  .268093E-02  .620569E-15 -.373766E-13  .998236E+00  .693263E-12 -
.407459E-10
  .253533E-14  .264455E-02 -.358470E-13  .282512E-11  .969003E+00 -
.389683E-10
 -.500376E-11 -.117464E-11  .220780E-02 -.538408E-08 -.126365E-08
.538826E+00]
hs= [-.111115E-03 -.105072E-15  .207388E-12
 -.105072E-15 -.447799E-03  .198901E-12
  .207388E-12  .198901E-12 -.122502E-01
 -.149314E-06 -.706645E-19  .141946E-15
 -.706645E-19 -.605490E-06  .136333E-15
  .141946E-15  .136333E-15 -.181295E-04]
cs=[ 0 0 0 1 0 0
     0 0 0 0 1 0
     0 0 0 0 0 1]
ds=[  .000000E+00  .000000E+00  .000000E+00
  .000000E+00  .000000E+00  .000000E+00
```

```
   .000000E+00   .000000E+00   .000000E+00]
Gs=gs;
Hs=hs;
Cs=cs;
Ds=ds;
```

APPENDIX B

DATA INPUT PROCEDURE
(STARS–CFDASE)

B.1 Introduction

Section B.2 thru B.10 provide description of data files Figure 5 .1 needed for a CFD-based AE and ASE analysis; Sections B.11 and B.12 depict the respective run streams for usual Euler and ARMA solutions, respectively.

B.2 Input Data for Background Grid (job.bac)

B.2.1 $ Title for Background Grid File
Format (FREE)

1. Description: Title card for the background grid file.

2. Note:

A maximum of 80 characters on one line of data.

B.2.2 NPBG, NEBG, NPS, NLS, NTS
Format (FREE)

1. Description: Basic data parameters.

2. Notes:

NPBG = number of points in the background grid

NEPG = number of tetrahedral elements in the background grid

NPS = number of point sources

NLS = number of line sources

NTS = number of triangular plane sources

B.2.3 JP, XP, YP, ZP

Format (FREE)

B.2.4 (DBG(I, 1), DBG(I, 2), DBG(I, 3), DBG(I, 4)), I=1, 3)

Format (FREE)

1. Description: NPBG sets of background grid nodal data.

2. Notes:

JP = index defining the point number

XP = X coordinate of the point

YP = Y coordinate of the point

ZP = Z coordinate of the point

DBG(I, 1) = x local-global coordinate

DBG(I, 2) = y local-global coordinate

DBG(I, 3) = z local-global coordinate

DBG(I, 4) = scale factor; a unit length along this axis is subdivided into approximately 1.0/DBG(I,4) divisions, with finer divisions being made near point I.

B.2.5 (JE, KEL(I), I=1, 4)

Format (FREE)

1. Description: NEBG sets of background grid element data.

2. Notes:

JE = index defining the element number

KEL(I) = node defining a vertex of the tetrahedral element

The background grid is required to completely enclose the computational domain as defined in the surface data file. The fineness of the generated grid is controlled mainly by the parameter DBG(I,4). The smaller this value is, the larger the number of elements there are.

B.2.6 $ Point Sources Data

Format (FREE)

B.2.6.1 $ Text

Format (FREE)

B.2.6.2 X, Y, Z, S, R, D

Format (FREE)

1. Description: Localized background weighting caused by point sources.

2. Notes:

UNIVERSITY OF WALES SWANSEA LIBRARY

X, Y, Z = Cartesian coordinates at the point sources

S = weight at the point source

R = radius of the sphere with a constant weight, S

D = distance from the source at which the spacing is 2 □S

Data for sections B.2.6.1 and B.2.6.2 are repeated NPS times.

B.2.7 $ Line Sources Data

Format (FREE)

B.2.7.1 $ Text

Format (FREE)

B.2.7.2 X1, Y1, Z1, S1, R1, D1

Format (FREE)

B.2.7.3 X2, Y2, Z2, S2, R2, D2

Format (FREE)

1. Description: Localized background weighting caused by line sources.

2. Note:

Data for sections B.2.7.1 through B.2.7.3 are repeated NLS times; definition as above pertains to two points defining the line source.

B.2.8 $ Plane Triangular Sources Data

Format (FREE)

B.2.8.1 $ Text

Format (FREE)

B.2.8.2 X1, Y1, Z1, S1, R1, D1

Format (FREE)

B.2.8.3 X2, Y2, Z2, S2, R2, D2

Format (FREE)

B.2.8.4 X3, Y3, Z3, S3, R3, D3

Format (FREE)

1. Description: Localized background weighting caused by triangular surface sources.
2. Note:

Data for sections B.2.8.1 through B.2.8.4 are repeated NTS times; definition as above pertains to three points defining the triangular plane source.

B.3 Input Data for Surface Grid (job.sur)

B.3.1 $ Title for Surface Definition File

Format (FREE)

1. Description: Title card for the surface definition file.
2. Note:

A maximum of 80 characters on one line of data.

B.3.1.1 NIS, NSF

Format (FREE)

1. Description: Basic data parameters.

2. Notes:

NIS = number of boundary edges for defining normals

NSF = number of support surfaces defining normals

Multiple surfaces can be defined in each support surface region.

B.3.2 $ Boundary-Edge Definitions

Format (FREE)

B.3.2.1 JS, ITIS

Format (FREE)

B.3.2.2 NIP

Format (FREE)

B.3.2.3 ((CIP(I, J), J=1, 3), I=1, NIP)

Format (FREE)

1. Description: NIS sets of boundary-edge definition data.

2. Notes:

JS = index defining the boundary edge

ITIS = index defining the type of boundary edge

= 1, normal generation (Ferguson)

NIP = number of points on the boundary edge

CIP(I, 1) = X coordinate of a point defining the boundary edge

CIP(I, 2) = Y coordinate of a point defining the boundary edge

CIP(I, 3) = Z coordinate of a point defining the boundary edge

B.3.3 $ Support-Surface Definitions and Orientation

Format (FREE)

B.3.3.1 ISS, ITSF,

Format (FREE)

B.3.3.2 NU, NV

Format (FREE)

B.3.3.3 ((CSP(I, J), J=1, 3), I=1, NU*NV)

Format (FREE)

1. Description: NSF sets of support-surface definition data.

2. Notes:

ISS = index defining the support surface

ITSF = index defining support-surface type

= 1, composite surfaces, curved (Ferguson)

NU = number of points in the U parametric direction

NV = number of points in the V parametric direction

CSP(I, 1) = X coordinate of a point defining the support surface

CSP(I, 2) = Y coordinate of a point defining the support surface

CSP(I, 3) = Z coordinate of a point defining the support surface

For NV > 1, the first set of NU is read, then the second, and so forth. The normal for a plane determined by these points should point into the computational domain. For a composite surface, the *u* axis is along the first input line, and the *v* axis is along the line connecting the first node on each line.

B.3.4 $ Curved-Edge Definition

Format (FREE)

B.3.4.1 NSG, NRG

Format (FREE)

1. Description: Number of surface-region data sets.

2. Notes:

NSG = number of curved segments

NRG = number of surfaces regions

These data define the regions of interest on each support surface; see section B.3.1.1.

B.3.4.2 $ Text

Format (FREE)

B.3.4.3 ISG IDCV ITSG

Format (FREE)

1. Description: NSG sets of curved-segment data
2. Notes:

ISG = index defining the curved segment

IDCV = index defining the boundary edge from section 5.3.1.1

ITSG = index defining the generation type

= 1

B.3.5 $ Support-Region Definition by Boundary Edges

Format (FREE)

B.3.5.1 IRG, IDSF, ITRG

Format (FREE)

B.3.5.2 NN

Format (FREE)

(ISBS(I), I=1, NN)

Format (FREE)

1. Description: NRG sets of surface-region data.
2. Notes:

IRG = index defining the surface number

IDSF = index defining the support-surface from section B.3.1.1

ITRG = index defining the generation type

= 1

NN = number of curved segments

ISBS(I) = indices of curved segments along the mesh region

The edges should be listed in such a manner that the direction of the normal points into the computational domain, and the edges are traversed in the opposite sense of their above definition when given a negative sign.

3. Additional notes:

This data file contains the geometrical definition of the boundary of the computational domain. The general data contains the number of boundary edges and the number of support surfaces. First, each support surface is defined as a plane, composite, or degenerate surface. Secondly, each support surface is defined by traveling about it, along the boundary edges, to obtain the direction normal to the surface points into the computational domain for all of the surfaces (using the right-hand rule). The normals in sections B.3.3.1 and B.3.5.1 should be consistent. If one is traveling along a boundary edge in the opposite sense of its original definition, its index is given a negative value.

B.4 Input Data for Boundary Conditions (job.bco)

B.4.1 $ Title for Boundary-Condition File

Format (FREE)

1. Description: Title card for the boundary-condition file.
2. Note:

A maximum of 80 characters on one line of data.

B.4.2 NRG, NSG, NIDEA

Format (FREE)

1. Description: Number of data sets.
2. Notes:

NRG = number of boundary surfaces

NSG = number of boundary segments

NIDEA = 0, grid generated by CFDASERUN (no normal calculation)
1, grid generated by IDEA (need normal calculation)

These numbers should match those in section 5.3.4.1.

B.4.3 $ Surface-Region Boundary-Condition Definitions

Format (FREE)

B.4.4 IRG, IBCO

Format (FREE)

1. Description: NRG sets of surface-region boundary-condition data.
2. Notes:

IRG = index defining the surface number

IBCO = index defining the surface boundary condition

= 1, wall

= 2, symmetry

= 3 and 4, far field

= 5 and 6, engine inlet

= 7 and 8, engine outlet

B.4.5 $ Curve-Segment Boundary-Condition Definitions

Format (FREE)

B.4.6 JS, ICBCO

Format (FREE)

1. Description: NSG sets of curved-segment boundary-condition data.
2. Notes:

JS = index defining the curved segment

IBCO = index defining the curved-segments boundary-condition

= 0, no singularity

= 1, all are singular

= 2, singular point at first and last

= 3, singular point at first only

= 4, singular point at last only

B.5 Input Data of Control File for Steady-State Computational Fluid Dynamics (Euler) Solution (job.cons)

1. Description: Parameters for a name list control file used in the steady-state Euler solution.
2. Notes:

Each name parameter must begin with "&control" and end with "/". These parameters are on their own lines. Each parameter must be separated with a comma, even if each appears on a separate line. If the parameters are not specified by the user, they will be automatically set to their default values, which are listed in parentheses after each definition.

&control

nstep = total number of solution time steps (1)

nstou = number of time substeps for writing the unknowns file job.un1
(ncycl substeps for each time step) (5)
writing also occurs after each solution time step
if nstou ≥ ncycl, writing occurs once every solution time step

nstage = number of stages in the Runge-Kutta time integration, to a maximum of 5 (5)

cfl = value of the CFL (Courant-Friederich-Lax) number (2.8)

diss1 = first dissipation constant (1.0)

diss2 = second dissipation constant (1.0)

relax = boundary-condition relaxation factor (1.0)

mach = free stream Mach number (0.6)

alpha = free-stream angle of attack (0.0)

beta = free-stream angle of sideslip (0.0)

restart = index defining restart option (.false.)
= .true., restart run
= .false., initial run

nlimit = limiter function type (1)
= 1, minmod
= 2, Thomas

lg = multigrid cycle (1)

nite0 = presmoothing iterations (1)

nite1 = smoothing iterations (1)

nite2 = postsmoothing iterations (1)

ncycl = number of substeps for each time step (1000)

ncyci = ncycl (1000)

tlr = stopping tolerance (0.0)

debug = debugging option (.false.)
= .true., debug
= .false., do not debug meshc = coarsest mesh (mmesh from the file *.geo)

meshf = starting mesh (1)

cbt(1), cbt(2), cbt(3), cbt(4),
cbt(5) = beta1, beta2, beta3, beta4, beta5 (1.0, 0.5, 0.0, 0.0, 0.0)

bulkvis = index for computing bulk viscosity (.false.)
= .true., compute bulk viscosity
= .false., do not compute bulk viscosity
for Mach > 2.5, set bulkvis = .true.

disx, xc1, xc2,
xc3, xc4 = parameters defining the bulk viscosity (6.0, –1.2, –0.2, 0.014, 0.0714)

nsmth = number of residual smoothing iterations (0)

smofc = residual smoothing coefficient (0.25)

low = order of solution (.false.)
= .true., low-order solution
= .false., high-order solution

trans = index for defining transient analysis (.false.)
= .true., transient analysis
= .false., no transient analysis
for steady flow, set to .false.

gamma = ratio of specific heats (1.4)

epslm = harten fix constant, (0.05)

/ = end file

B.6 STARS–AEROS–GENMASS Data (genmass.dat)

Purpose: Prepare genmass.dat data file.

Description: Computes a generalized mass matrix.

B.6.1 $ Job Description

Format (FREE)

B.6.2 ISTMN, NLVN, GR

Format (2I5, E10.4)

1. Description: Generalized mass-matrix generation data.
2. Notes:

ISTMN = integer specifying the starting mode number

NLVN = number of laterally vibrating aerodynamic interpolation node points (0)

GR = gravitational constant(=1)

B.7 Input Data for Control (job.control)

B.7.1 $ Size of A matrix and column of the B matrix of the controller, starting step

Format (FREE)

B.7.2 NCRA, NCCB, NCRC, GAINR, GAINC, NSTAR, NAND

Format (FREE)

1. Description: Number of roots for the damping solution.
2. Note:

NCRA = size of the controller A matrix

NCCB = number of column of the controller B matrix

NCRC = number of row of the controller C matrix

GAINR = number of row of the $\tilde{\mathbf{K}}$ gain matrix

GAINC = number of column of the $\tilde{\mathbf{K}}$ matrix

NSTAR = step to where controller is turned on

NAND = 1, controller matrices are analog

2, controller matrices are digitized

B.7.3 $ The controller $\mathbf{A}_c$ matrix

Format (FREE)

B.7.4 ((AC(I,J),J=1,NCRA), I=1,NCRA)

Format (FREE)

1. Description: The state-space matrix of the controller.
2. Note:

AC = the controller **A** matrix

B.7.5 $ The controller B_c matrix

Format (FREE)

B.7.6 ((BC(I,J),J=1,NCCB), I=1,NCRA

Format (FREE)

1. Description: the state space matrix of the controller.
2. Note:

BC = the controller **B** matrix.

B.7.7 $ The controller C_c matrix

Format (FREE)

B.7.8 ((CC(I,J),J=1,NCRA), I=1,NCRC

Format (FREE)

1. Description: the state space matrix of the controller.
2. Note:

CC = the controller **C** matrix.

B.7.9 $ The controller D_c matrix

Format (FREE)

B.7.10 ((DC(I,J),J=1,NCCB), I=1,NCRC

Format (FREE)

1. Description: the state space matrix of the controller.
2. Note:

DC = the controller **D** matrix.

B.7.11 $ The gain matrix

Format (FREE)

B.7.12 ((GM(I, J), J=1, GAINC),I=1,GAINR)

Format (FREE)

1. Description: vector to direct the output of the controller back into the aeroelastic state vector.
2. Note:

GM(I, J) = the components for the gain matrix.

B.7.13 $ The matrix correlate the output of control with structure output

Format (FREE)

B.7.14 (G(I), J=1, 2NR)

Format (FREE)

1. Description: vector to direct the output of the controller back into the aeroelastic state vector.
2. Note:

GM(I, J) = the components for the gain matrix.

B.8 Input Data for Unsteady Flow (job.scalars)

B.8.1 $ Title for Scalars File

Format (FREE)

1. Description: Title card for the scalars file.
2. Note:

A maximum of 80 characters on one line of data.

B.8.2 $ Basic Parameters

Format (FREE)

B.8.3 NR, IBCX, RBCX,ISIZE

Format (FREE)

1. Description: Basic data parameters.
2. Notes:

NR = number of mode shapes used in the unsteady analysis

IBCX = index defining ARMA control parameters

= 0, structure is free to move due aerodynamic forces (Euler/ARMA)

= 1, displacement is set to the RBCX value (Euler) structure is clamped, all generalized displacement are zero(ARMA)

= 2, aeroservoelastic analysis (Euler/ARMA, Piston/ARMA)

= 3, displacement is set to RBCX plus velocity (Euler)

= 4, apply multistep 3211 training signal to each generalized input signal(ARMA)

RBCX = mode-shape multiplication factor (Euler)
a floating point magnitude for the multistep 3211 (ARMA)

ISIZE = an integer scaling factor for the multistep 3211 size(ARMA)

B.8.4 NNR, (NS(I), I=1, NNR)

Format (FREE)

1. Description: Boundary-condition modification data.
2. Notes:

NNR = number of surfaces upon which the boundary condition needs to be modified

NS = index defining the surface number

B.8.5 $ I/O Parameters

Format (FREE)

B.8.6 IRFORM, IPFORM

Format (FREE)

1. Description: Indices to set data input and output formats.
2. Notes:

IRFORM = index defining the input read format
= 1, free format, ASCII file
= 2, binary file

IPRINT = index defining the output print format
= 0, no print out
= 2, print out k, m, and c generalized matrices

B.8.7 $ Dimensional Parameters

Format (FREE)

B.8.8 MACHI, RHOI, AI, GAMMA, PINF

Format (FREE)

1. Description: Dimensional parameters at infinity.
2. Notes:

MACHI = Mach number at infinity

RHOI = density at infinity

AI = speed of sound at infinity

GAMMA = gamma constant, c_v/c_p

PINF = air pressure at infinity

B.8.9 $ Shift Factor and Gravitational Constant

Format (FREE)

B.8.10 SCF, GR

Format (FREE)

1. Description: Basic constants.
2. Notes:

SCF = scaling factor, as defined in section 9.7.4

GR = gravity constant, as defined in section 6.1.2

B.8.11 $ Impulse-Force Data

Format (FREE)

B.8.12 IFLAG, FFI, NS/XS, NE/XE

Format (FREE)

1. Description: Data for specifying the impulse force.
2. Notes:

IFLAG = index defining the generalized impulse-force input mode

= 1, applied from times XS to XE (real time)

= 2, applied from steps NS to NE step

FFI = magnitude of the generalized impulse force

NS/XS = starting step or time

NE/XE = ending step or time

B.8.13 $ Force Activation Parameters

Format (FREE)

B.8.14 ICFA, ICFI

Format (FREE)

1. Description: Parameters to activate aerodynamic and applied generalized forces.
2. Notes:

ICFA = index defining the activation of aerodynamic force
= 0, do not activate
= 1, activate

ICFI = index defining the activation of applied generalized force
= 0, do not activate
= 1, activate

B.8.15 $ Transition Matrix Parameters

Format (FREE)

B.8.16 NTERMS, NSTEPS

Format (FREE)

1. Description: Parameters used in calculating the transition matrix, $e^{A\Delta t}$.
2. Notes:

NTERMS = number of terms used in the calculation of $e^{A\Delta t}$.

NSTEPS = option to calculate the transition matrix $e^{A\Delta t}$ at specified intervals

B.8.17 $ Input for ARMA Option: NA, NB

Format (FREE)

2. Notes:

NA = order of the A_i coefficients, in ARMA equation (4.24)

NB = order of the B_m coefficients, in ARMA equation (4.24)

B.9 Input Data of Control File for Unsteady Computational Fluid Dynamics (Euler) Solution (job.conu)

1. Description: Parameters for a name list control file used in the unsteady Euler solution.
2. Notes:

The data below are to be augmented with the data in section B.5; nstou from section B.5 is replaced by nout. See section B.5 for other details regarding using the name list.

&control

nout = number of time steps for writing the unknowns file job.uni (1)

restart = index defining the restart option (1)

= 0, start from a far-field boundary condition

= 1, start from the steady-state solution/unsteady f_a convergence check solution

= 2, restart from the last unsteady solution

freq = size adjustment of the time step for a transient analysis (0.0)

nstpe = size adjustment of the time step of the transient analysis (1)

x0, y0 ,z0 = center of rotation (0.0, 0.0, 0.0)

wux, wuy,
wyz = axis of rotation (0.0, 0.0, 0.0)

phase = angle, phi, used to switch an input signal from a sine to a cosine wave,
A x sin(Δt+ phi), in the pitching problem (0.0)

amplitude = magnitude, A, of the input signal (0.0)

iflow_sol = index for solution type

= 1, use the CFD unsteady Euler solver (also for ARMA steps 1 and 2)

= 2, use the alternative piston and modified Newtonian impact theory

= 3, ARMA, Euler or piston

/ = end file

B.10 Input Data of Control File for STEADYDP (job.consdp)

B.10.1 NLINES

Format (FREE)

1. Description: Specifies the number of the following comment lines.
2. Note:

NLINES = number of comment lines to follow

B.10.1.1 $ Comment Lines

Format (FREE)

1. Description: NLINES sets of comment lines.
2. Note:

A maximum of 80 characters for each line of comments.

B.10.2 $ Problem Dimension

Format (FREE)

1. Note:

Comment line. Not included in NLINES.

B.10.2.1 NDIM

Format (FREE)

1. Description: Problem dimension size.
2. Note:

NDIM = number of dimensions in the problem
= 3

B.10.3 $ Problem Size Parameters

Format (FREE)

B.10.3.1 NELEM, NPOIN, NBOUN

Format (FREE)

1. Description: Basic data parameters.
2. Notes:

NELEM = number of tetrahedral elements

NPOIN = number of points

NBOUN = number of boundary elements

B.10.4 $ Solution Acceleration Parameters

Format (FREE)

B.10.4.1 KACCEL, NACCEL

Format (FREE)

1. Description: Parameters to accelerate the solution.
2. Notes:

KACCEL = number of iterations between acceleration

NACCEL = index defining the starting acceleration time step

If no acceleration is desired, set NACCEL to significantly exceed the expected value of NTIME+ITIN, as defined in sections 9.10.10.1 and 9.10.18.1, respectively.

B.10.5 $ General Parameters

Format (FREE)

B.10.5.1 GAMMA, C1, IDIFF, EPS, IVISC, WBR

Format (FREE)

1. Description: Basic fluid data parameters.
2. Notes:

GAMMA = gas constant
= 1.4, for air

C1 = pressure switch coefficient
= 0.3, recommended for completely subsonic
= 0.5–0.8, recommended for transonic
= 1.0, recommended for transonic to hypersonic

IDIFF = index defining the smoothing type for artificial dissipation
= 0, metric weighted, acting on the sides
= 1, area weighted, acting on the sides (old code)
= 2, area weighted, acting at the element level (new code)
= 3, new diffusion scheme with side eigenvalues

EPS = pressure switch tolerance; it must be set to a small number or 0.0
= 0.1, normally

If EPS = 0.0, a pressure switch of the type $(M_C - M_L)p/(M_C - M_L)$ is evaluated; otherwise, the pressure switch is evaluated as $psw = \sum (P_i - P_j) \;/\sum (| P_i - P_j |)$

, and EPS is used to avoid division by zero. Because of the way that the division by zero has been avoided, if EPS = 1, the pressure switch is evaluated as $\sum (P_i - P_j)$ /PMEAN, where PMEAN is the mean value in the surrounding elements.

IVISC = viscous flow indicator

= 0, for Euler

WBR = wall boundary relaxation parameter, to be used when strong boundary conditions are applied (pointwise velocity projection at wall)

WBR normalizes wall boundary conditions at each step to avoid big jumps. At each step, 0.2 would normalize by 20 percent. Even 1.0 will normally work. Hypersonically, problems may exist. For unsteady flow, set WBR to 1.0 to be time accurate.

B.10.6 $ Far-Field Boundary Condition Parameter

Format (FREE)

B.10.6.1 NFFBC

Format (FREE)

1. Description: Number of far-field boundary conditions.
2. Note:

NFFBC = number of far-field boundary conditions

B.10.7 $ Far-Field Boundary Condition Data

Format (FREE)

B.10.7.1 ROINF, UXINF, UYINF, UZINF, PINF, MACHINF

Format (FREE)

1. Description: NFFBC sets of far-field boundary-condition data.
2. Notes:

ROINF = density at infinity

UXINF = velocity in X at infinity

UYINF = velocity in Y at infinity

UZINF = velocity in Z at infinity

PINF = pressure at infinity

= ROINF/(GAMMA*MACHINF**2)

MACHINF = Mach number at infinity

B.10.8 $ Engine Intake/Outlet Boundary-Condition Parameter

Format (FREE)

B.10.8.1 NENBC

Format (FREE)

1. Description: Number of engine inlet/exit boundary conditions.
2. Note:

NENBC = number of engine inlet/exit boundary conditions

B.10.9 $ Engine Boundary-Condition Data (Required if NENBC $\neq$ 0)

Format (FREE)

B.10.9.1 ROENG, UXENG, UYENG, UZENG, PENG, MACHENG (Required if NENBC $\neq$ 0)

Format (FREE)

1. Description: NENBC sets of far-field boundary-condition data.
2. Notes:

ROENG = specified density

UXENG = velocity in X

UYENG = velocity in Y

UZENG = velocity in Z

PENG = specified pressure

MACHENG = specified Mach number

B.10.10 $ Iteration Parameters

Format (FREE)

B.10.10.1 NTIME, NITER, ILOT

Format (FREE)

1. Description: Parameters to set the number of solution time steps.

2. Notes:

NTIME = maximum number of iterations

NITER = number of mass-consistent iterations
= 1, mass-lumped solution used (steady state)
= 2, mass-consistent solution used (transient)

ILOTS = time-stepping indicator
= 0, global time stepping (steady or transient)
= 1, local time stepping (steady, faster than 0)

B.10.11 $ General Convergence Parameters

Format (FREE)

B.10.11.1 CSAFE, IFCT, NQUAN, (IDO(I), I = 1, NQUAN), CLIMAX

Format (FREE)

1. Description: Data to specify solution convergence.
2. Notes:

CSAFE = Taylor-Galerkin safety factor; usually, $0.0 \leq \text{CSAFE} \leq 1.0$
= 0.7, a reasonable value

IFCT = FCT routine switch
= 0, no FCT
= 1, FCT
= −1, low order only (not generally used)

NQUAN = number of FCT quantities to limit; set to 1, 2, or 3

IDO(I) = variable to be limited for FCT
= 1, density
= 2, energy
= 3, pressure

CLIMAX = maximum limiter allowed; usually 0.00 to 0.95

The FCT should decrease "smearing" near a strong shock but does not always work and increases the solution time. Normally, this option would not be used.

B.10.12 $ File Formats and I/O Direction

Format (FREE)

B.10.12.1 INFOG, INFOU, OUFO, NIOUT

Format (FREE)

1. Description: Indices to specify input and output.
2. Notes:

INFOG = index defining the geometry file format specification
= 0, input file is formatted in ASCII
= −1, input file is unformatted

INFOU = index defining the restart initial values file format specification
= 0, input file is formatted in ASCII
= −1, input file is unformatted
= −2, input file is not required, initial values are generated from far-field specifications

OUFO = index defining the output file specification
= 3, unformatted output on channel 15 (graphics)
= 2, formatted output to channel 4; five unknowns at each point in mesh
= 1, unformatted output to the front end (VAX)
= 0, formatted output to the front end
= −1, formatted output to a Cray computer with the name FILE3 and overwriting
= −2, no output file written
= −3, unformatted output to a Cray computer with the name FILE3 and overwriting
= −4, formatted output to a Cray computer with a new file generated every NIOUT iteration with the name FILE3iter
= −5, unformatted output to a Cray computer with a new file generated every NIOUT iteration with the name FILE3iter

NIOUT = number of iterations between outputs
= 0, output written only at the end of the job

WARNING: If OUFO = 0 or 1, (for example, a result file sent to the front end), an unformatted copy of the file (named FILE3) is also sent to the Cray computer.

Note: For INFOU set to 0 or −1, use the previous output file for FILE4 in section 5.10.19.1 for the initial values. Remember to update ITIN in section 5.10.18.1 as well.

B.10.13 $ Residuals Smoothing Parameters

Format (FREE)

B.10.13.1 CSMOO, NSMOO

Format (FREE)

1. Description: Data for defining residuals smoothing.
2. Notes:

CSMOO = residual smoothing coefficient
= 0.25 for Jamesons's method

NSMOO = number of smoothing iterations
= 2 for Jamesons's method

B.10.14 $ Enthalpy Damping Coefficient

Format (FREE)

B.10.14.1 ALPHA

Format (FREE)

1. Description: Enthalpy damping coefficient.
2. Notes:

ALPHA = enthalpy damping coefficient to enforce constant enthalpy; does not always work
= 1.0, normally

B.10.15 $ Residuals and Lift Parameters

Format (FREE)

B.10.15.1 IRPR, IRLOG, ILPR, ILLOG, AXIS(I, I = 1, 3), RCHORD

Format (FREE)

1. Description: Data for residuals and lift.
2. Notes:

IRPR = number of iterations between evaluations of diffusive fluxes for a Taylor-Galerkin scheme

IRLOG = type of logging for residuals

= 0, print to log file only

= 1, print to RESID, and print to log file

= 2, print to RESID

ILPR = number of iterations between outputs of lift, drag, and moment coefficients; uses the centroids of the elements with a boundary condition of 2

= 0, no output for lift

ILLOG = type of logging for lift

= 0, print to log file

= 1, print to LIFT, and print to log file

= 2, print to LIFT

AXIS(I) = end points of a position vector, in x, y, and z, parallel to which the lift acts

RCHORD = reference chord for use in lift and moment calculations

B.10.16 $ Residual Smoothing Iteration Parameters

Format (FREE)

B.10.16.1 IRFR, IRFS

Format (FREE)

1. Description: Data for defining residuals smoothing iterations.
2. Notes:

IRFR = number of iterations between smoothing residuals, starting from iteration N; this parameter is a tradeoff with the CSAFE parameter

= 1, if CSAFE = 1.2

= 3, if CSAFE ≈ 0.9

IRFS = number of initial iterations before an alternate evaluation of diffusive fluxes

For Taylor-Galerkin schemes, irrespective of IRFR, the diffusive fluxes are evaluated at every time step for the first IRFS iterations. This option is not presently used.

B.10.17 $ Boundary-Condition Types and Geometry Checking

Format (FREE)

B.10.17.1 ISTRON, ICHECK

Format (FREE)

1. Description: Specifies boundary-condition types.
2. Notes:

ISTRON = boundary-condition type
= 0, weak boundary conditions; flux is corrected on the outer bounds
= 1, strong boundary conditions with velocity projection at the sides included into the right-side boundary integral
= 2, strong boundary conditions with full boundary integral evaluation

ICHECK = geometry consistency-checking parameter
= 0, no checking
= 1, checking done

B.10.18 $ Initial Time and Iterations

Format (FREE)

B.10.18.1 TIMEIN, ITIN

Format (FREE)

1. Description: Parameters to control starting times.
2. Notes:

TIMEIN = initial time (only for transient)

ITIN = initial iteration number; the iteration counter starts at (ITIN+1)

3. Additional notes:

This code does not check itself for convergence and stop automatically. Convergence is generally said to have occurred when a drop of 4 to 5 orders of magnitude has occurred in the average of the residuals. The lower the Mach number is, the slower the convergence is.

B.10.19 $ File Names

Format (FREE)

B.10.19.1 FILE3, FILE2, FILE4

Format (FREE)

1. Description: Listing of files for input and output control.
2. Notes:

FILE3	=	output file for the results
FILE2	=	input geometry file
FILE4	=	restart the input file with initial values

Each file name can have a maximum of 16 characters. Only the prefix is required.

B.10.20 $ CPU Parameters

Format (FREE)

B.10.20.1 NCPU

Format (FREE)

1. Description: Number of central processing units (CPUs) to be used in the solution.
2. Notes:

NCPU = Number of CPUs requested
Set to 0 or 1 for a nonmultitasked version.

B.11 CFD-Based Aeroelastic and Aeroservoelastic Analysis

Three solution options are available (A) Euler CFD-based (B) Euler CFD-based with piston perturbation(unsteady piston calculation using steady Euler solution) and (C) piston, respectively (Table B.1).

Table B.1. Time-marched aeroelastic and aeroservoelastic solution option.

Solution step	CFD-based (A)	Piston Perturbation (B)	Piston (C)
1	Euler steady	Euler steady	None
2	Euler unsteady (iflow_sol=1,restart=1)	Piston unsteady (iflow_sol=2,restart=1)	Piston unsteady (iflow_sol=2,restart=0)

```
$ cfdaserun
> 1 'surface'   - job.sur, job.bac → [job.fro], is the output file
> 2 'volume'    - job.bac, [job.fro] → [job.gri]
> 4 'setbnd2'   - job.bco, [job.fro, job.gri] → [job.geo, job.plt ]
> 6 'steady'    - job.cons, [job.geo] → [job.unl; change to job.unk for restart
                  or to run unsteady]
> 7 'Interface'
> 7-2 'srun'      - solids.dat → [solids.out.1&2, fort.46, fort.*]

> 7-3 'genmass' - genmass.dat, [fort.46] → [genmass.out (freq., $\hat{M}$, $\hat{K}$, $\hat{D}$),
                  genmass.binary]
> 7-4 'intpolsf'  - [solids.out.2, job.fro], vibrating surface numbers →
                  [job.phia, fort.21,...,fort(nr+20)]
> 7-5 'arrays'    - [job.fro, genmass.out, job.phia], specify mode #'s → [job.arrays]
> 8 'unsteady' - job.conu, job.scalars, job.control, [job.geo, job.unk, job.arrays,
                  job.fro] → [job.uni, xn.dat]
```

Plot xn.dat (generalized displacements q 's, velocities $\dot{q}$'s, and forces f_a 's) and calculate damping for the altitude.

```
$ xp
read xn.dat
select 1
plot x1
⋮
sel 4
plot x4
repeat for other modes.
```

(plots q_1, q_2, $\cdots$, q_{nr},$\dot{q}_1$, $\dot{q}_2$, $\cdots$, $\dot{q}_{nr}$)

B.12 CFD-Based ARMA Aeroelastic and Aeroservoelastic Analysis

Three solution options are available (A) Euler CFD-based (B) Euler CFD-based with piston perturbation (unsteady piston calculation using steady Euler solution) and (C) piston, respectively (Table B.2).

Table B.2. State space ARMA aeroelastic and aeroservoelastic solution options.

Solution step	CFD-based (A)	Piston Perturbation (B)	Piston (C)
1	Euler steady	Euler steady	None
1a	Euler unsteady (iflow_sol=1,restart=1)	Piston unsteady (iflow_sol=2,restart=1)	None
2	Training ARMA (iflow_sol=1,restart=1)	Training ARMA (iflow_sol=2,restart=1)	Training the ARMA (iflow_sol=2,restart=0)
3	Least Square curve fit for the ARMA model	Least Square curve fit for the ARMA model	Least Square curve fit for the ARMA model

4	Evaluate AMA model	Evaluate ARMA model	Evaluate ARMA model
5	ARMA solution (iflow_sol =3)	ARMA solution (iflow_sol =3)	ARMA solution (iflow_sol =3)

Solution Steps:

Step 1. Steady solution and input data preparation for unsteady analysis

```
$ cfdaserun
> 1 'surface'   - job.sur, job.bac → [job.fro], is the output file
> 2 'volume'    - job.bac, [job.fro] → [job.gri]
> 3 'setbnd2'   - job.bco, [job.fro, job.gri] → [job.geo, job.plt ]
> 6 'steady'    - job.cons, [job.geo] → [job.un1; change to job.unk for restart
                                                           or to run unsteady]
> 7 'Interface'
> 7-2 'srun'      - solids.dat → [solids.out.1&2, fort.46, fort.*]

> 7-3 'genmass' - genmass.dat, [fort.46] → [genmass.out (freq., M̂, K̂, D̂),
                                                              genmass.binary]
> 7-4 'intpolsf'  - [solids.out.2, job.fro], vibrating surface numbers →
                                                 [job.phia, fort.21,...,fort(nr+20)]
> 7-5 'arrays'    - [job.fro, genmass.out, job.phia], specify mode #'s → [job.arrays]
```

Step 1a. 'Unsteady' solution convergence study of the clamped structure.

Modify:

job.scalars: ibcx=1 (structure clamped, generalized displacement zero)

job.conu: iflow_sol=1 (1-euler, 2-piston, 3-ARMA)

restart=1 (from job.unk of **step 1** steady run) nstep =100 or so (enough for f_a's to converge to a flat line)

```
$ cfdaserun
```

> 8 'unsteady' -> [xn.dat, generalized displacements q's, and $\dot{q}$'s,

and generalized force f_a's]

To check convergence of generalized forces (to be a straight line without oscillation), plot the xn.dat.

```
$ xp
read xn.dt
sel 1
plot f1
sel 2
plot f2
```

If f_a's did not converge restart and run **step 1a** again for more solution steps.

Step 2. Training the ARMA - ARMA multistep "unsteady' solution for 3-2-1-1 input signal – nstep or so for a Mach number

Modify:

```
job.scalars:    ibcx = 4 (input 3211 signals)
                     = 5 (variable amplitude multistep input signal)
                isize = an integer scaling factor for the multistep size
                rho-inf = a specified  training altitude density
job.conu:       iflow_sol=1 (1-euler, 2-piston, 3-ARMA)
                nstep = 5 + isize*( 4*nr + 3 ) for ibcx =4
                      = 5 + isize*( 16*nr + 3 ) for ibcx = 5
                restart=1 (from job.unk of step 1a)
```

```
$ cfdaserun
> 8 'unsteady' -> [xn.dat, renamed multi.dat]
```

Step 3. Least squares curve fitting for the ARMA model

Modify:

```
job.scalars:    ibcx=4 (input 3211 signals)
                     na = # number
```

nb = # number

rho-inf = same free stream density used in **step 2**

job.conu: iflow_sol=1 (1-euler, 2-piston, 3-ARMA)

restart= ignored in this step

nstep = same number of steps used in **step 2**

```
$ cfdaserun
> 9 'arma_utility'
```

> 9 – 1 cfdmdl-> [job.mdl (coefficients for state space $\mathbf{G}_a, \mathbf{H}_a, \mathbf{C}_a, \mathbf{D}_a$ matrices)]

Note: For Piston solution (restart =0) the range for na and nb are

na =0 and nb=3 or 4

For Piston–perturbation (restart=1) solution range for na and nb are

na = 1 and nb= 3 or 4 (due to nonlinearities in the mean flow job.unk file)

For Euler solution the range for na and nb

0 < na < 5 and 0< nb < 15

The training input signal needs to be at least 1/2 of a highest frequency cycle length.

Step 4. Evaluate the ARMA model ($\mathbf{G}_a$, $\mathbf{H}_a$, $\mathbf{C}_a$, $\mathbf{D}_a$)

Modify:

job.scalars: ibcx=4 (input 3211 signals)

na = # number same as **step 3**

nb = # number same as **step 3**

rho-inf = same free stream density used in **step 2**

job.conu: iflow_sol=3 (1-euler, 2-piston, 3-ARMA)

restart= ignored in this step

nstep = same number of steps used in **step 2**

```
$ cfdaserun
```

> 8 'unsteady' -> [xn.dat, using $\mathbf{G}_a$, $\mathbf{H}_a$, $\mathbf{C}_a$, $\mathbf{D}_a$; Copy to xn.nanb]

Plot xn.dat and multi.dat to ensure that the signal $f_a's$ of the xn.dat match up with the $f_a's$ of the multi.dat signal.

```
$ xp
```

```
read multi.dat
read xn.dat 1
plot f1 f1.1
plot f2 f2.1
```

(do this for *nr* f_a, all the f_a need to match up real good.)

If f_a in xn.dat does not match with the multi.dat's f_a then change the *na* and *nb* parameters and rerun **step 3** and **step 4** again until the f_a's for xn.dat matches with multi.dat.

```
$ cfdaserun
> 9  'ARMA utility'
```

$>$ 9-2 'asemdl' -> - [job.amtx ($\mathbf{G}_a$, $\mathbf{H}_a$, $\mathbf{C}_a$, $\mathbf{D}_a$), job.smtx ($\mathbf{G}_s$, $\mathbf{H}_s$, $\mathbf{C}_s$, $\mathbf{D}_s$), job.eig]

$>$ 9-3 'gleigplt' -> plots root locus from job.eig; if unstable obtain a control law design employing the state-space matrices, yielding the gain matrix (job.control)

Step 5. ARMA solution

Modify:

job.scalars:
ibcx= 0   for aeroelastic analysis
ibcx= 2   for aeroservoelastic analysis (need job.control file)
na = # number same as **step3**
nb = # number same as **step 3**
rho-inf = any altitude

job.conu:
iflow_sol=3 (1-euler, 2-piston, 3-ARMA)
restart= ignored in this step
nstep = any number of steps enough to compute damping

```
$ cfdaserun
> 8  'unsteady' -  job.conu, job.scalars, job.control, [ job.geo, job.unk, job.arrays,
                   job.fro] -> [xn.dat, using  Ga, Ha, Ca, Da; copy xn.dat to
                   xn.density]
```

Plot xn.dat and compute damping of the signal for this density.

```
$ xp
read xn.density
sel 1
plot x1
sel 2
plot x2
sel 3
plot x3
sel 4
plot x4 ( and so on)
```

Repeat solution for other relevant densities for the same Mach number.

APPENDIX C

Input Data For ASE Analysis of Cantilever Wing

The following input data follows the sequence as in the Figure 6.1. Data for the surface file, **wing.sur**, are given first.

STARS–CFDASE input data:

```
$  STARS 5.3.1 wing.sur quasi-2D naca0012
C  STARS 5.3.1.1  NIS, NSF
  36   16
$  STARS 5.3.2 Boundary-edge  definitions
C  STARS 5.3.2.1  JS, ITIS
       1   1
C  STARS 5.3.2.2  NIP  Number of point on the boundary edge
   41
C  STARS 5.3.2.3  ((CIP(I,P),j=1,3),I=1,NIP)
        0.10089E+01     0.0      0.00000E+00
        0.10069E+01     0.0     -0.28900E-03
        0.10013E+01     0.0     -0.10810E-02
        0.99239E+00     0.0     -0.23220E-02
        0.98043E+00     0.0     -0.39740E-02
        0.96555E+00     0.0     -0.59930E-02
        0.94792E+00     0.0     -0.83390E-02
        0.92771E+00     0.0     -0.10971E-01
        0.90508E+00     0.0     -0.13843E-01
        0.88019E+00     0.0     -0.16915E-01
        0.85323E+00     0.0     -0.20146E-01
        0.82436E+00     0.0     -0.23494E-01
        0.79375E+00     0.0     -0.26920E-01
        0.76160E+00     0.0     -0.30386E-01
        0.72808E+00     0.0     -0.33853E-01
        0.69336E+00     0.0     -0.37281E-01
        0.65765E+00     0.0     -0.40632E-01
        0.62111E+00     0.0     -0.43863E-01
        0.58394E+00     0.0     -0.46931E-01
        0.54633E+00     0.0     -0.49791E-01
        0.50846E+00     0.0     -0.52398E-01
        0.47053E+00     0.0     -0.54701E-01
        0.43273E+00     0.0     -0.56653E-01
        0.39526E+00     0.0     -0.58203E-01
        0.35831E+00     0.0     -0.59303E-01
        0.32208E+00     0.0     -0.59908E-01
        0.28677E+00     0.0     -0.59978E-01
        0.25259E+00     0.0     -0.59475E-01
        0.21973E+00     0.0     -0.58374E-01
        0.18841E+00     0.0     -0.56655E-01
        0.15882E+00     0.0     -0.54310E-01
        0.13117E+00     0.0     -0.51339E-01
        0.10564E+00     0.0     -0.47753E-01
        0.82428E-01     0.0     -0.43572E-01
        0.61717E-01     0.0     -0.38825E-01
        0.43684E-01     0.0     -0.33541E-01
        0.28501E-01     0.0     -0.27752E-01
        0.16337E-01     0.0     -0.21479E-01
        0.73750E-02     0.0     -0.14730E-01
        0.18480E-02     0.0     -0.75170E-02
        0.00000E+00     0.0      0.00000E+00
   2    1
  41
        0.00000E+00     0.0     0.00000E+00
        0.18480E-02     0.0     0.75170E-02
        0.73750E-02     0.0     0.14730E-01
        0.16338E-01     0.0     0.21479E-01
        0.28501E-01     0.0     0.27752E-01
        0.43684E-01     0.0     0.33541E-01
        0.61716E-01     0.0     0.38825E-01
        0.82428E-01     0.0     0.43572E-01
        0.10564E+00     0.0     0.47753E-01
        0.13117E+00     0.0     0.51339E-01
        0.15882E+00     0.0     0.54310E-01
        0.18841E+00     0.0     0.56656E-01
        0.21973E+00     0.0     0.58374E-01
        0.25259E+00     0.0     0.59476E-01
```

```
      0.28677E+00     0.0     0.59978E-01
      0.32208E+00     0.0     0.59909E-01
      0.35831E+00     0.0     0.59304E-01
      0.39526E+00     0.0     0.58203E-01
      0.43273E+00     0.0     0.56653E-01
      0.47054E+00     0.0     0.54702E-01
      0.50846E+00     0.0     0.52398E-01
      0.54633E+00     0.0     0.49792E-01
      0.58394E+00     0.0     0.46931E-01
      0.62111E+00     0.0     0.43863E-01
      0.65765E+00     0.0     0.40632E-01
      0.69336E+00     0.0     0.37282E-01
      0.72808E+00     0.0     0.33853E-01
      0.76160E+00     0.0     0.30387E-01
      0.79375E+00     0.0     0.26920E-01
      0.82436E+00     0.0     0.23494E-01
      0.85323E+00     0.0     0.20146E-01
      0.88019E+00     0.0     0.16915E-01
      0.90508E+00     0.0     0.13843E-01
      0.92771E+00     0.0     0.10971E-01
      0.94792E+00     0.0     0.83390E-02
      0.96555E+00     0.0     0.59930E-02
      0.98043E+00     0.0     0.39740E-02
      0.99239E+00     0.0     0.23220E-02
      0.10013E+01     0.0     0.10810E-02
      0.10069E+01     0.0     0.28900E-03
      0.10089E+01     0.0     0.00000E+00
  3   1
41
      0.10089E+01   2.0178       0.00000E+00
      0.10069E+01   2.0178      -0.28900E-03
      0.10013E+01   2.0178      -0.10810E-02
      0.99239E+00   2.0178      -0.23220E-02
      0.98043E+00   2.0178      -0.39740E-02
      0.96555E+00   2.0178      -0.59930E-02
      0.94792E+00   2.0178      -0.83390E-02
      0.92771E+00   2.0178      -0.10971E-01
      0.90508E+00   2.0178      -0.13843E-01
      0.88019E+00   2.0178      -0.16915E-01
      0.85323E+00   2.0178      -0.20146E-01
      0.82436E+00   2.0178      -0.23494E-01
      0.79375E+00   2.0178      -0.26920E-01
      0.76160E+00   2.0178      -0.30386E-01
      0.72808E+00   2.0178      -0.33853E-01
      0.69336E+00   2.0178      -0.37281E-01
      0.65765E+00   2.0178      -0.40632E-01
      0.62111E+00   2.0178      -0.43863E-01
      0.58394E+00   2.0178      -0.46931E-01
      0.54633E+00   2.0178      -0.49791E-01
      0.50846E+00   2.0178      -0.52398E-01
      0.47053E+00   2.0178      -0.54701E-01
      0.43273E+00   2.0178      -0.56653E-01
      0.39526E+00   2.0178      -0.58203E-01
      0.35831E+00   2.0178      -0.59303E-01
      0.32208E+00   2.0178      -0.59908E-01
      0.28677E+00   2.0178      -0.59978E-01
      0.25259E+00   2.0178      -0.59475E-01
      0.21973E+00   2.0178      -0.58374E-01
      0.18841E+00   2.0178      -0.56655E-01
      0.15882E+00   2.0178      -0.54310E-01
      0.13117E+00   2.0178      -0.51339E-01
      0.10564E+00   2.0178      -0.47753E-01
      0.82428E-01   2.0178      -0.43572E-01
      0.61717E-01   2.0178      -0.38825E-01
      0.43684E-01   2.0178      -0.33541E-01
      0.28501E-01   2.0178      -0.27752E-01
      0.16337E-01   2.0178      -0.21479E-01
      0.73750E-02   2.0178      -0.14730E-01
      0.18480E-02   2.0178      -0.75170E-02
      0.00000E+00   2.0178       0.00000E+00
      4    1
41
      0.00000E+00   2.0178      0.00000E+00
      0.18480E-02   2.0178      0.75170E-02
      0.73750E-02   2.0178      0.14730E-01
      0.16338E-01   2.0178      0.21479E-01
      0.28501E-01   2.0178      0.27752E-01
      0.43684E-01   2.0178      0.33541E-01
      0.61716E-01   2.0178      0.38825E-01
      0.82428E-01   2.0178      0.43572E-01
      0.10564E+00   2.0178      0.47753E-01
      0.13117E+00   2.0178      0.51339E-01
      0.15882E+00   2.0178      0.54310E-01
      0.18841E+00   2.0178      0.56656E-01
      0.21973E+00   2.0178      0.58374E-01
      0.25259E+00   2.0178      0.59476E-01
      0.28677E+00   2.0178      0.59978E-01
      0.32208E+00   2.0178      0.59909E-01
      0.35831E+00   2.0178      0.59304E-01
      0.39526E+00   2.0178      0.58203E-01
      0.43273E+00   2.0178      0.56653E-01
      0.47054E+00   2.0178      0.54702E-01
      0.50846E+00   2.0178      0.52398E-01
      0.54633E+00   2.0178      0.49792E-01
      0.58394E+00   2.0178      0.46931E-01
```

```
   0.62111E+00   2.0178      0.43863E-01
   0.65765E+00   2.0178      0.40632E-01
   0.69336E+00   2.0178      0.37282E-01
   0.72808E+00   2.0178      0.33853E-01
   0.76160E+00   2.0178      0.30387E-01
   0.79375E+00   2.0178      0.26920E-01
   0.82436E+00   2.0178      0.23494E-01
   0.85323E+00   2.0178      0.20146E-01
   0.88019E+00   2.0178      0.16915E-01
   0.90508E+00   2.0178      0.13843E-01
   0.92771E+00   2.0178      0.10971E-01
   0.94792E+00   2.0178      0.83390E-02
   0.96555E+00   2.0178      0.59930E-02
   0.98043E+00   2.0178      0.39740E-02
   0.99239E+00   2.0178      0.23220E-02
   0.10013E+01   2.0178      0.10810E-02
   0.10069E+01   2.0178      0.28900E-03
   0.10089E+01   2.0178      0.00000E+00
 5   1
   2
          0.      0.       0.
          0.      .9074    0.
 6   1
   2
          1.0089    0      0.
          1.0089  .9074    0.
 7   1
   2
        -15.        0.     0.
          0.        0.     0.
 8   1
   2
          1.0089    0.     0.
         15.        0.     0.
 9   1
   2
        -15.        0.     0.
        -15.        0.    10.
10   1
   2
         15.        0.     0.
         15.        0.    10.
11   1
   2
        -15.        0.   -10.
        -15.        0.     0.
12   1
   2
         15.        0.   -10.
         15.        0.     0.
13   1
   2
        -15.        0.   -10.
         15.        0.   -10.
14   1
   2
        -15.        0.    10.
         15.        0.    10.
15   1
   2
        -15.       10.    10.
         15.       10.    10.
16   1
   2
        -15.       10.   -10.
         15.       10.   -10.
17   1
   2
        -15.        0.    10.
        -15.       10.    10.
18   1
   2
        -15.       10.    10.
        -15.       10.   -10.
19   1
   2
        -15.        0.   -10.
        -15.       10.   -10.
20   1
   2
         15.        0.    10.
         15.       10.    10.
21   1
   2
         15.       10.    10.
         15.       10.   -10.
22   1
   2
         15.        0.   -10.
         15.       10.   -10.
23   1
 29
   0.00000E+00    .9074   0.00000E+00
   0.18480E-02    .9074   0.75170E-02
   0.73750E-02    .9074   0.14730E-01
```

```
      0.16338E-01     .9074    0.21479E-01
      0.28501E-01     .9074    0.27752E-01
      0.43684E-01     .9074    0.33541E-01
      0.61716E-01     .9074    0.38825E-01
      0.82428E-01     .9074    0.43572E-01
      0.10564E+00     .9074    0.47753E-01
      0.13117E+00     .9074    0.51339E-01
      0.15882E+00     .9074    0.54310E-01
      0.18841E+00     .9074    0.56656E-01
      0.21973E+00     .9074    0.58374E-01
      0.25259E+00     .9074    0.59476E-01
      0.28677E+00     .9074    0.59978E-01
      0.32208E+00     .9074    0.59909E-01
      0.35831E+00     .9074    0.59304E-01
      0.39526E+00     .9074    0.58203E-01
      0.43273E+00     .9074    0.56653E-01
      0.47054E+00     .9074    0.54702E-01
      0.50846E+00     .9074    0.52398E-01
      0.54633E+00     .9074    0.49792E-01
      0.58394E+00     .9074    0.46931E-01
      0.62111E+00     .9074    0.43863E-01
      0.65765E+00     .9074    0.40632E-01
      0.69336E+00     .9074    0.37282E-01
      0.72808E+00     .9074    0.33853E-01
      0.76160E+00     .9074    0.30387E-01
      0.79375E+00     .9074    0.26920E-01
   24     1
   13
      0.79375E+00     .9074    0.26920E-01
      0.82436E+00     .9074    0.23494E-01
      0.85323E+00     .9074    0.20146E-01
      0.88019E+00     .9074    0.16915E-01
      0.90508E+00     .9074    0.13843E-01
      0.92771E+00     .9074    0.10971E-01
      0.94792E+00     .9074    0.83390E-02
      0.96555E+00     .9074    0.59930E-02
      0.98043E+00     .9074    0.39740E-02
      0.99239E+00     .9074    0.23220E-02
      0.10013E+01     .9074    0.10810E-02
      0.10069E+01     .9074    0.28900E-03
      0.10089E+01     .9074    0.00000E+00
   25    1
   13
      0.10089E+01     .9074     0.00000E+00
      0.10069E+01     .9074    -0.28900E-03
      0.10013E+01     .9074    -0.10810E-02
      0.99239E+00     .9074    -0.23220E-02
      0.98043E+00     .9074    -0.39740E-02
      0.96555E+00     .9074    -0.59930E-02
      0.94792E+00     .9074    -0.83390E-02
      0.92771E+00     .9074    -0.10971E-01
      0.90508E+00     .9074    -0.13843E-01
      0.88019E+00     .9074    -0.16915E-01
      0.85323E+00     .9074    -0.20146E-01
      0.82436E+00     .9074    -0.23494E-01
      0.79375E+00     .9074    -0.26920E-01
  26     1
  29
      0.79375E+00     .9074    -0.26920E-01
      0.76160E+00     .9074    -0.30386E-01
      0.72808E+00     .9074    -0.33853E-01
      0.69336E+00     .9074    -0.37281E-01
      0.65765E+00     .9074    -0.40632E-01
      0.62111E+00     .9074    -0.43863E-01
      0.58394E+00     .9074    -0.46931E-01
      0.54633E+00     .9074    -0.49791E-01
      0.50846E+00     .9074    -0.52398E-01
      0.47053E+00     .9074    -0.54701E-01
      0.43273E+00     .9074    -0.56653E-01
      0.39526E+00     .9074    -0.58203E-01
      0.35831E+00     .9074    -0.59303E-01
      0.32208E+00     .9074    -0.59908E-01
      0.28677E+00     .9074    -0.59978E-01
      0.25259E+00     .9074    -0.59475E-01
      0.21973E+00     .9074    -0.58374E-01
      0.18841E+00     .9074    -0.56655E-01
      0.15882E+00     .9074    -0.54310E-01
      0.13117E+00     .9074    -0.51339E-01
      0.10564E+00     .9074    -0.47753E-01
      0.82428E-01     .9074    -0.43572E-01
      0.61717E-01     .9074    -0.38825E-01
      0.43684E-01     .9074    -0.33541E-01
      0.28501E-01     .9074    -0.27752E-01
      0.16337E-01     .9074    -0.21479E-01
      0.73750E-02     .9074    -0.14730E-01
      0.18480E-02     .9074    -0.75170E-02
      0.00000E+00     .9074     0.00000E+00
 27    1
  29
      0.00000E+00   1.51312   0.00000E+00
      0.18480E-02   1.51312   0.75170E-02
      0.73750E-02   1.51312   0.14730E-01
      0.16338E-01   1.51312   0.21479E-01
      0.28501E-01   1.51312   0.27752E-01
      0.43684E-01   1.51312   0.33541E-01
```

```
    0.61716E-01   1.51312  0.38825E-01
    0.82428E-01   1.51312  0.43572E-01
    0.10564E+00   1.51312  0.47753E-01
    0.13117E+00   1.51312  0.51339E-01
    0.15882E+00   1.51312  0.54310E-01
    0.18841E+00   1.51312  0.56656E-01
    0.21973E+00   1.51312  0.58374E-01
    0.25259E+00   1.51312  0.59476E-01
    0.28677E+00   1.51312  0.59978E-01
    0.32208E+00   1.51312  0.59909E-01
    0.35831E+00   1.51312  0.59304E-01
    0.39526E+00   1.51312  0.58203E-01
    0.43273E+00   1.51312  0.56653E-01
    0.47054E+00   1.51312  0.54702E-01
    0.50846E+00   1.51312  0.52398E-01
    0.54633E+00   1.51312  0.49792E-01
    0.58394E+00   1.51312  0.46931E-01
    0.62111E+00   1.51312  0.43863E-01
    0.65765E+00   1.51312  0.40632E-01
    0.69336E+00   1.51312  0.37282E-01
    0.72808E+00   1.51312  0.33853E-01
    0.76160E+00   1.51312  0.30387E-01
    0.79375E+00   1.51312  0.26920E-01
28   1
 13
    0.79375E+00   1.51312  0.26920E-01
    0.82436E+00   1.51312  0.23494E-01
    0.85323E+00   1.51312  0.20146E-01
    0.88019E+00   1.51312  0.16915E-01
    0.90508E+00   1.51312  0.13843E-01
    0.92771E+00   1.51312  0.10971E-01
    0.94792E+00   1.51312  0.83390E-02
    0.96555E+00   1.51312  0.59930E-02
    0.98043E+00   1.51312  0.39740E-02
    0.99239E+00   1.51312  0.23220E-02
    0.10013E+01   1.51312  0.10810E-02
    0.10069E+01   1.51312  0.28900E-03
    0.10089E+01   1.51312  0.00000E+00
29    1
  13
    0.10089E+01   1.51312   0.00000E+00
    0.10069E+01   1.51312  -0.28900E-03
    0.10013E+01   1.51312  -0.10810E-02
    0.99239E+00   1.51312  -0.23220E-02
    0.98043E+00   1.51312  -0.39740E-02
    0.96555E+00   1.51312  -0.59930E-02
    0.94792E+00   1.51312  -0.83390E-02
    0.92771E+00   1.51312  -0.10971E-01
    0.90508E+00   1.51312  -0.13843E-01
    0.88019E+00   1.51312  -0.16915E-01
    0.85323E+00   1.51312  -0.20146E-01
    0.82436E+00   1.51312  -0.23494E-01
    0.79375E+00   1.51312  -0.26920E-01
 30    1
 29
    0.79375E+00   1.51312  -0.26920E-01
    0.76160E+00   1.51312  -0.30386E-01
    0.72808E+00   1.51312  -0.33853E-01
    0.69336E+00   1.51312  -0.37281E-01
    0.65765E+00   1.51312  -0.40632E-01
    0.62111E+00   1.51312  -0.43863E-01
    0.58394E+00   1.51312  -0.46931E-01
    0.54633E+00   1.51312  -0.49791E-01
    0.50846E+00   1.51312  -0.52398E-01
    0.47053E+00   1.51312  -0.54701E-01
    0.43273E+00   1.51312  -0.56653E-01
    0.39526E+00   1.51312  -0.58203E-01
    0.35831E+00   1.51312  -0.59303E-01
    0.32208E+00   1.51312  -0.59908E-01
    0.28677E+00   1.51312  -0.59978E-01
    0.25259E+00   1.51312  -0.59475E-01
    0.21973E+00   1.51312  -0.58374E-01
    0.18841E+00   1.51312  -0.56655E-01
    0.15882E+00   1.51312  -0.54310E-01
    0.13117E+00   1.51312  -0.51339E-01
    0.10564E+00   1.51312  -0.47753E-01
    0.82428E-01   1.51312  -0.43572E-01
    0.61717E-01   1.51312  -0.38825E-01
    0.43684E-01   1.51312  -0.33541E-01
    0.28501E-01   1.51312  -0.27752E-01
    0.16337E-01   1.51312  -0.21479E-01
    0.73750E-02   1.51312  -0.14730E-01
    0.18480E-02   1.51312  -0.75170E-02
    0.00000E+00   1.51312   0.00000E+00
 31    1
  2
    0.79375E+00    .9074    0.26920E-01
    0.79375E+00   1.51312   0.26920E-01
 32    1
  2
    0.79375E+00    .9074   -0.26920E-01
    0.79375E+00   1.51312  -0.26920E-01
 33    1
  2
    0.10089E+01    .9074   0.00000E+00
```

```
        0.10089E+01   1.51312  0.00000E+00
     34    1
      2
        0.10089E+01   1.51312  0.00000E+00
        0.10089E+01   2.0178  0.00000E+00
     35    1
      2
        0.00000E+00    .9074   0.00000E+00
        0.00000E+00   1.51312  0.00000E+00
     36    1
      2
        0.00000E+00   1.51312  0.00000E+00
        0.00000E+00   2.0178  0.00000E+00
$ STARS 5.3.3  Support Surfaces Definitions and Orientation
C STARS 5.3.3.1 ISS, ITSF
    1  1
C STARS 5.3.3.2 NU, NV
   41   2
C STARS 5.3.3.3 ((CSP(I,J), J=1,3),I=1,NU*NV)
        0.10089E+01     0.0     0.00000E+00
        0.10069E+01     0.0    -0.28900E-03
        0.10013E+01     0.0    -0.10810E-02
        0.99239E+00     0.0    -0.23220E-02
        0.98043E+00     0.0    -0.39740E-02
        0.96555E+00     0.0    -0.59930E-02
        0.94792E+00     0.0    -0.83390E-02
        0.92771E+00     0.0    -0.10971E-01
        0.90508E+00     0.0    -0.13843E-01
        0.88019E+00     0.0    -0.16915E-01
        0.85323E+00     0.0    -0.20146E-01
        0.82436E+00     0.0    -0.23494E-01
        0.79375E+00     0.0    -0.26920E-01
        0.76160E+00     0.0    -0.30386E-01
        0.72808E+00     0.0    -0.33853E-01
        0.69336E+00     0.0    -0.37281E-01
        0.65765E+00     0.0    -0.40632E-01
        0.62111E+00     0.0    -0.43863E-01
        0.58394E+00     0.0    -0.46931E-01
        0.54633E+00     0.0    -0.49791E-01
        0.50846E+00     0.0    -0.52398E-01
        0.47053E+00     0.0    -0.54701E-01
        0.43273E+00     0.0    -0.56653E-01
        0.39526E+00     0.0    -0.58203E-01
        0.35831E+00     0.0    -0.59303E-01
        0.32208E+00     0.0    -0.59908E-01
        0.28677E+00     0.0    -0.59978E-01
        0.25259E+00     0.0    -0.59475E-01
        0.21973E+00     0.0    -0.58374E-01
        0.18841E+00     0.0    -0.56655E-01
        0.15882E+00     0.0    -0.54310E-01
        0.13117E+00     0.0    -0.51339E-01
        0.10564E+00     0.0    -0.47753E-01
        0.82428E-01     0.0    -0.43572E-01
        0.61717E-01     0.0    -0.38825E-01
        0.43684E-01     0.0    -0.33541E-01
        0.28501E-01     0.0    -0.27752E-01
        0.16337E-01     0.0    -0.21479E-01
        0.73750E-02     0.0    -0.14730E-01
        0.18480E-02     0.0    -0.75170E-02
        0.00000E+00     0.0     0.00000E+00
        0.10089E+01   .9074         0.00000E+00
        0.10069E+01    .9074       -0.28900E-03
        0.10013E+01    .9074       -0.10810E-02
        0.99239E+00    .9074       -0.23220E-02
        0.98043E+00    .9074       -0.39740E-02
        0.96555E+00    .9074       -0.59930E-02
        0.94792E+00    .9074       -0.83390E-02
        0.92771E+00    .9074       -0.10971E-01
        0.90508E+00    .9074       -0.13843E-01
        0.88019E+00    .9074       -0.16915E-01
        0.85323E+00    .9074       -0.20146E-01
        0.82436E+00    .9074       -0.23494E-01
        0.79375E+00    .9074       -0.26920E-01
        0.76160E+00    .9074       -0.30386E-01
        0.72808E+00    .9074       -0.33853E-01
        0.69336E+00    .9074       -0.37281E-01
        0.65765E+00    .9074       -0.40632E-01
        0.62111E+00    .9074       -0.43863E-01
        0.58394E+00    .9074       -0.46931E-01
        0.54633E+00    .9074       -0.49791E-01
        0.50846E+00    .9074       -0.52398E-01
        0.47053E+00    .9074       -0.54701E-01
        0.43273E+00    .9074       -0.56653E-01
        0.39526E+00    .9074       -0.58203E-01
        0.35831E+00    .9074       -0.59303E-01
        0.32208E+00    .9074       -0.59908E-01
        0.28677E+00    .9074       -0.59978E-01
        0.25259E+00    .9074       -0.59475E-01
        0.21973E+00    .9074       -0.58374E-01
        0.18841E+00    .9074       -0.56655E-01
        0.15882E+00    .9074       -0.54310E-01
        0.13117E+00    .9074       -0.51339E-01
        0.10564E+00    .9074       -0.47753E-01
        0.82428E-01    .9074       -0.43572E-01
        0.61717E-01    .9074       -0.38825E-01
      0.43684E-01    .9074       -0.33541E-01
      0.28501E-01    .9074       -0.27752E-01
      0.16337E-01    .9074       -0.21479E-01
      0.73750E-02    .9074       -0.14730E-01
      0.18480E-02    .9074       -0.75170E-02
      0.00000E+00    .9074        0.00000E+00
 2  1
41   2
     0.00000E+00     0.0     0.00000E+00
      0.18480E-02     0.0     0.75170E-02
      0.73750E-02     0.0     0.14730E-01
      0.16338E-01     0.0     0.21479E-01
      0.28501E-01     0.0     0.27752E-01
      0.43684E-01     0.0     0.33541E-01
      0.61716E-01     0.0     0.38825E-01
      0.82428E-01     0.0     0.43572E-01
      0.10564E+00     0.0     0.47753E-01
      0.13117E+00     0.0     0.51339E-01
      0.15882E+00     0.0     0.54310E-01
      0.18841E+00     0.0     0.56656E-01
      0.21973E+00     0.0     0.58374E-01
      0.25259E+00     0.0     0.59476E-01
      0.28677E+00     0.0     0.59978E-01
      0.32208E+00     0.0     0.59909E-01
      0.35831E+00     0.0     0.59304E-01
      0.39526E+00     0.0     0.58203E-01
      0.43273E+00     0.0     0.56653E-01
      0.47054E+00     0.0     0.54702E-01
      0.50846E+00     0.0     0.52398E-01
      0.54633E+00     0.0     0.49792E-01
      0.58394E+00     0.0     0.46931E-01
      0.62111E+00     0.0     0.43863E-01
      0.65765E+00     0.0     0.40632E-01
      0.69336E+00     0.0     0.37282E-01
      0.72808E+00     0.0     0.33853E-01
      0.76160E+00     0.0     0.30387E-01
      0.79375E+00     0.0     0.26920E-01
      0.82436E+00     0.0     0.23494E-01
      0.85323E+00     0.0     0.20146E-01
      0.88019E+00     0.0     0.16915E-01
      0.90508E+00     0.0     0.13843E-01
      0.92771E+00     0.0     0.10971E-01
      0.94792E+00     0.0     0.83390E-02
      0.96555E+00     0.0     0.59930E-02
      0.98043E+00     0.0     0.39740E-02
      0.99239E+00     0.0     0.23220E-02
      0.10013E+01     0.0     0.10810E-02
      0.10069E+01     0.0     0.28900E-03
      0.10089E+01     0.0     0.00000E+00
      0.00000E+00    .9074       0.00000E+00
      0.18480E-02    .9074       0.75170E-02
      0.73750E-02    .9074       0.14730E-01
      0.16338E-01    .9074       0.21479E-01
      0.28501E-01    .9074       0.27752E-01
      0.43684E-01    .9074       0.33541E-01
      0.61716E-01    .9074       0.38825E-01
      0.82428E-01    .9074       0.43572E-01
      0.10564E+00    .9074       0.47753E-01
      0.13117E+00    .9074       0.51339E-01
      0.15882E+00    .9074       0.54310E-01
      0.18841E+00    .9074       0.56656E-01
      0.21973E+00    .9074       0.58374E-01
      0.25259E+00    .9074       0.59476E-01
      0.28677E+00    .9074       0.59978E-01
      0.32208E+00    .9074       0.59909E-01
      0.35831E+00    .9074       0.59304E-01
      0.39526E+00    .9074       0.58203E-01
      0.43273E+00    .9074       0.56653E-01
      0.47054E+00    .9074       0.54702E-01
      0.50846E+00    .9074       0.52398E-01
      0.54633E+00    .9074       0.49792E-01
      0.58394E+00    .9074       0.46931E-01
      0.62111E+00    .9074       0.43863E-01
      0.65765E+00    .9074       0.40632E-01
      0.69336E+00    .9074       0.37282E-01
      0.72808E+00    .9074       0.33853E-01
      0.76160E+00    .9074       0.30387E-01
      0.79375E+00    .9074       0.26920E-01
      0.82436E+00    .9074       0.23494E-01
      0.85323E+00    .9074       0.20146E-01
      0.88019E+00    .9074       0.16915E-01
      0.90508E+00    .9074       0.13843E-01
      0.92771E+00    .9074       0.10971E-01
      0.94792E+00    .9074       0.83390E-02
      0.96555E+00    .9074       0.59930E-02
      0.98043E+00    .9074       0.39740E-02
      0.99239E+00    .9074       0.23220E-02
      0.10013E+01    .9074       0.10810E-02
      0.10069E+01    .9074       0.28900E-03
      0.10089E+01    .9074       0.00000E+00
 3    1
 2    41
      0.00000E+00   2.0178       0.00000E+00
      0.00000E+00   2.0178       0.00000E+00
      0.18480E-02   2.0178      -0.75170E-02
      0.18480E-02   2.0178       0.75170E-02
      0.73750E-02   2.0178      -0.14730E-01
      0.73750E-02   2.0178       0.14730E-01
      0.16338E-01   2.0178      -0.21479E-01
      0.16338E-01   2.0178       0.21479E-01
      0.28501E-01   2.0178      -0.27752E-01
      0.28501E-01   2.0178       0.27752E-01
      0.43684E-01   2.0178      -0.33541E-01
      0.43684E-01   2.0178       0.33541E-01
      0.61716E-01   2.0178      -0.38825E-01
      0.61716E-01   2.0178       0.38825E-01
      0.82428E-01   2.0178      -0.43572E-01
      0.82428E-01   2.0178       0.43572E-01
      0.10564E+00   2.0178      -0.47753E-01
      0.10564E+00   2.0178       0.47753E-01
      0.13117E+00   2.0178      -0.51339E-01
      0.13117E+00   2.0178       0.51339E-01
      0.15882E+00   2.0178      -0.54310E-01
      0.15882E+00   2.0178       0.54310E-01
      0.18841E+00   2.0178      -0.56656E-01
      0.18841E+00   2.0178       0.56656E-01
      0.21973E+00   2.0178      -0.58374E-01
      0.21973E+00   2.0178       0.58374E-01
      0.25259E+00   2.0178      -0.59476E-01
      0.25259E+00   2.0178       0.59476E-01
      0.28677E+00   2.0178      -0.59978E-01
      0.28677E+00   2.0178       0.59978E-01
      0.32208E+00   2.0178      -0.59909E-01
      0.32208E+00   2.0178       0.59909E-01
      0.35831E+00   2.0178      -0.59304E-01
      0.35831E+00   2.0178       0.59304E-01
      0.39526E+00   2.0178      -0.58203E-01
      0.39526E+00   2.0178       0.58203E-01
      0.43273E+00   2.0178      -0.56653E-01
      0.43273E+00   2.0178       0.56653E-01
      0.47054E+00   2.0178      -0.54702E-01
      0.47054E+00   2.0178       0.54702E-01
      0.50846E+00   2.0178      -0.52398E-01
      0.50846E+00   2.0178       0.52398E-01
      0.54633E+00   2.0178      -0.49792E-01
      0.54633E+00   2.0178       0.49792E-01
      0.58394E+00   2.0178      -0.46931E-01
      0.58394E+00   2.0178       0.46931E-01
      0.62111E+00   2.0178      -0.43863E-01
      0.62111E+00   2.0178       0.43863E-01
      0.65765E+00   2.0178      -0.40632E-01
      0.65765E+00   2.0178       0.40632E-01
      0.69336E+00   2.0178      -0.37282E-01
      0.69336E+00   2.0178       0.37282E-01
      0.72808E+00   2.0178      -0.33853E-01
      0.72808E+00   2.0178       0.33853E-01
      0.76160E+00   2.0178      -0.30387E-01
      0.76160E+00   2.0178       0.30387E-01
      0.79375E+00   2.0178      -0.26920E-01
      0.79375E+00   2.0178       0.26920E-01
      0.82436E+00   2.0178      -0.23494E-01
      0.82436E+00   2.0178       0.23494E-01
      0.85323E+00   2.0178      -0.20146E-01
      0.85323E+00   2.0178       0.20146E-01
      0.88019E+00   2.0178      -0.16915E-01
      0.88019E+00   2.0178       0.16915E-01
      0.90508E+00   2.0178      -0.13843E-01
      0.90508E+00   2.0178       0.13843E-01
      0.92771E+00   2.0178      -0.10971E-01
      0.92771E+00   2.0178       0.10971E-01
      0.94792E+00   2.0178      -0.83390E-02
      0.94792E+00   2.0178       0.83390E-02
      0.96555E+00   2.0178      -0.59930E-02
      0.96555E+00   2.0178       0.59930E-02
      0.98043E+00   2.0178      -0.39740E-02
      0.98043E+00   2.0178       0.39740E-02
      0.99239E+00   2.0178      -0.23220E-02
      0.99239E+00   2.0178       0.23220E-02
      0.10013E+01   2.0178      -0.10810E-02
      0.10013E+01   2.0178       0.10810E-02
      0.10069E+01   2.0178      -0.28900E-03
      0.10069E+01   2.0178       0.28900E-03
      0.10089E+01   2.0178       0.00000E+00
      0.10089E+01   2.0178       0.00000E+00
4    1
2    2
          -15.         10.     10.
           15.         10.     10.
          -15.          0.     10.
           15.          0.     10.
5    1
2    2
          -15.         10.    -10.
           15.         10.    -10.
          -15.         10.     10.
           15.         10.     10.
6    1
2    2
          -15.          0.    -10.
           15.          0.    -10.
```

```
         -15.        10.   -10.
          15.        10.   -10.
 7   1
  2   2
         -15.         0.   -10.
         -15.        10.   -10.
         -15.         0.    10.
         -15.        10.    10.
 8   1
  2   2
          15.         0.    10.
          15.        10.    10.
          15.         0.   -10.
          15.        10.   -10.
 9   1
 2   2
         -15.      0       10.
          15.      0       10.
         -15.      0.      0.
          15.      0.      0.
 10    1
  2    2
         -15       0.      0.
          15.      0.      0.
         -15.      0.     -10.
          15.      0.     -10.
11   1
 29    2
      0.79375E+00    .9074   -0.26920E-01
      0.76160E+00    .9074   -0.30386E-01
      0.72808E+00    .9074   -0.33853E-01
      0.69336E+00    .9074   -0.37281E-01
      0.65765E+00    .9074   -0.40632E-01
      0.62111E+00    .9074   -0.43863E-01
      0.58394E+00    .9074   -0.46931E-01
      0.54633E+00    .9074   -0.49791E-01
      0.50846E+00    .9074   -0.52398E-01
      0.47053E+00    .9074   -0.54701E-01
      0.43273E+00    .9074   -0.56653E-01
      0.39526E+00    .9074   -0.58203E-01
      0.35831E+00    .9074   -0.59303E-01
      0.32208E+00    .9074   -0.59908E-01
      0.28677E+00    .9074   -0.59978E-01
      0.25259E+00    .9074   -0.59475E-01
      0.21973E+00    .9074   -0.58374E-01
      0.18841E+00    .9074   -0.56655E-01
      0.15882E+00    .9074   -0.54310E-01
      0.13117E+00    .9074   -0.51339E-01
      0.10564E+00    .9074   -0.47753E-01
      0.82428E-01    .9074   -0.43572E-01
      0.61717E-01    .9074   -0.38825E-01
      0.43684E-01    .9074   -0.33541E-01
      0.28501E-01    .9074   -0.27752E-01
      0.16337E-01    .9074   -0.21479E-01
      0.73750E-02    .9074   -0.14730E-01
      0.18480E-02    .9074   -0.75170E-02
      0.00000E+00    .9074    0.00000E+00
      0.79375E+00  1.51312   -0.26920E-01
      0.76160E+00  1.51312   -0.30386E-01
      0.72808E+00  1.51312   -0.33853E-01
      0.69336E+00  1.51312   -0.37281E-01
      0.65765E+00  1.51312   -0.40632E-01
      0.62111E+00  1.51312   -0.43863E-01
      0.58394E+00  1.51312   -0.46931E-01
      0.54633E+00  1.51312   -0.49791E-01
      0.50846E+00  1.51312   -0.52398E-01
      0.47053E+00  1.51312   -0.54701E-01
      0.43273E+00  1.51312   -0.56653E-01
      0.39526E+00  1.51312   -0.58203E-01
      0.35831E+00  1.51312   -0.59303E-01
      0.32208E+00  1.51312   -0.59908E-01
      0.28677E+00  1.51312   -0.59978E-01
      0.25259E+00  1.51312   -0.59475E-01
      0.21973E+00  1.51312   -0.58374E-01
      0.18841E+00  1.51312   -0.56655E-01
      0.15882E+00  1.51312   -0.54310E-01
      0.13117E+00  1.51312   -0.51339E-01
      0.10564E+00  1.51312   -0.47753E-01
      0.82428E-01  1.51312   -0.43572E-01
      0.61717E-01  1.51312   -0.38825E-01
      0.43684E-01  1.51312   -0.33541E-01
      0.28501E-01  1.51312   -0.27752E-01
      0.16337E-01  1.51312   -0.21479E-01
      0.73750E-02  1.51312   -0.14730E-01
      0.18480E-02  1.51312   -0.75170E-02
      0.00000E+00  1.51312    0.00000E+00
12   1
  13  2
      0.10089E+01    .9074    0.00000E+00
      0.10069E+01    .9074   -0.28900E-03
      0.10013E+01    .9074   -0.10810E-02
      0.99239E+00    .9074   -0.23220E-02
      0.98043E+00    .9074   -0.39740E-02
      0.96555E+00    .9074   -0.59930E-02
      0.94792E+00    .9074   -0.83390E-02
```

```
          0.92771E+00     .9074    -0.10971E-01
          0.90508E+00     .9074    -0.13843E-01
          0.88019E+00     .9074    -0.16915E-01
          0.85323E+00     .9074    -0.20146E-01
          0.82436E+00     .9074    -0.23494E-01
          0.79375E+00     .9074    -0.26920E-01
          0.10089E+01    1.51312    0.00000E+00
          0.10069E+01    1.51312   -0.28900E-03
          0.10013E+01    1.51312   -0.10810E-02
          0.99239E+00    1.51312   -0.23220E-02
          0.98043E+00    1.51312   -0.39740E-02
          0.96555E+00    1.51312   -0.59930E-02
          0.94792E+00    1.51312   -0.83390E-02
          0.92771E+00    1.51312   -0.10971E-01
          0.90508E+00    1.51312   -0.13843E-01
          0.88019E+00    1.51312   -0.16915E-01
          0.85323E+00    1.51312   -0.20146E-01
          0.82436E+00    1.51312   -0.23494E-01
          0.79375E+00    1.51312   -0.26920E-01
 13    1
  29    2
         0.00000E+00     .9074    0.00000E+00
          0.18480E-02     .9074    0.75170E-02
          0.73750E-02     .9074    0.14730E-01
          0.16338E-01     .9074    0.21479E-01
          0.28501E-01     .9074    0.27752E-01
          0.43684E-01     .9074    0.33541E-01
          0.61716E-01     .9074    0.38825E-01
          0.82428E-01     .9074    0.43572E-01
          0.10564E+00     .9074    0.47753E-01
          0.13117E+00     .9074    0.51339E-01
          0.15882E+00     .9074    0.54310E-01
          0.18841E+00     .9074    0.56656E-01
          0.21973E+00     .9074    0.58374E-01
          0.25259E+00     .9074    0.59476E-01
          0.28677E+00     .9074    0.59978E-01
          0.32208E+00     .9074    0.59909E-01
          0.35831E+00     .9074    0.59304E-01
          0.39526E+00     .9074    0.58203E-01
          0.43273E+00     .9074    0.56653E-01
          0.47054E+00     .9074    0.54702E-01
          0.50846E+00     .9074    0.52398E-01
          0.54633E+00     .9074    0.49792E-01
          0.58394E+00     .9074    0.46931E-01
          0.62111E+00     .9074    0.43863E-01
          0.65765E+00     .9074    0.40632E-01
          0.69336E+00     .9074    0.37282E-01
          0.72808E+00     .9074    0.33853E-01
          0.76160E+00     .9074    0.30387E-01
          0.79375E+00     .9074    0.26920E-01
          0.00000E+00    1.51312   0.00000E+00
          0.18480E-02    1.51312   0.75170E-02
          0.73750E-02    1.51312   0.14730E-01
          0.16338E-01    1.51312   0.21479E-01
          0.28501E-01    1.51312   0.27752E-01
          0.43684E-01    1.51312   0.33541E-01
          0.61716E-01    1.51312   0.38825E-01
          0.82428E-01    1.51312   0.43572E-01
          0.10564E+00    1.51312   0.47753E-01
          0.13117E+00    1.51312   0.51339E-01
          0.15882E+00    1.51312   0.54310E-01
          0.18841E+00    1.51312   0.56656E-01
          0.21973E+00    1.51312   0.58374E-01
          0.25259E+00    1.51312   0.59476E-01
          0.28677E+00    1.51312   0.59978E-01
          0.32208E+00    1.51312   0.59909E-01
          0.35831E+00    1.51312   0.59304E-01
          0.39526E+00    1.51312   0.58203E-01
          0.43273E+00    1.51312   0.56653E-01
          0.47054E+00    1.51312   0.54702E-01
          0.50846E+00    1.51312   0.52398E-01
          0.54633E+00    1.51312   0.49792E-01
          0.58394E+00    1.51312   0.46931E-01
          0.62111E+00    1.51312   0.43863E-01
          0.65765E+00    1.51312   0.40632E-01
          0.69336E+00    1.51312   0.37282E-01
          0.72808E+00    1.51312   0.33853E-01
          0.76160E+00    1.51312   0.30387E-01
          0.79375E+00    1.51312   0.26920E-01
 14    1
 13    2
          0.79375E+00     .9074    0.26920E-01
          0.82436E+00     .9074    0.23494E-01
          0.85323E+00     .9074    0.20146E-01
          0.88019E+00     .9074    0.16915E-01
          0.90508E+00     .9074    0.13843E-01
          0.92771E+00     .9074    0.10971E-01
          0.94792E+00     .9074    0.83390E-02
          0.96555E+00     .9074    0.59930E-02
          0.98043E+00     .9074    0.39740E-02
          0.99239E+00     .9074    0.23220E-02
          0.10013E+01     .9074    0.10810E-02
          0.10069E+01     .9074    0.28900E-03
          0.10089E+01     .9074    0.00000E+00
          0.79375E+00    1.51312   0.26920E-01
         0.82436E+00   1.51312  0.23494E-01
         0.85323E+00   1.51312  0.20146E-01
         0.88019E+00   1.51312  0.16915E-01
         0.90508E+00   1.51312  0.13843E-01
         0.92771E+00   1.51312  0.10971E-01
         0.94792E+00   1.51312  0.83390E-02
         0.96555E+00   1.51312  0.59930E-02
         0.98043E+00   1.51312  0.39740E-02
         0.99239E+00   1.51312  0.23220E-02
         0.10013E+01   1.51312  0.10810E-02
         0.10069E+01   1.51312  0.28900E-03
         0.10089E+01   1.51312  0.00000E+00
15   1
 41  2
         0.10089E+01   1.51312       0.00000E+00
         0.10069E+01   1.51312      -0.28900E-03
         0.10013E+01   1.51312      -0.10810E-02
         0.99239E+00   1.51312      -0.23220E-02
         0.98043E+00   1.51312      -0.39740E-02
         0.96555E+00   1.51312      -0.59930E-02
         0.94792E+00   1.51312      -0.83390E-02
         0.92771E+00   1.51312      -0.10971E-01
         0.90508E+00   1.51312      -0.13843E-01
         0.88019E+00   1.51312      -0.16915E-01
         0.85323E+00   1.51312      -0.20146E-01
         0.82436E+00   1.51312      -0.23494E-01
         0.79375E+00   1.51312      -0.26920E-01
         0.76160E+00   1.51312      -0.30386E-01
         0.72808E+00   1.51312      -0.33853E-01
         0.69336E+00   1.51312      -0.37281E-01
         0.65765E+00   1.51312      -0.40632E-01
         0.62111E+00   1.51312      -0.43863E-01
         0.58394E+00   1.51312      -0.46931E-01
         0.54633E+00   1.51312      -0.49791E-01
         0.50846E+00   1.51312      -0.52398E-01
         0.47053E+00   1.51312      -0.54701E-01
         0.43273E+00   1.51312      -0.56653E-01
         0.39526E+00   1.51312      -0.58203E-01
         0.35831E+00   1.51312      -0.59303E-01
         0.32208E+00   1.51312      -0.59908E-01
         0.28677E+00   1.51312      -0.59978E-01
         0.25259E+00   1.51312      -0.59475E-01
         0.21973E+00   1.51312      -0.58374E-01
         0.18841E+00   1.51312      -0.56655E-01
         0.15882E+00   1.51312      -0.54310E-01
         0.13117E+00   1.51312      -0.51339E-01
         0.10564E+00   1.51312      -0.47753E-01
         0.82428E-01   1.51312      -0.43572E-01
         0.61717E-01   1.51312      -0.38825E-01
         0.43684E-01   1.51312      -0.33541E-01
         0.28501E-01   1.51312      -0.27752E-01
         0.16337E-01   1.51312      -0.21479E-01
         0.73750E-02   1.51312      -0.14730E-01
         0.18480E-02   1.51312      -0.75170E-02
         0.00000E+00   1.51312       0.00000E+00
         0.10089E+01   2.0178        0.00000E+00
         0.10069E+01   2.0178       -0.28900E-03
         0.10013E+01   2.0178       -0.10810E-02
         0.99239E+00   2.0178       -0.23220E-02
         0.98043E+00   2.0178       -0.39740E-02
         0.96555E+00   2.0178       -0.59930E-02
         0.94792E+00   2.0178       -0.83390E-02
         0.92771E+00   2.0178       -0.10971E-01
         0.90508E+00   2.0178       -0.13843E-01
         0.88019E+00   2.0178       -0.16915E-01
         0.85323E+00   2.0178       -0.20146E-01
         0.82436E+00   2.0178       -0.23494E-01
         0.79375E+00   2.0178       -0.26920E-01
         0.76160E+00   2.0178       -0.30386E-01
         0.72808E+00   2.0178       -0.33853E-01
         0.69336E+00   2.0178       -0.37281E-01
         0.65765E+00   2.0178       -0.40632E-01
         0.62111E+00   2.0178       -0.43863E-01
         0.58394E+00   2.0178       -0.46931E-01
         0.54633E+00   2.0178       -0.49791E-01
         0.50846E+00   2.0178       -0.52398E-01
         0.47053E+00   2.0178       -0.54701E-01
         0.43273E+00   2.0178       -0.56653E-01
         0.39526E+00   2.0178       -0.58203E-01
         0.35831E+00   2.0178       -0.59303E-01
         0.32208E+00   2.0178       -0.59908E-01
         0.28677E+00   2.0178       -0.59978E-01
         0.25259E+00   2.0178       -0.59475E-01
         0.21973E+00   2.0178       -0.58374E-01
         0.18841E+00   2.0178       -0.56655E-01
         0.15882E+00   2.0178       -0.54310E-01
         0.13117E+00   2.0178       -0.51339E-01
         0.10564E+00   2.0178       -0.47753E-01
         0.82428E-01   2.0178       -0.43572E-01
         0.61717E-01   2.0178       -0.38825E-01
         0.43684E-01   2.0178       -0.33541E-01
         0.28501E-01   2.0178       -0.27752E-01
         0.16337E-01   2.0178       -0.21479E-01
         0.73750E-02   2.0178       -0.14730E-01
         0.18480E-02   2.0178       -0.75170E-02
         0.00000E+00   2.0178        0.00000E+00
   16    1
   41    2
         0.00000E+00  1.51312       0.00000E+00
         0.18480E-02  1.51312       0.75170E-02
         0.73750E-02  1.51312       0.14730E-01
         0.16338E-01  1.51312       0.21479E-01
         0.28501E-01  1.51312       0.27752E-01
         0.43684E-01  1.51312       0.33541E-01
         0.61716E-01  1.51312       0.38825E-01
         0.82428E-01  1.51312       0.43572E-01
         0.10564E+00  1.51312       0.47753E-01
         0.13117E+00  1.51312       0.51339E-01
         0.15882E+00  1.51312       0.54310E-01
         0.18841E+00  1.51312       0.56656E-01
         0.21973E+00  1.51312       0.58374E-01
         0.25259E+00  1.51312       0.59476E-01
         0.28677E+00  1.51312       0.59978E-01
         0.32208E+00  1.51312       0.59909E-01
         0:35831E+00  1.51312       0.59304E-01
         0.39526E+00  1.51312       0.58203E-01
         0.43273E+00  1.51312       0.56653E-01
         0.47054E+00  1.51312       0.54702E-01
         0.50846E+00  1.51312       0.52398E-01
         0.54633E+00  1.51312       0.49792E-01
         0.58394E+00  1.51312       0.46931E-01
         0.62111E+00  1.51312       0.43863E-01
         0.65765E+00  1.51312       0.40632E-01
         0.69336E+00  1.51312       0.37282E-01
         0.72808E+00  1.51312       0.33853E-01
         0.76160E+00  1.51312       0.30387E-01
         0.79375E+00  1.51312       0.26920E-01
         0.82436E+00  1.51312       0.23494E-01
         0.85323E+00  1.51312       0.20146E-01
         0.88019E+00  1.51312       0.16915E-01
         0.90508E+00  1.51312       0.13843E-01
         0.92771E+00  1.51312       0.10971E-01
         0.94792E+00  1.51312       0.83390E-02
         0.96555E+00  1.51312       0.59930E-02
         0.98043E+00  1.51312       0.39740E-02
         0.99239E+00  1.51312       0.23220E-02
         0.10013E+01  1.51312       0.10810E-02
         0.10069E+01  1.51312       0.28900E-03
         0.10089E+01  1.51312       0.00000E+00
         0.00000E+00   2.0178       0.00000E+00
         0.18480E-02   2.0178       0.75170E-02
         0.73750E-02   2.0178       0.14730E-01
         0.16338E-01   2.0178       0.21479E-01
         0.28501E-01   2.0178       0.27752E-01
         0.43684E-01   2.0178       0.33541E-01
         0.61716E-01   2.0178       0.38825E-01
         0.82428E-01   2.0178       0.43572E-01
         0.10564E+00   2.0178       0.47753E-01
         0.13117E+00   2.0178       0.51339E-01
         0.15882E+00   2.0178       0.54310E-01
         0.18841E+00   2.0178       0.56656E-01
         0.21973E+00   2.0178       0.58374E-01
         0.25259E+00   2.0178       0.59476E-01
         0.28677E+00   2.0178       0.59978E-01
         0.32208E+00   2.0178       0.59909E-01
         0.35831E+00   2.0178       0.59304E-01
         0.39526E+00   2.0178       0.58203E-01
         0.43273E+00   2.0178       0.56653E-01
         0.47054E+00   2.0178       0.54702E-01
         0.50846E+00   2.0178       0.52398E-01
         0.54633E+00   2.0178       0.49792E-01
         0.58394E+00   2.0178       0.46931E-01
         0.62111E+00   2.0178       0.43863E-01
         0.65765E+00   2.0178       0.40632E-01
         0.69336E+00   2.0178       0.37282E-01
         0.72808E+00   2.0178       0.33853E-01
         0.76160E+00   2.0178       0.30387E-01
         0.79375E+00   2.0178       0.26920E-01
         0.82436E+00   2.0178       0.23494E-01
         0.85323E+00   2.0178       0.20146E-01
         0.88019E+00   2.0178       0.16915E-01
         0.90508E+00   2.0178       0.13843E-01
         0.92771E+00   2.0178       0.10971E-01
         0.94792E+00   2.0178       0.83390E-02
         0.96555E+00   2.0178       0.59930E-02
         0.98043E+00   2.0178       0.39740E-02
         0.99239E+00   2.0178       0.23220E-02
         0.10013E+01   2.0178       0.10810E-02
         0.10069E+01   2.0178       0.28900E-03
         0.10089E+01   2.0178       0.00000E+00
$ STARS 5.3.4 Curved-Edge Definition
C STARS 5.3.4.1  NSG, NRG
   36   16
$ STARS 5.3.4.2 Segments reference
C STARS 5.3.4.3  ISG, IDCV, ITSG
    1    1    1
    2    2    1
    3    3    1
    4    4    1
    5    5    1
   6   6   1
   7   7   1
   8   8   1
   9   9   1
  10  10   1
  11  11   1
  12  12   1
  13  13   1
  14  14   1
  15  15   1
  16  16   1
  17  17   1
  18  18   1
  19  19   1
  20  20   1
  21  21   1
  22  22   1
  23  23   1
  24  24   1
  25  25   1
  26  26   1
  27  27   1
  28  28   1
  29  29   1
  30  30   1
  31  31   1
  32  32   1
  33  33   1
  34  34  ·1
  35  35   1
  36  36   1
$ STARS 5.3.5 Support-Region Definition by Boundary Edges
C STARS 5.3.5.1  IRG, IDSF, ITRG
  1 1 1
C STARS 5.3.5.2  NN
  5
C STARS 5.3.5.2  (ISBS(I),I=1,NN)
       5 -26 -25 -6  1
  2 2 1
  5
      2    6   -24 -23 -5
  3 3 1
  2
      4   3
  4 4 1
  4
    -20  -14  17   15
  5 5 1
  4
      18  16   -21 -15
  6 6 1
  4
     13   22   -16   -19
  7 7 1
  5
     -18   -17  -9 -11  19
  8 8 1
  5
      20  21   -22  12   10
  9  9  1
  6
      14   -10  -8   -2   -7   9
  10  10  1
  6
       7    -1    8   -12  -13   11
  11  11   1
   4
  35 -30  -32   26
  12  12    1
  4
  32  -29 -33 25
  13  13    1
   4
  23  31  -27 -35
  14   14    1
   4
  24  33  -28  -31
  15   15    1
   5
  36  -3  -34  29  30
  16   16   1
  5
  -36  27  28  34  -4
```

Data for the background grid file, **wing.bac**, are given below.

STARS–CFDASE input data:

```
$ STARS 5.2.1 wing.bac - Background mesh ... quasi-2D NACA0012
C STARS 5.2.2 Basic data parmeters:NPBG NEBG NPS NLS NTS
     8     6   0   4   4
```

```
C STARS 5.2.3 Node, nodal coordinates
     1   .10000E+06  -.10000E+06  -.10000E+06
C STARS 5.2.4 x,y,z local-global coordinates, scales factors
   1.00     .00     .00        3.000
    .00    1.00     .00        3.000
    .00     .00    1.00        3.000
     2   .10000E+06   .10000E+06  -.10000E+06
   1.00     .00     .00        3.000
    .00    1.00     .00        3.000
    .00     .00    1.00        3.000
     3  -.10000E+06   .10000E+06  -.10000E+06
   1.00     .00     .00        3.000
    .00    1.00     .00        3.000
    .00     .00    1.00        3.000
     4  -.10000E+06  -.10000E+06  -.10000E+06
   1.00     .00     .00        3.000
    .00    1.00     .00        3.000
    .00     .00    1.00        3.000
     5   .10000E+06  -.10000e+06   .10000E+06
   1.00     .00     .00        3.000
    .00    1.00     .00        3.000
    .00     .00    1.00        3.000
     6   .10000E+06   .10000E+06   .10000E+06
   1.00     .00     .00        3.000
    .00    1.00     .00        3.000
    .00     .00    1.00        3.000
     7  -.10000E+06   .10000E+06   .10000E+06
   1.00     .00     .00        3.000
    .00    1.00     .00        3.000
    .00     .00    1.00        3.000
     8  -.10000E+06  -.10000E+06   .10000E+06
   1.00     .00     .00        3.000
    .00    1.00     .00        3.000
    .00     .00    1.00        3.000
C STARS 5.2.5 Element number, tetrahedral connectivity for background domain
     1     2     1     8     4
     2     2     8     7     4
     3     2     3     4     7
     4     2     8     1     6
     5     2     7     8     6
     6     1     6     8     5
$ STARS 5.2.6 Point Sources Data
$ STARS 5.2.7 Lines Sources Data
$ STARS 5.2.7.1   1.-  leading edge
C STARS 5.2.7.2 Point coordinates: x1,y1,z1,s1,r1,d1
    .00000E+00   .00000E+00   .00000E+00       .015       .050       .089
C STARS 5.2.7.3 Point coordinates: x2,y2,z2,s2,r2,d2
    .00000E+00   .21000E+01   .00000E+01       .015       .050       .089
 2.-  leading edge
    .00000E+00   .00000E+00   .00000E+00       .040       .100       .308
    .00000E+00   .21000E+01   .0000E+01       .040       .100       .308
 3.-  trailing edge
   .1007E+01   .00000E+00   .00000E+00       .025       .050       .179
   .1007E+01   .21000E+01   .00000E+00       .025       .050       .179
 4.-  trailing edge
   .1007E+01   .00000E+00   .00000E+00       .040       .100       .377
   .1007E+01   .21000E+01   .00000E+00       .040       .100       .377
$ STARS 5.2.8 Plane Triangular Sources Data
$ STARS 5.2.8.1   1.- wing
C STARS 5.2.8.2 Point coordinates: x1,y1,z1,s1,r1,d1
   -.10000E+00   .000000E+00   .00000E+00       .04       .160       .500
C STARS 5.2.8.3 Point coordinates: x2,y2,z2,s2,r2,d2
   -.10000E+00   .210000E+01   .00000E+00       .04       .160       .500
C STARS 5.2.8.4 Point coordinates: x3,y3,z3,s3,r3,d3
   .101E+01   .210000E+01   .00000E+00       .04       .160       .500
 2.- wing
   .101E+01   .21000E+01   .00000E+00       .04       .160       .500
   .101E+01   .00000E+00   .00000E+00       .04       .160       .500
   -.10000E+00   .00000E+00   .00000E+00    .04       .160       .50
 3.- control surface
.785           .89          0.                 .01       .02   .05
.785          1.55          0.                 .01       .02   .05
1.01          1.55          0.                0.01       .02   .05
 4.-control surface
1.01          1.55          0.                0.01       .02   .05
1.01           .89          0.                 .01       .02   .05
.785           .89           0.                .01       .02   .05
```

Data for the boundary-condition file, **wing.bco**, are given below.

STARS–CFDASE input data:

```
$ STARS 5.4.1 wing.bco Boundary Condition Flags
C STARS 5.4.2  NRG, NSG
   16,  36,    0
$ STARS 5.4.3 Surface Regions Boundary-Condition Definitions
C STARS 5.4.4  IRG, IBCO
    1   1
```

```
     2   1
     3   1
     4   3
     5   3
     6   3
     7   3
     8   3
     9   2
    10   2
    11   1
    12   1
    13   1
    14   1
    15   1
    16   1
$ STARS 5.4.5 Curved Segments Boundary-Condition Definitions
C STARS 5.4.6  JS, ICBCO
     1    0
     2    0
     3    3
     4    4
     5    0
     6    1
     7    0
     8    0
     9    0
    10    0
    11    0
    12    0
    13    0
    14    0
    15    0
    16    0
    17    0
    18    0
    19    0
    20    0
    21    0
    22    0
    23    0
    24    4
    25    3
    26    0
    27    0
    28    4
    29    3
    30    0
    31    0
    32    0
    33    1
    34    1
    35    0
    36    0
```

Data for the steady CFD solution control file, **wing.cons**, are given below.

STARS–CFDASE input data:

```
 &control
C  STARS 5.5 wing.cons  file, steady state solution control parameters
  nstep     = 700,
  nstou     = 200,
  nstage    = 4,
  cfl       = 1.0,
  diss1     = 1.0,
  diss2     = 1.0,
  relax     = 1.0,
  mach      = 2.0,
  alpha     = 0.0,
  beta      = 0.0,
  restart   = .false.,
  nlimit    = 2,
  lg        = 1,
  nite0     = 1,
  nite1     = 1,
  nite2     = 0,
  ncycl     = 25,
  ncyci     = 25,
  tlr       = 0.0001,
  debug     = .false.,
  meshc     = 1,
  meshf     = 1,
  cbt(1)    = 1.0,
  cbt(2)    = 0.5,
  cbt(3)    = 0.0,
  cbt(4)    = 0.0,
  trans     = .false.,
 /
```

Data for the solids file, **wing.dat**, are given below.

STARS–SOLIDS input data:

```
$ wing solid model for structural analysis.   wing.dat  from preprocess
  486, 1549,    2,    4,    1,    2,    0,    0,    0,    0
    0,    0,    0,    1,    0,    0,    0,    0,    0,    0, 0, 0
    1,    0,    0,    0,    0,    0,    0,    0,    0,    2
    2,    0,    2,    0,    1,    0,    0,    1,    1,    0
    1,   10,    0, 600.0,  0.0,  0.0, 0.0
$ NODAL DATA
     1      .0000     .0000      .0000    1    1    1    1    1    1    0    0    0
     2      .0000     .1000      .0000    0    0    0    0    0    0    0    0    0
    21      .0000    2.0178      .0000    0    0    0    0    0    0    0    0    1
    22      .0074     .0000      .0147    1    1    1    1    1    1    0    0    0
    23      .0074     .1000      .0147    0    0    0    0    0    0    0    0    0
    42      .0074    2.0178      .0147    0    0    0    0    0    0    0    0    1
    43      .0285     .0000      .0277    1    1    1    1    1    1    0    0    0
    44      .0285     .1000      .0277    0    0    0    0    0    0    0    0    0
    63      .0285    2.0178      .0277    0    0    0    0    0    0    0    0    1
    64      .1056     .0000      .0478    1    1    1    1    1    1    0    0    0
    65      .1056     .1000      .0478    0    0    0    0    0    0    0    0    0
    84      .1056    2.0178      .0478    0    0    0    0    0    0    0    0    1
    85      .2197     .0000      .0584    1    1    1    1    1    1    0    0    0
    86      .2197     .1000      .0584    0    0    0    0    0    0    0    0    0
   105      .2197    2.0178      .0584    0    0    0    0    0    0    0    0    1
   106      .3583     .0000      .0593    1    1    1    1    1    1    0    0    0
   107      .3583     .1000      .0593    0    0    0    0    0    0    0    0    0
   126      .3583    2.0178      .0593    0    0    0    0    0    0    0    0    1
   127      .5085     .0000      .0524    1    1    1    1    1    1    0    0    0
   128      .5085     .1000      .0524    0    0    0    0    0    0    0    0    0
   147      .5085    2.0178      .0524    0    0    0    0    0    0    0    0    1
   148      .6576     .0000      .0406    1    1    1    1    1    1    0    0    0
   149      .6576     .1000      .0406    0    0    0    0    0    0    0    0    0
   168      .6576    2.0178      .0406    0    0    0    0    0    0    0    0    1
   169      .7937     .0000      .0269    1    1    1    1    1    1    0    0    0
   170      .7937     .1000      .0269    0    0    0    0    0    0    0    0    0
   189      .7937    2.0178      .0269    0    0    0    0    0    0    0    0    1
   190      .9051     .0000      .0138    1    1    1    1    1    1    0    0    0
   191      .9051     .1000      .0138    0    0    0    0    0    0    0    0    0
   210      .9051    2.0178      .0138    0    0    0    0    0    0    0    0    1
   211      .9804     .0000      .0040    1    1    1    1    1    1    0    0    0
   212      .9804     .1000      .0040    0    0    0    0    0    0    0    0    0
   231      .9804    2.0178      .0040    0    0    0    0    0    0    0    0    1
   232     1.0089     .0000      .0000    1    1    1    1    1    1    0    0    0
   233     1.0089     .1000      .0000    0    0    0    0    0    0    0    0    0
   252     1.0089    2.0178      .0000    0    0    0    0    0    0    0    0    1
   253      .0074     .0000     -.0147    1    1    1    1    1    1    0    0    0
   254      .0074     .1000     -.0147    0    0    0    0    0    0    0    0    0
   273      .0074    2.0178     -.0147    0    0    0    0    0    0    0    0    1
   274      .0285     .0000     -.0277    1    1    1    1    1    1    0    0    0
   275      .0285     .1000     -.0277    0    0    0    0    0    0    0    0    0
   294      .0285    2.0178     -.0277    0    0    0    0    0    0    0    0    1
   295      .1056     .0000     -.0478    1    1    1    1    1    1    0    0    0
   296      .1056     .1000     -.0478    0    0    0    0    0    0    0    0    0
   315      .1056    2.0178     -.0478    0    0    0    0    0    0    0    0    1
   316      .2197     .0000     -.0584    1    1    1    1    1    1    0    0    0
   317      .2197     .1000     -.0584    0    0    0    0    0    0    0    0    0
   336      .2197    2.0178     -.0584    0    0    0    0    0    0    0    0    1
   337      .3583     .0000     -.0593    1    1    1    1    1    1    0    0    0
   338      .3583     .1000     -.0593    0    0    0    0    0    0    0    0    0
   357      .3583    2.0178     -.0593    0    0    0    0    0    0    0    0    1
   358      .5085     .0000     -.0524    1    1    1    1    1    1    0    0    0
   359      .5085     .1000     -.0524    0    0    0    0    0    0    0    0    0
   378      .5085    2.0178     -.0524    0    0    0    0    0    0    0    0    1
   379      .6576     .0000     -.0406    1    1    1    1    1    1    0    0    0
   380      .6576     .1000     -.0406    0    0    0    0    0    0    0    0    0
   399      .6576    2.0178     -.0406    0    0    0    0    0    0    0    0    1
   400      .7937     .0000     -.0269    1    1    1    1    1    1    0    0    0
   401      .7937     .1000     -.0269    0    0    0    0    0    0    0    0    0
   420      .7937    2.0178     -.0269    0    0    0    0    0    0    0    0    1
   421      .9051     .0000     -.0138    1    1    1    1    1    1    0    0    0
   422      .9051     .1000     -.0138    0    0    0    0    0    0    0    0    0
   441      .9051    2.0178     -.0138    0    0    0    0    0    0    0    0    1
   442      .9804     .0000     -.0040    1    1    1    1    1    1    0    0    0
   443      .9804     .1000     -.0040    0    0    0    0    0    0    0    0    0
   462      .9804    2.0178     -.0040    0    0    0    0    0    0    0    0    1
   463     1.0089     .9175      .0000    0    0    0    0    0    0    0    0    0
   464     1.0089    1.5031      .0000    0    0    0    0    0    0    0    0    0
   465      .8244     .9175      .0235    0    0    0    0    0    0    0    0    0
   471      .8244    1.5031      .0235    0    0    0    0    0    0    0    0    1
   472      .9051     .9175      .0138    0    0    0    0    0    0    0    0    0
   473      .9051    1.5031      .0138    0    0    0    0    0    0    0    0    0
   474      .9804     .9175      .0040    0    0    0    0    0    0    0    0    0
   475      .9804    1.5031      .0040    0    0    0    0    0    0    0    0    0
   476      .8244     .9175     -.0235    0    0    0    0    0    0    0    0    0
   482      .8244    1.5031     -.0235    0    0    0    0    0    0    0    0    1
   483      .9051     .9175     -.0138    0    0    0    0    0    0    0    0    0
  484      .9051     1.5031     -.0138    0    0    0    0    0    0    0    0    0
  485      .9804      .9175     -.0040    0    0    0    0    0    0    0    0    0
  486      .9804     1.5031     -.0040    0    0    0    0    0    0    0    0    0
$ ELEMENT CONNECTIVITY CONDITIONS
    3    1    1    2   23    0    0    0    0    0    1    1    0    0    0    0
    3   20   20   21   42    0    0    0    0    0    1    1    0    0    0    1
    3   21   23   22    1    0    0    0    0    0    1    1    0    0    0    0
    3   40   42   41   20    0    0    0    0    0    1    1    0    0    0    1
    3   41   22   23   44    0    0    0    0    0    1    1    0    0    0    0
    3   60   41   42   63    0    0    0    0    0    1    1    0    0    0    1
    3   61   44   43   22    0    0    0    0    0    1    1    0    0    0    0
    3   80   63   62   41    0    0    0    0    0    1    1    0    0    0    1
    3   81   43   44   65    0    0    0    0    0    1    1    0    0    0    0
    3  100   62   63   84    0    0    0    0    0    1    1    0    0    0    1
    3  101   65   64   43    0    0    0    0    0    1    1    0    0    0    0
    3  120   84   83   62    0    0    0    0    0    1    1    0    0    0    1
    3  121   64   65   86    0    0    0    0    0    1    1    0    0    0    0
    3  140   83   84  105    0    0    0    0    0    1    1    0    0    0    1
    3  141   86   85   64    0    0    0    0    0    1    1    0    0    0    0
    3  160  105  104   83    0    0    0    0    0    1    1    0    0    0    1
    3  161   85   86  107    0    0    0    0    0    1    1    0    0    0    0
    3  180  104  105  126    0    0    0    0    0    1    1    0    0    0    1
    3  181  107  106   85    0    0    0    0    0    1    1    0    0    0    0
    3  200  126  125  104    0    0    0    0    0    1    1    0    0    0    1
    3  201  106  107  128    0    0    0    0    0    1    1    0    0    0    0
    3  220  125  126  147    0    0    0    0    0    1    1    0    0    0    1
    3  221  128  127  106    0    0    0    0    0    1    1    0    0    0    0
    3  240  147  146  125    0    0    0    0    0    1    1    0    0    0    1
    3  241  127  128  149    0    0    0    0    0    1    1    0    0    0    0
    3  260  146  147  168    0    0    0    0    0    1    1    0    0    0    1
    3  261  149  148  127    0    0    0    0    0    1    1    0    0    0    0
    3  280  168  167  146    0    0    0    0    0    1    1    0    0    0    1
    3  281  148  149  170    0    0    0    0    0    1    1    0    0    0    0
    3  300  167  168  189    0    0    0    0    0    1    1    0    0    0    1
    3  301  170  169  148    0    0    0    0    0    1    1    0    0    0    0
    3  320  189  188  167    0    0    0    0    0    1    1    0    0    0    1
    3  321  169  170  191    0    0    0    0    0    1    1    0    0    0    0
    3  329  177  178  199    0    0    0    0    0    1    1    0    0    0    1
    3  330  465  466  200    0    0    0    0    0    2    2    0    0    0    0
    3  334  469  470  204    0    0    0    0    0    2    2    0    0    0    1
    3  335  470  471  473    0    0    0    0    0    2    2    0    0    0    0
    3  336  184  185  206    0    0    0    0    0    1    1    0    0    0    0
    3  340  188  189  210    0    0    0    0    0    1    1    0    0    0    1
    3  341  191  190  169    0    0    0    0    0    1    1    0    0    0    0
    3  349  199  198  177    0    0    0    0    0    1    1    0    0    0    1
    3  350  200  472  465    0    0    0    0    0    2    2    0    0    0    0
    3  351  201  200  466    0    0    0    0    0    2    2    0    0    0    0
    3  354  204  203  469    0    0    0    0    0    2    2    0    0    0    1
    3  355  473  204  470    0    0    0    0    0    2    2    0    0    0    0
    3  356  206  205  184    0    0    0    0    0    1    1    0    0    0    0
    3  360  210  209  188    0    0    0    0    0    1    1    0    0    0    1
    3  361  190  191  212    0    0    0    0    0    1    1    0    0    0    0
    3  369  198  199  220    0    0    0    0    0    1    1    0    0    0    1
    3  370  472  200  221    0    0    0    0    0    2    2    0    0    0    0
    3  371  200  201  222    0    0    0    0    0    2    2    0    0    0    0
    3  374  203  204  225    0    0    0    0    0    2    2    0    0    0    1
    3  375  204  473  475    0    0    0    0    0    2    2    0    0    0    0
    3  376  205  206  227    0    0    0    0    0    1    1    0    0    0    0
    3  380  209  210  231    0    0    0    0    0    1    1    0    0    0    1
    3  381  212  211  190    0    0    0    0    0    1    1    0    0    0    0
    3  389  220  219  198    0    0    0    0    0    1    1    0    0    0    1
    3  390  221  474  472    0    0    0    0    0    2    2    0    0    0    0
    3  391  222  221  200    0    0    0    0    0    2    2    0    0    0    0
    3  394  225  224  203    0    0    0    0    0    2    2    0    0    0    1
    3  395  475  225  204    0    0    0    0    0    2    2    0    0    0    0
    3  396  227  226  205    0    0    0    0    0    1    1    0    0    0    0
    3  400  231  230  209    0    0    0    0    0    1    1    0    0    0    1
    3  401  211  212  233    0    0    0    0    0    1    1    0    0    0    0
    3  409  219  220  241    0    0    0    0    0    1    1    0    0    0    1
    3  410  474  221  242    0    0    0    0    0    2    2    0    0    0    0
    3  411  221  222  243    0    0    0    0    0    2    2    0    0    0    0
    3  414  224  225  246    0    0    0    0    0    2    2    0    0    0    1
    3  415  225  475  464    0    0    0    0    0    2    2    0    0    0    0
    3  416  226  227  248    0    0    0    0    0    1    1    0    0    0    0
    3  420  230  231  252    0    0    0    0    0    1    1    0    0    0    1
    3  421  233  232  211    0    0    0    0    0    1    1    0    0    0    0
    3  429  241  240  219    0    0    0    0    0    1    1    0    0    0    1
    3  430  242  463  474    0    0    0    0    0    2    2    0    0    0    0
    3  431  243  242  221    0    0    0    0    0    2    2    0    0    0    0
    3  434  246  245  224    0    0    0    0    0    2    2    0    0    0    1
    3  435  464  246  225    0    0    0    0    0    2    2    0    0    0    0
    3  436  248  247  226    0    0    0    0    0    1    1    0    0    0    0
    3  440  252  251  230    0    0    0    0    0    1    1    0    0    0    1
    3  441    2    1  253    0    0    0    0    0    1    1    0    0    0    0
    3  460   21   20  272    0    0    0    0    0    1    1    0    0    0    1
    3  461  253  254    2    0    0    0    0    0    1    1    0    0    0    0
    3  480  272  273   21    0    0    0    0    0    1    1    0    0    0    1
    3  481  254  253  274    0    0    0    0    0    1    1    0    0    0    0
    3  500  273  272  293    0    0    0    0    0    1    1    0    0    0    1
    3  501  274  275  254    0    0    0    0    0    1    1    0    0    0    0
    3  520  293  294  273    0    0    0    0    0    1    1    0    0    0    1
    3  521  275  274  295    0    0    0    0    0    1    1    0    0    0    0
    3  540  294  293  314    0    0    0    0    0    1    1    0    0    0    1
    3  541  295  296  275    0    0    0    0    0    1    1    0    0    0    0
    3  560  314  315  294    0    0    0    0    0    1    1    0    0    0    1
```

3	561	296	295	316	0	0	0	0	0	1	1	0	0	0	0
3	580	315	314	335	0	0	0	0	0	1	1	0	0	0	1
3	581	316	317	296	0	0	0	0	0	1	1	0	0	0	0
3	600	335	336	315	0	0	0	0	0	1	1	0	0	0	1
3	601	317	316	337	0	0	0	0	0	1	1	0	0	0	0
3	620	336	335	356	0	0	0	0	0	1	1	0	0	0	1
3	621	337	338	317	0	0	0	0	0	1	1	0	0	0	0
3	640	356	357	336	0	0	0	0	0	1	1	0	0	0	1
3	641	338	337	358	0	0	0	0	0	1	1	0	0	0	0
3	660	357	356	377	0	0	0	0	0	1	1	0	0	0	1
3	661	358	359	338	0	0	0	0	0	1	1	0	0	0	0
3	680	377	378	357	0	0	0	0	0	1	1	0	0	0	1
3	681	359	358	379	0	0	0	0	0	1	1	0	0	0	0
3	700	378	377	398	0	0	0	0	0	1	1	0	0	0	1
3	701	379	380	359	0	0	0	0	0	1	1	0	0	0	0
3	720	398	399	378	0	0	0	0	0	1	1	0	0	0	1
3	721	380	379	400	0	0	0	0	0	1	1	0	0	0	0
3	740	399	398	419	0	0	0	0	0	1	1	0	0	0	1
3	741	400	401	380	0	0	0	0	0	1	1	0	0	0	0
3	760	419	420	399	0	0	0	0	0	1	1	0	0	0	1
3	761	401	400	421	0	0	0	0	0	1	1	0	0	0	0
3	769	409	408	429	0	0	0	0	0	1	1	0	0	0	1
3	770	477	476	483	0	0	0	0	0	2	2	0	0	0	0
3	771	478	477	431	0	0	0	0	0	2	2	0	0	0	0
3	775	482	481	435	0	0	0	0	0	2	2	0	0	0	1
3	776	416	415	436	0	0	0	0	0	1	1	0	0	0	0
3	780	420	419	440	0	0	0	0	0	1	1	0	0	0	1
3	781	421	422	401	0	0	0	0	0	1	1	0	0	0	0
3	789	429	430	409	0	0	0	0	0	1	1	0	0	0	1
3	790	483	431	477	0	0	0	0	0	2	2	0	0	0	0
3	791	431	432	478	0	0	0	0	0	2	2	0	0	0	0
3	794	434	435	481	0	0	0	0	0	2	2	0	0	0	1
3	795	435	484	482	0	0	0	0	0	2	2	0	0	0	0
3	796	436	437	416	0	0	0	0	0	1	1	0	0	0	0
3	800	440	441	420	0	0	0	0	0	1	1	0	0	0	1
3	801	422	421	442	0	0	0	0	0	1	1	0	0	0	0
3	809	430	429	450	0	0	0	0	0	1	1	0	0	0	1
3	810	431	483	485	0	0	0	0	0	2	2	0	0	0	0
3	811	432	431	452	0	0	0	0	0	2	2	0	0	0	0
3	814	435	434	455	0	0	0	0	0	2	2	0	0	0	1
3	815	484	435	456	0	0	0	0	0	2	2	0	0	0	0
3	816	437	436	457	0	0	0	0	0	1	1	0	0	0	0
3	820	441	440	461	0	0	0	0	0	1	1	0	0	0	1
3	821	442	443	422	0	0	0	0	0	1	1	0	0	0	0
3	829	450	451	430	0	0	0	0	0	1	1	0	0	0	1
3	830	485	452	431	0	0	0	0	0	2	2	0	0	0	0
3	831	452	453	432	0	0	0	0	0	2	2	0	0	0	0
3	834	455	456	435	0	0	0	0	0	2	2	0	0	0	1
3	835	456	486	484	0	0	0	0	0	2	2	0	0	0	0
3	836	457	458	437	0	0	0	0	0	1	1	0	0	0	0
3	840	461	462	441	0	0	0	0	0	1	1	0	0	0	1
3	841	443	442	232	0	0	0	0	0	1	1	0	0	0	0
3	849	451	450	240	0	0	0	0	0	1	1	0	0	0	1
3	850	452	485	463	0	0	0	0	0	2	2	0	0	0	0
3	851	453	452	242	0	0	0	0	0	2	2	0	0	0	0
3	854	456	455	245	0	0	0	0	0	2	2	0	0	0	1
3	855	486	456	246	0	0	0	0	0	2	2	0	0	0	0
3	856	458	457	247	0	0	0	0	0	1	1	0	0	0	0
3	860	462	461	251	0	0	0	0	0	1	1	0	0	0	1
3	861	232	233	443	0	0	0	0	0	1	1	0	0	0	0
3	869	240	241	451	0	0	0	0	0	1	1	0	0	0	1
3	870	463	242	452	0	0	0	0	0	2	2	0	0	0	0
3	871	242	243	453	0	0	0	0	0	2	2	0	0	0	0
3	874	245	246	456	0	0	0	0	0	2	2	0	0	0	1
3	875	246	464	486	0	0	0	0	0	2	2	0	0	0	0
3	876	247	248	458	0	0	0	0	0	1	1	0	0	0	0
3	880	251	252	462	0	0	0	0	0	1	1	0	0	0	1
3	881	21	42	273	0	0	0	0	0	1	1	0	0	0	0
3	882	42	63	273	0	0	0	0	0	1	1	0	0	0	0
3	883	294	273	63	0	0	0	0	0	1	1	0	0	0	0
3	884	63	84	315	0	0	0	0	0	1	1	0	0	0	0
3	885	315	294	63	0	0	0	0	0	1	1	0	0	0	0
3	886	84	105	315	0	0	0	0	0	1	1	0	0	0	0
3	887	336	315	105	0	0	0	0	0	1	1	0	0	0	0
3	888	105	126	357	0	0	0	0	0	1	1	0	0	0	0
3	889	357	336	105	0	0	0	0	0	1	1	0	0	0	0
3	890	126	147	357	0	0	0	0	0	1	1	0	0	0	0
3	891	378	357	147	0	0	0	0	0	1	1	0	0	0	0
3	892	147	168	399	0	0	0	0	0	1	1	0	0	0	0
3	893	399	378	147	0	0	0	0	0	1	1	0	0	0	0
3	894	168	189	399	0	0	0	0	0	1	1	0	0	0	0
3	895	420	399	189	0	0	0	0	0	1	1	0	0	0	0
3	896	189	210	441	0	0	0	0	0	1	1	0	0	0	0
3	897	441	420	189	0	0	0	0	0	1	1	0	0	0	0
3	898	210	231	441	0	0	0	0	0	1	1	0	0	0	0
3	899	462	441	231	0	0	0	0	0	1	1	0	0	0	0
3	900	231	252	462	0	0	0	0	0	1	1	0	0	0	0
3	901	17	38	269	0	0	0	0	0	1	1	0	0	0	0
3	902	38	59	269	0	0	0	0	0	1	1	0	0	0	0
3	903	290	269	59	0	0	0	0	0	1	1	0	0	0	0
3	904	59	80	311	0	0	0	0	0	1	1	0	0	0	0
3	905	311	290	59	0	0	0	0	0	1	1	0	0	0	0
3	906	80	101	311	0	0	0	0	0	1	1	0	0	0	0
3	907	332	311	101	0	0	0	0	0	1	1	0	0	0	0
3	908	101	122	353	0	0	0	0	0	1	1	0	0	0	0

```
3  909  353  332  101    0    0    0    0    0    1    1    0    0    0    0
3  910  122  143  353    0    0    0    0    0    1    1    0    0    0    0
3  911  374  353  143    0    0    0    0    0    1    1    0    0    0    0
3  912  143  164  395    0    0    0    0    0    1    1    0    0    0    0
3  913  395  374  143    0    0    0    0    0    1    1    0    0    0    0
3  914  164  185  395    0    0    0    0    0    1    1    0    0    0    0
3  915  416  395  185    0    0    0    0    0    1    1    0    0    0    0
3  916  185  206  437    0    0    0    0    0    1    1    0    0    0    0
3  917  437  416  185    0    0    0    0    0    1    1    0    0    0    0
3  918  206  227  437    0    0    0    0    0    1    1    0    0    0    0
3  919  458  437  227    0    0    0    0    0    1    1    0    0    0    0
3  920  227  248  458    0    0    0    0    0    1    1    0    0    0    0
3  921   13   34  265    0    0    0    0    0    1    1    0    0    0    0
3  922   34   55  265    0    0    0    0    0    1    1    0    0    0    0
3  923  286  265   55    0    0    0    0    0    1    1    0    0    0    0
3  924   55   76  307    0    0    0    0    0    1    1    0    0    0    0
3  925  307  286   55    0    0    0    0    0    1    1    0    0    0    0
3  926   76   97  307    0    0    0    0    0    1    1    0    0    0    0
3  927  328  307   97    0    0    0    0    0    1    1    0    0    0    0
3  928   97  118  349    0    0    0    0    0    1    1    0    0    0    0
3  929  349  328   97    0    0    0    0    0    1    1    0    0    0    0
3  930  118  139  349    0    0    0    0    0    1    1    0    0    0    0
3  931  370  349  139    0    0    0    0    0    1    1    0    0    0    0
3  932  139  160  391    0    0    0    0    0    1    1    0    0    0    0
3  933  391  370  139    0    0    0    0    0    1    1    0    0    0    0
3  934  160  181  391    0    0    0    0    0    1    1    0    0    0    0
3  935  412  391  181    0    0    0    0    0    1    1    0    0    0    0
3  941    9   30  261    0    0    0    0    0    1    1    0    0    0    0
3  942   30   51  261    0    0    0    0    0    1    1    0    0    0    0
3  943  282  261   51    0    0    0    0    0    1    1    0    0    0    0
3  944   51   72  303    0    0    0    0    0    1    1    0    0    0    0
3  945  303  282   51    0    0    0    0    0    1    1    0    0    0    0
3  946   72   93  303    0    0    0    0    0    1    1    0    0    0    0
3  947  324  303   93    0    0    0    0    0    1    1    0    0    0    0
3  948   93  114  345    0    0    0    0    0    1    1    0    0    0    0
3  949  345  324   93    0    0    0    0    0    1    1    0    0    0    0
3  950  114  135  345    0    0    0    0    0    1    1    0    0    0    0
3  951  366  345  135    0    0    0    0    0    1    1    0    0    0    0
3  952  135  156  387    0    0    0    0    0    1    1    0    0    0    0
3  953  387  366  135    0    0    0    0    0    1    1    0    0    0    0
3  954  156  177  387    0    0    0    0    0    1    1    0    0    0    0
3  955  408  387  177    0    0    0    0    0    1    1    0    0    0    0
3  956  177  198  429    0    0    0    0    0    1    1    0    0    0    0
3  957  429  408  177    0    0    0    0    0    1    1    0    0    0    0
3  958  198  219  429    0    0    0    0    0    1    1    0    0    0    0
3  959  450  429  219    0    0    0    0    0    1    1    0    0    0    0
3  960  219  240  450    0    0    0    0    0    1    1    0    0    0    0
3  961    5   26  257    0    0    0    0    0    1    1    0    0    0    0
3  962   26   47  257    0    0    0    0    0    1    1    0    0    0    0
3  963  278  257   47    0    0    0    0    0    1    1    0    0    0    0
3  964   47   68  299    0    0    0    0    0    1    1    0    0    0    0
3  965  299  278   47    0    0    0    0    0    1    1    0    0    0    0
3  966   68   89  299    0    0    0    0    0    1    1    0    0    0    0
3  967  320  299   89    0    0    0    0    0    1    1    0    0    0    0
3  968   89  110  341    0    0    0    0    0    1    1    0    0    0    0
3  969  341  320   89    0    0    0    0    0    1    1    0    0    0    0
3  970  110  131  341    0    0    0    0    0    1    1    0    0    0    0
3  971  362  341  131    0    0    0    0    0    1    1    0    0    0    0
3  972  131  152  383    0    0    0    0    0    1    1    0    0    0    0
3  973  383  362  131    0    0    0    0    0    1    1    0    0    0    0
3  974  152  173  383    0    0    0    0    0    1    1    0    0    0    0
3  975  404  383  173    0    0    0    0    0    1    1    0    0    0    0
3  976  173  194  425    0    0    0    0    0    1    1    0    0    0    0
3  977  425  404  173    0    0    0    0    0    1    1    0    0    0    0
3  978  194  215  425    0    0    0    0    0    1    1    0    0    0    0
3  979  446  425  215    0    0    0    0    0    1    1    0    0    0    0
3  980  215  236  446    0    0    0    0    0    1    1    0    0    0    0
3 1499  485  463  474    0    0    0    0    0    1    1    0    0    0    0
3 1500  483  485  474    0    0    0    0    0    1    1    0    0    0    0
3 1501  474  472  483    0    0    0    0    0    1    1    0    0    0    0
3 1502  476  483  472    0    0    0    0    0    1    1    0    0    0    0
3 1503  472  465  476    0    0    0    0    0    1    1    0    0    0    0
3 1504  465  476  477    0    0    0    0    0    1    1    0    0    0    0
3 1509  470  481  482    0    0    0    0    0    1    1    0    0    0    1
3 1510  477  466  465    0    0    0    0    0    1    1    0    0    0    0
3 1515  482  471  470    0    0    0    0    0    1    1    0    0    0    1
3 1516  484  482  471    0    0    0    0    0    1    1    0    0    0    0
3 1517  471  473  484    0    0    0    0    0    1    1    0    0    0    0
3 1518  486  484  473    0    0    0    0    0    1    1    0    0    0    0
3 1519  473  475  486    0    0    0    0    0    1    1    0    0    0    0
3 1520  464  486  475    0    0    0    0    0    1    1    0    0    0    0
1  981    1   22   23    0    0    0    0    0    1    1    0    0    0    0
1  991  211  232  233    0    0    0    0    0    1    1    0    0    0   21
1  992  253  274  275    0    0    0    0    0    1    1    0    0    0    0
1 1000  421  442  443    0    0    0    0    0    1    1    0    0    0   21
1 1001    2   23   24    0    0    0    0    0    1    1    0    0    0    0
1 1011  212  233  234    0    0    0    0    0    1    1    0    0    0   21
1 1012  254  275  276    0    0    0    0    0    1    1    0    0    0    0
1 1020  422  443  444    0    0    0    0    0    1    1    0    0    0   21
1 1021    3   24   25    0    0    0    0    0    1    1    0    0    0    0
1 1031  213  234  235    0    0    0    0    0    1    1    0    0    0   21
1 1032  255  276  277    0    0    0    0    0    1    1    0    0    0    0
1 1040  423  444  445    0    0    0    0    0    1    1    0    0    0   21
1 1041    4   25   26    0    0    0    0    0    1    1    0    0    0    0
1 1051  214  235  236    0    0    0    0    0    1    1    0    0    0   21
```

```
1 1052  256  277  278    0    0    0    0    0    1    1    0    0    0    0
1 1060  424  445  446    0    0    0    0    0    1    1    0    0    0   21
1 1061    5   26   27    0    0    0    0    0    1    1    0    0    0    0
1 1071  215  236  237    0    0    0    0    0    1    1    0    0    0   21
1 1072  257  278  279    0    0    0    0    0    1    1    0    0    0    0
1 1080  425  446  447    0    0    0    0    0    1    1    0    0    0   21
1 1081    6   27   28    0    0    0    0    0    1    1    0    0    0    0
1 1091  216  237  238    0    0    0    0    0    1    1    0    0    0   21
1 1092  258  279  280    0    0    0    0    0    1    1    0    0    0    0
1 1100  426  447  448    0    0    0    0    0    1    1    0    0    0   21
1 1101    7   28   29    0    0    0    0    0    1    1    0    0    0    0
1 1111  217  238  239    0    0    0    0    0    1    1    0    0    0   21
1 1112  259  280  281    0    0    0    0    0    1    1    0    0    0    0
1 1120  427  448  449    0    0    0    0    0    1    1    0    0    0   21
1 1121    8   29   30    0    0    0    0    0    1    1    0    0    0    0
1 1131  218  239  240    0    0    0    0    0    1    1    0    0    0   21
1 1132  260  281  282    0    0    0    0    0    1    1    0    0    0    0
1 1140  428  449  450    0    0    0    0    0    1    1    0    0    0   21
1 1141    9   30   31    0    0    0    0    0    1    1    0    0    0    0
1 1151  219  240  241    0    0    0    0    0    1    1    0    0    0   21
1 1152  261  282  283    0    0    0    0    0    1    1    0    0    0    0
1 1160  429  450  451    0    0    0    0    0    1    1    0    0    0   21
1 1161   10   31   32    0    0    0    0    0    1    1    0    0    0    0
1 1171  220  241  242    0    0    0    0    0    1    1    0    0    0   21
1 1172  262  283  284    0    0    0    0    0    1    1    0    0    0    0
1 1180  430  451  452    0    0    0    0    0    1    1    0    0    0   21
1 1181   11   32   33    0    0    0    0    0    1    1    0    0    0    0
1 1188  158  179  180    0    0    0    0    0    1    1    0    0    0   21
1 1189  466  200  201    0    0    0    0    0    1    1    0    0    0    0
1 1190  200  221  222    0    0    0    0    0    1    1    0    0    0    0
1 1191  221  242  243    0    0    0    0    0    1    1    0    0    0    0
1 1192  263  284  285    0    0    0    0    0    1    1    0    0    0    0
1 1198  389  410  411    0    0    0    0    0    1    1    0    0    0   21
1 1199  477  431  432    0    0    0    0    0    1    1    0    0    0    0
1 1200  431  452  453    0    0    0    0    0    1    1    0    0    0    0
1 1201   12   33   34    0    0    0    0    0    1    1    0    0    0    0
1 1208  159  180  181    0    0    0    0    0    1    1    0    0    0   21
1 1209  467  201  202    0    0    0    0    0    1    1    0    0    0    0
1 1210  201  222  223    0    0    0    0    0    1    1    0    0    0    0
1 1211  222  243  244    0    0    0    0    0    1    1    0    0    0    0
1 1212  264  285  286    0    0    0    0    0    1    1    0    0    0    0
1 1218  390  411  412    0    0    0    0    0    1    1    0    0    0   21
1 1219  478  432  433    0    0    0    0    0    1    1    0    0    0    0
1 1220  432  453  454    0    0    0    0    0    1    1    0    0    0    0
1 1221   13   34   35    0    0    0    0    0    1    1    0    0    0    0
1 1228  160  181  182    0    0    0    0    0    1    1    0    0    0   21
1 1229  468  202  203    0    0    0    0    0    1    1    0    0    0    0
1 1230  202  223  224    0    0    0    0    0    1    1    0    0    0    0
1 1231  223  244  245    0    0    0    0    0    1    1    0    0    0    0
1 1232  265  286  287    0    0    0    0    0    1    1    0    0    0    0
1 1238  391  412  413    0    0    0    0    0    1    1    0    0    0   21
1 1239  479  433  434    0    0    0    0    0    1    1    0    0    0    0
1 1240  433  454  455    0    0    0    0    0    1    1    0    0    0    0
1 1241   14   35   36    0    0    0    0    0    1    1    0    0    0    0
1 1248  161  182  183    0    0    0    0    0    1    1    0    0    0   21
1 1249  469  203  204    0    0    0    0    0    1    1    0    0    0    0
1 1250  203  224  225    0    0    0    0    0    1    1    0    0    0    0
1 1251  224  245  246    0    0    0    0    0    1    1    0    0    0    0
1 1252  266  287  288    0    0    0    0    0    1    1    0    0    0    0
1 1258  392  413  414    0    0    0    0    0    1    1    0    0    0   21
1 1259  480  434  435    0    0    0    0    0    1    1    0    0    0    0
1 1260  434  455  456    0    0    0    0    0    1    1    0    0    0    0
1 1261   15   36   37    0    0    0    0    0    1    1    0    0    0    0
1 1268  162  183  184    0    0    0    0    0    1    1    0    0    0   21
1 1269  470  204  205    0    0    0    0    0    1    1    0    0    0    0
1 1270  204  225  226    0    0    0    0    0    1    1    0    0    0    0
1 1271  225  246  247    0    0    0    0    0    1    1    0    0    0    0
1 1272  267  288  289    0    0    0    0    0    1    1    0    0    0    0
1 1278  393  414  415    0    0    0    0    0    1    1    0    0    0   21
1 1279  481  435  436    0    0    0    0    0    1    1    0    0    0    0
1 1280  435  456  457    0    0    0    0    0    1    1    0    0    0    0
1 1281   16   37   38    0    0    0    0    0    1    1    0    0    0    0
1 1291  226  247  248    0    0    0    0    0    1    1    0    0    0   21
1 1292  268  289  290    0    0    0    0    0    1    1    0    0    0    0
1 1300  436  457  458    0    0    0    0    0    1    1    0    0    0   21
1 1301   17   38   39    0    0    0    0    0    1    1    0    0    0    0
1 1311  227  248  249    0    0    0    0    0    1    1    0    0    0   21
1 1312  269  290  291    0    0    0    0    0    1    1    0    0    0    0
1 1320  437  458  459    0    0    0    0    0    1    1    0    0    0   21
1 1321   18   39   40    0    0    0    0    0    1    1    0    0    0    0
1 1331  228  249  250    0    0    0    0    0    1    1    0    0    0   21
1 1332  270  291  292    0    0    0    0    0    1    1    0    0    0    0
1 1340  438  459  460    0    0    0    0    0    1    1    0    0    0   21
1 1341   19   40   41    0    0    0    0    0    1    1    0    0    0    0
1 1351  229  250  251    0    0    0    0    0    1    1    0    0    0   21
1 1352  271  292  293    0    0    0    0    0    1    1    0    0    0    0
1 1360  439  460  461    0    0    0    0    0    1    1    0    0    0   21
1 1361   20   41   42    0    0    0    0    0    1    1    0    0    0    0
1 1371  230  251  252    0    0    0    0    0    1    1    0    0    0   21
1 1372  272  293  294    0    0    0    0    0    1    1    0    0    0    0
1 1380  440  461  462    0    0    0    0    0    1    1    0    0    0   21
1 1381   21   42   43    0    0    0    0    0    1    1    0    0    0    0
1 1391  231  252  251    0    0    0    0    0    1    1    0    0    0   21
1 1392  273  294  295    0    0    0    0    0    1    1    0    0    0    0
1 1400  441  462  461    0    0    0    0    0    1    1    0    0    0   21
```

```
  1 1401    1  253  254    0    0    0    0    0    1    1    0    0    0    0
  1 1420   20  272  273    0    0    0    0    0    1    1                   1
  1 1421   21  273  272    0    0    0    0    0    1    1    0    0    0    0
  1 1422  232  442  443    0    0    0    0    0    1    1    0    0    0    0
  1 1441  251  461  462                             1    1                   1
  1 1442  252  462  461    0    0    0    0    0    1    1    0    0    0    0
  1 1443    1    3  252    0    0    0    0    0    1    1    0    0    0    0
  1 1452   19   21  252    0    0    0    0    0    1    1    0    0    0    2
  1 1453  232  234    1    0    0    0    0    0    1    1    0    0    0    0
  1 1456  238  240    1    0    0    0    0    0    1    1    0    0    0    2
  1 1457  248  250    1    0    0    0    0    0    1    1    0    0    0    0
  1 1458  250  252    1    0    0    0    0    0    1    1    0    0    0    0
  3 1459  241  451  220    0    0    0    0    0    1    1    0    0    0    0
  3 1460  247  226  457    0    0    0    0    0    1    1    0    0    0    0
  2 1461  451  430  199  220    0    0    0    0    1    1    0    0    0    0
  2 1462  430  409  178  199    0    0    0    0    1    1    0    0    0    0
  2 1463  178  409  410  179    0    0    0    0    1    1    0    0    0    0
  2 1468  183  414  415  184    0    0    0    0    1    1    0    0    0    1
  2 1469  436  205  184  415    0    0    0    0    1    1    0    0    0    0
  2 1470  457  226  205  436    0    0    0    0    1    1    0    0    0    0
  1 1521  466  467  180    0    0    0    0    0    1    1    0    0    0    0
  1 1523  470  471  184    0    0    0    0    0    1    1    0    0    0    2
  1 1524  477  478  411    0    0    0    0    0    1    1    0    0    0    0
  1 1526  481  482  415    0    0    0    0    0    1    1    0    0    0    2
  1 1600  463  242  221                             1    1
  1 1527  242  243   11    0    0    0    0    0    1    1    0    0    0    0
  1 1601  243  244   11                             1    1
  1 1528  244  245   11    0    0    0    0    0    1    1    0    0    0    0
  1 1602  245  246   11                             1    1                   0
  1 1529  246  464   16    0    0    0    0    0    1    1    0    0    0    0
  1 1530  240  241  220    0    0    0    0    0    1    1    0    0    0    0
  1 1531  247  248  227    0    0    0    0    0    1    1    0    0    0    0
  1 1532  465  472  200    0    0    0    0    0    1    1    0    0    0    0
  1 1533  472  474  221    0    0    0    0    0    1    1    0    0    0    0
  1 1534  474  463  242    0    0    0    0    0    1    1    0    0    0    0
  1 1535  463  485  452    0    0    0    0    0    1    1    0    0    0    0
  1 1536  485  483  431    0    0    0    0    0    1    1    0    0    0    0
  1 1537  483  476  477    0    0    0    0    0    1    1    0    0    0    0
  1 1538  471  473  204    0    0    0    0    0    1    1    0    0    0    0
  1 1539  473  475  225    0    0    0    0    0    1    1    0    0    0    0
  1 1540  475  464  246    0    0    0    0    0    1    1    0    0    0    0
  1 1541  464  486  456    0    0    0    0    0    1    1    0    0    0    0
  1 1542  486  484  435    0    0    0    0    0    1    1    0    0    0    0
  1 1543  484  482  481    0    0    0    0    0    1    1    0    0    0    0
  1 1544  465  476  477    0    0    0    0    0    1    1    0    0    0    0
  1 1549  470  481  482    0    0    0    0    0    1    1    0    0    0    1
  1 1550  471  482  481    0    0    0    0    0    1    1    0    0    0    0
  1 1551  466  179  467    0    0    0    0    0    2    1    0    0    0    0
  1 1555  470  183  471    0    0    0    0    0    2    1    0    0    0    0
  1 1556  477  410  411    0    0    0    0    0    2    1    0    0    0    0
  1 1560  481  414  415    0    0    0    0    0    2    1    0    0    0    0
  1 1471  178  179  157    0    0    0    0    0    1    1    0    0    0    0
  1 1472  179  180  163    0    0    0    0    0    1    1    0    0    0    0
  1 1476  183  184  163    0    0    0    0    0    1    1    0    0    0    1
  1 1477  409  410  389    0    0    0    0    0    1    1    0    0    0    0
  1 1478  410  411  394    0    0    0    0    0    1    1    0    0    0    0
  1 1482  414  415  394    0    0    0    0    0    1    1    0    0    0    1
  1 1483  178  409  185    0    0    0    0    0    1    1    0    0    0    0
  1 1489  184  415  185    0    0    0    0    0    1    1    0    0    0    1
  1 1561  465  466  200                             1    1
  1 1563  469  470  204                             1    1                   2
  1 1564  476  477  431                             1    1
  1 1566  480  481  435                             1    1                   2
$ LINE ELEMENT BASIC PROPERTIES
  1 .6452E-03 .6937E-07 .3469E-07 .3469E-07 .0000E+00 .0000E+00
$ SHELL ELEMENT THICKNESSES
  1 .1000E-03 .1000E-03 .1000E-03
  2 .1000E-03 .1000E-03 .1000E-03
$ MATERIAL PROPERTIES
  1    1
.6895E+11 .3000E+00 .0000E+00 .2765E+04 .0000E+00 .0000E+00
  2    1
.2105E+09 .3000E+00 .0000E+00 .7765E+02 .0000E+00 .0000E+00
  1 .1000E-03 .1000E-03 .1000E-03
```

Data for the aeroelastic scalars file, **wing.scalars**, are given below.

STARS–CFDASE input data:

```
$ STARS 5.8.1 wing.scalars file, Euler unsteady  run.
$ STARS 5.8.2 NR, IBCX, RBCX, ISIZE   Basic parameters
   3, 0, 1.0, 4
C STARS 5.8.4 NNR, (NS(I),I=1,NNR) Boundary-condition modification data
   12,  1, 2, 3, 4, 5, 6, 11, 12, 13, 14, 15, 16
$ STARS 5.8.5 I/O parameter
C STARS 5.8.6 IRFORM, IPRINT
   2,    1
```

```
$ STARS 5.8.7 dimensional parameters
C STARS 5.8.8 mach-inf, rho-inf(kg/m**3), a-inf(m/sec), gamma, pinf
      2.0       0.915          340.29        1.4    0.0
$ STARS 5.8.9 shift factor and gravity constant
C STARS 5.8.10  SCF, GR
   6102.01554752     1.
$ STARS 5.8.11 Impulse-Force Data
C STARS 5.8.12 IFLAG, FFI, NS,  NE
    2,   10.,  3,   5
$ STARS 5.8.13 Force activation Parameters
C STARS 5.8.14 ICFA,ICFI
   1,   1
$ STARS 5.8.15 Transition Matrix Parameters
C STARS 5.8.16 NTERMS, NSTEPS
      20,      2
$ STARS 5.8.17 NA, NB order of the ARMA model
   7, 9
```

Data for the unsteady CFD solution control file, **wing.conu**, are given below.

STARS–CFDASE input data:

```
 &control
C STARS 5.9 - wing.conu  file for Euler unsteady run.
  nstep     =  5401,
  nout      = 50,
  nstage    = 3,
  cfl       = .70,
  mach      = 2.,
  alpha     = 0.0,
  beta      = 0.0,
  restart   = 1,
  ncycl     = 40,
  ncyci     = 40,
  tlr       = 0.01,
  debug     = .false.,
  meshc     = 1,
  meshf     = 1,
  cbt(1)    = 1.,
  cbt(2)    = 0.5,
  cbt(3)    = 0.,
  cbt(4)    = 0.,
  nsmth     = 2,
  smofc     = 0.2,
  low       = .false.,
  trans     = .true.,
  freq      = 0.0125,
  nstpe     = 275,
  x0        = 0.0,
  y0        = 0.0,
  z0        = 0.0,
  wux       = 0.0,
  wuy       = 0.0,
  wuz       = 1.0,
  phase     = 0.0,
  iflow_sol= 1,
  amplitude= .1,
/
```

Data for the alternate steady CFD solution control file, **wing.consdp**, are given below.

STARS–CFDASE input data:

```
    4   (lines of title)
$ VERSION USING FILES FROM SURFACE, VOLUME, AND 'CFDASERUN' ROUTINE, JUNE 1990
$ cantilever wing
$ mach=0.5 alpha=0
$
$ PROBLEM DIMENSION
    3
$ NELEM, NPOIN, NBOUN
   297700,  54759,  12594
$ KACCEL, NACCEL
    100,  25000
$ GAMMA,  C1, IDIFF,   EPS, IVISC,  WBR
    1.4, 1.0,      2,   0.1,      0,  0.2
$ NFFBC
    1
$ ROINF,  UXINF, UYINF, UZINF,        PINF,      MACHINF
   1.0,    1.0,    0.0,    0.0,     .178571429,       2.
$ NENBC
    0
$ NTIME, NITER, ILOT
```

```
  2000,     1,    1
$ CSAFE, IFCT, NQUAN, IDO(1), IDO(2), CLIMAX
    0.7,    0,     2,      3,      1,   0.90
$ INFOG, INFOU, OUFO, NIOUT
     -1,    -2,    3,    500
$ CSMOO, NSMOO
     .2,     0
$ ENTHALPY DAMPING COEFFICIENT
    1.0
$ IRPR, IRLOG, ILPR, ILLOG, AX(1), AX(2), AX(3), RCHORD
     1,     1,    1,     1,   1.0,   0.0,   0.0,    2.5
$ IRFR, IRFS
     3, 5500
$ ISTRON, ICHECK
       2       1
$ TIMEIN, ITIM
     0.0,     0
$ FILE3, FILE2, FILE4 ( Output file name - geo file name - input file name )
fort.15_dp
manual.geodp
IN
$ NCPU
     1
```

The following section is concentrated on the ARMA modeling technique. Data for the aeroelastic scalars file for step 1a in the ARMA procedures, **wing.scalars**, are given below.

STARS–CFDASE input data:

```
$ STARS 5.8.1 wing.scalars1file, ARMA  unsteady  run step 1a.
$ STARS 5.8.2 NR, IBCX, RBCX, ISIZE   Basic parameters
   3, 1, 1.0, 4
C STARS 5.8.4 NNR, (NS(I),I=1,NNR) Boundary-condition modification data
   12,  1, 2, 3, 4, 5, 6, 11, 12, 13, 14, 15, 16
$ STARS 5.8.5 I/O parameter
C STARS 5.8.6 IRFORM, IPRINT
    2,     1
$ STARS 5.8.7 dimensional parameters
C STARS 5.8.8 mach-inf, rho-inf(kg/m**3), a-inf(m/sec), gamma, pinf
       2.0      1.225          340.29         1.4    0.0
$ STARS 5.8.9 shift factor and gravity constant
C STARS 5.8.10  SCF, GR
    6102.01554752     1.
$ STARS 5.8.11 Impulse-Force Data
C STARS 5.8.12 IFLAG, FFI, NS,  NE
     2,   10.,  3,   5
$ STARS 5.8.13 Force activation Parameters
C STARS 5.8.14 ICFA,ICFI
    1,   1
$ STARS 5.8.15 Transition Matrix Parameters
C STARS 5.8.16 NTERMS, NSTEPS
      20,       2
$ STARS 5.8.17 NA, NB order of the ARMA model
   7, 9
```

Data for the unsteady CFD solution control file, **wing.conu**, are given below.

STARS–CFDASE input data:

```
 &control
C STARS 5.9 - wing.conu1 file for Euler  ARMA unsteady run step 1a.
  nstep     =  5401,
  nout      = 50,
  nstage    = 3,
  cfl       = .70,
  mach      = 2.,
  alpha     = 0.0,
  beta      = 0.0,
  restart   = 1,
  ncycl     = 40,
  ncyci     = 40,
  tlr       = 0.01,
  debug     = .false.,
  meshc     = 1,
  meshf     = 1,
  cbt(1)    = 1.,
  cbt(2)    = 0.5,
  cbt(3)    = 0.,
  cbt(4)    = 0.,
  nsmth     = 2,
  smofc     = 0.2,
  low       = .false.,
  trans     = .true.,
  freq      = 0.0125,
  nstpe     = 275,
  x0        = 0.0,
  y0        = 0.0,
  z0        = 0.0,
  wux       = 0.0,
  wuy       = 0.0,
  wuz       = 1.0,
  phase     = 0.0,
  iflow_sol= 1,
  amplitude= .1,
/
```

Data for the aeroelastic scalars file for step 2 in the ARMA procedures, **wing.scalars**, are given below.

STARS–CFDASE input data:

```
$ STARS 5.8.1 wing.scalars2   file,ARMA unsteady flow STEP 2,
$ STARS 5.8.2 NR, IBCX, RBCX, ISIZE   Basic parameters
   3, 5, 1.0, 4
C STARS 5.8.4 NNR, (NS(I),I=1,NNR) Boundary-condition modification data
   12,  1, 2, 3, 4, 5, 6, 11, 12, 13, 14, 15, 16
$ STARS 5.8.5 I/O parameter
C STARS 5.8.6 IRFORM, IPRINT
    2,    1
$ STARS 5.8.7 dimensional parameters
C STARS 5.8.8 mach-inf, rho-inf(kg/m**3), a-inf(m/sec), gamma, pinf
       2.0      1.225          340.29        1.4    0.0
$ STARS 5.8.9 shift factor and gravity constant
C STARS 5.8.10  SCF, GR
    6102.01554752     1.
$ STARS 5.8.11 Impulse-Force Data
C STARS 5.8.12 IFLAG, FFI, NS,  NE
     2,   10.,  3,   5
$ STARS 5.8.13 Force activation Parameters
C STARS 5.8.14 ICFA,ICFI
    1,   1
$ STARS 5.8.15 Transition Matrix Parameters
C STARS 5.8.16 NTERMS, NSTEPS
      20,       2
$ STARS 5.8.17 NA, NB order of the ARMA model
   1, 3
```

Data for the unsteady CFD solution control file, **wing.conu**, are given below.

STARS–CFDASE input data:

```
 &control
C  STARS 5.9 -  wing.conu2  file for step 2 in ARMA modeling procedure
  nstep     =  401,
  nout      = 50,
  nstage    = 3,
  cfl       = .70,
  mach      = 2.,
  alpha     = 0.0,
  beta      = 0.0,
  restart   = 1,
  ncycl     = 40,
  ncyci     = 40,
  tlr       = 0.01,
  debug     = .false.,
  meshc     = 1,
  meshf     = 1,
  cbt(1)    = 1.,
  cbt(2)    = 0.5,
  cbt(3)    = 0.,
  cbt(4)    = 0.,
  nsmth     = 2,
  smofc     = 0.2,
  low       = .false.,
  trans     = .true.,
  freq      = 0.0125,
  nstpe     = 275,
  x0        = 0.0,
  y0        = 0.0,
  z0       = 0.0,
  wux      = 0.0,
  wuy      = 0.0,
  wuz      = 1.0,
  phase    = 0.0,
  iflow_sol= 1,
  amplitude= .1,
/
```

Data for the aeroelastic scalars file for step 3 and 4 in the ARMA procedures, **wing.scalars**, are given below.

STARS–CFDASE input data:

```
$ STARS 5.8.1 wing.scalars4 file, ARMA unsteady flow, STEP 4
$ STARS 5.8.2 NR, IBCX, RBCX, ISIZE   Basic parameters
   3, 5, 1.0, 4
C STARS 5.8.4 NNR, (NS(I),I=1,NNR) Boundary-condition modification data
   12,  1, 2, 3, 4, 5, 6, 11, 12, 13, 14, 15, 16
$ STARS 5.8.5 I/O parameter
C STARS 5.8.6 IRFORM, IPRINT
    2,    1
$ STARS 5.8.7 dimensional parameters
C STARS 5.8.8 mach-inf, rho-inf(kg/m**3), a-inf(m/sec), gamma, pinf
       2.0      1.225          340.29        1.4    0.0
$ STARS 5.8.9 shift factor and gravity constant
C STARS 5.8.10  SCF, GR
     6102.01554752      1.
$ STARS 5.8.11 Impulse-Force Data
C STARS 5.8.12 IFLAG, FFI, NS,  NE
      2,   10.,  3,   5
$ STARS 5.8.13 Force activation Parameters
C STARS 5.8.14 ICFA,ICFI
    1,    1
$ STARS 5.8.15 Transition Matrix Parameters
C STARS 5.8.16 NTERMS, NSTEPS
      20,       2
$ STARS 5.8.17 NA, NB order of the ARMA model
   7, 9
```

Data for the unsteady CFD solution control file, **wing.conu**, are given below.

STARS–CFDASE input data:

```
 &control
C  STARS 5.9 - wing.conu4 file for step 4 in ARMA modeling procedure
  nstep    =  401,
  nout     = 50,
  nstage   = 3,
  cfl      = .70,
  mach     = 2.,
  alpha    = 0.0,
  beta     = 0.0,
  restart  = 1,
  ncycl    = 40,
  ncyci    = 40,
  tlr      = 0.01,
  debug    = .false.,
  meshc    = 1,
  meshf    = 1,
  cbt(1)   = 1.,
  cbt(2)   = 0.5,
  cbt(3)   = 0.,
  cbt(4)   = 0.,
  nsmth    = 2,
  smofc    = 0.2,
  low      = .false.,
  trans    = .true.,
  freq     = 0.0125,
  nstpe    = 275,
  x0       = 0.0,
  y0       = 0.0,
  z0       = 0.0,
  wux      = 0.0,
  wuy      = 0.0,
  wuz      = 1.0,
  phase    = 0.0,
  iflow_sol= 3,
  amplitude= .1,
/
```

Data for the aeroelastic scalars file for step 5 in the ARMA procedures, **wing.scalars**, are given below.

STARS–CFDASE input data:

```
$ STARS 5.8.1 wing.scalars5   file, ARMA unsteady flow, STEP 5
$ STARS 5.8.2 NR, IBCX, RBCX, ISIZE   Basic parameters
   3, 0, 1.0, 4
C STARS 5.8.4 NNR, (NS(I),I=1,NNR) Boundary-condition modification data
   12,  1, 2, 3, 4, 5, 6, 11, 12, 13, 14, 15, 16
$ STARS 5.8.5 I/O parameter
C STARS 5.8.6 IRFORM, IPRINT
    2,    1
$ STARS 5.8.7 dimensional parameters
C STARS 5.8.8 mach-inf, rho-inf(kg/m**3), a-inf(m/sec), gamma, pinf
       2.0      0.995          340.29        1.4    0.0
$ STARS 5.8.9 shift factor and gravity constant
C STARS 5.8.10  SCF, GR
    6102.01554752     1.
$ STARS 5.8.11 Impulse-Force Data
C STARS 5.8.12 IFLAG, FFI, NS,  NE
     2,   10.,  3,   5
$ STARS 5.8.13 Force activation Parameters
C STARS 5.8.14 ICFA,ICFI
    1,   1
$ STARS 5.8.15 Transition Matrix Parameters
C STARS 5.8.16 NTERMS, NSTEPS
      20,      2
$ STARS 5.8.17 NA, NB order of the ARMA model
   7, 9
```

Data for the unsteady CFD solution control file, **wing.conu**, are given below.

STARS–CFDASE input data:

```
 &control
C  STARS 5.9 - wing.conu5 file for step 5 in ARMA modeling procedure
  nstep     =  2401,
  nout      = 5000,
  nstage    = 3,
  cfl       = .70,
  mach      = 2.,
  alpha     = 0,0,
  beta      = 0.0,
  restart   = 1,
  ncycl     = 40,
  ncyci     = 40,
  tlr       = 0.01,
  debug     = .false.,
  meshc     = 1,
  meshf     = 1,
  cbt(1)    = 1.,
  cbt(2)    = 0.5,
  cbt(3)    = 0.,
  cbt(4)    = 0.,
  nsmth     = 2,
  smofc     = 0.2,
  low       = .false.,
  trans     = .true.,
  freq      = 0.0125,
  nstpe     = 275,
  x0        = 0.0,
  y0        = 0.0,
  z0        = 0.0,
  wux       = 0.0,
  wuy       = 0.0,
  wuz       = 1.0,
  phase     = 0.0,
  iflow_sol= 3,
  amplitude= .1,
/
```

Data for the unsteady CFD solution control file, **wing.control**, are given below.

STARS–CFDASE input data:

```
$ STARS 5.7 - wing.control file
$     na       nb  nc   gainr  gainc   ncstars    anal/digit (1/2)
      5         3   1     3      6       0          2
$ amatrix
```

```
    1.4554   -0.6082   -0.3573   -0.0816   -0.1207
    1.0000         0         0         0         0
         0         0    0.5179    0.4651   -0.2160
         0         0   -0.4492    0.8606    0.0859
         0         0   -0.2170   -0.0726    0.6776
$ bmatrix
         0         0         0
         0         0         0
    0.6303   -0.3140   -0.0427
   -0.1496    0.1331    0.0058
    0.1913   -0.1502   -0.0148
$ cmatrix
 0.1688    0.1429         0         0         0
$ dmatrix
 0     0     0
$ Transformation  matrix
   1  0  0  0  0  0
   0  1  0  0  0  0
   0  0  1  0  0  0
$ controller output to xn
  0  0  1  0  0  0
```

BIBLIOGRAPHY

[1]Bisplinghoff, R. L., Ashley H. and Halfman,R. L., *Aeroelasticity*, Addison-Wesley Publishing Company, Inc., New York, 1957.

[2]Garrick, I. E., *Aerodynamic Flutter*, AIAA Selected Reprint Series, Vol. 5, March 1969.

[3]Dowell, E. H. (Editor), Crawley, E. F.,Curtiss, H. C., Jr., Peters, D. A., Scanlan, R. H. and Sisto, F., *A Modern Course in Aeroelasticity*, Kluwer Acadamic Publisher, Dordrecht, The Netherlands,1995.

[4]Geising, J. P., Kalman, T. P., and Rodden, W. P., *Subsonic Unsteady Aerodynamics for General Configurations*, Vol. 1 and 2, AFFDL-TR-71-5, November 1971.

[5]Appa, K., "Constant Pressure Panel Method for Supersonic Unsteady Airload Analysis," *Journal of Aircraft*, Vol. 24, No. 10, pp 696–702, October 1987.

[6] Batina, J. T., "Unsteady Euler Airfoil Solutions Using Unstrtuctured Dynamic meshes," AIAA 89-0115, 27th Aerospace Sciences Meeting & Exhibit, Reno, Nevada, January 9-12, 1989.

[7] Bendiksen, O., "A New Approach to Computational Aeroelasticity," AIAA 91-0939, April 1991.

[8] Geuzaine, P., Brown G. and Farhat. C., "Three Field-Based Nonlinear Aeroelastic Simulation Technology: Status and Application to the Flutter Analysis of an F16 Configuration," AIAA 2002-0870, 40th Aerospace Sciences Meeting & Exhibit, Reno, Nevada, January14-17, 2002.

[9] Lesoinne, M. and Farhat, C., "Stability Analysis of Dynamic Meshes for Transient Aeroelastic Computations," AIAA 93-3325, July 1993.

[10] Bendiksen, O. O., "Eulerian-Lagrangian Simulations of Transonic Flutter Instabilities," Symposium on Fluid-Structure Interaction and Aeroelasticity, ASME winter Annual Meeting, Chicago, IL, November 11, 1994.

[11] Bendiksen, O. O., "A Mixed Eulerian-Langrangian Computational Method for Flutter Calculations," Paper 91-091, Presented at the International Forum on Aeroelasticity and Structural Dynamics, Aachen, Germany, June 3-6, 1991.

[12] Bendiksen, O. O., "Numerical Simulations of Unsteady Flow and Flutter in Transonic Cascades," Sixth Int. Symposium on Unsteady Aerodynamics, Aeroacoustics and Aeroelasticity of Turbomachinse and Propellers, Univ. of Notre Dame, In, Sept 15-19, 1991.

[13] Hsiao, C. and Bendiksen, O. O., "Finite Element Euler Calculations of Transonic Flutter in Cascades," AiAA 93-2083, 29th AIAA/ASME/SAE/ASEE Joint Propulsion Conf., Monterey, CA, June 28-30,1993.

[14] Davis, G. A. and Bendiksen, O. O., "Transonic Panel Flutter," AIAA 93-1479, AIAA/ASME/ASCE/AHS/ASCE 34th SDM Conf. La Jolla, CA., April 19-22, 1993.

[15] Bendiksen, O. O., "Nonclassical Aileron Buzz in Transonic Flow," AIAA 93-1479, AIAA/ASME/ASCE/AHS/ASCE 34th SDM Conf., La Jolla, CA, April 19-22, 1993.

[16] Gupta, K. K., *STARS —A Integrated General-Purpose Finite Element Structural, Aeroelastic, and Aeroservoelastic analysis Computer Program*, NASA TM-4795, May 1997.

[17]Gupta, K. K. and Meek, J. L., *Finite Element Multidisciplinary Analysis*, AIAA Education Series, July 2000.

[18] Przemieniecki, J. S., *Theory of Matrix Structural Analysis*, Dover Publications, Inc., New York, 1985.

[19] Zienkiewicz, O. C., and Taylor, R. L., *The Finite Element Method,* Fourth edition, McGraw Hill Book Company, London, 1994.

[20] Huebner, Kenneth H. and Thornton, Earl A., *The Finite Element Method for Engineers*, Second edition, John Wiley and Sons, New York, 1982.

[21] Gupta, K. K., "Solution of Quadratic matrix equations for Free Vibration Analysis of Structures " *International Journal for Numerical Methods in Engineering*, Vol. 6, pp 129–135, 1973.

[22] Gupta, K. K., "Solution of Eigenvalue Problem by Sturm Sequence Method," *International Journal for Numerical Methods in Engineering*, Vol. 6, pp. 379-404, 1972.

[23] Gupta, K. K., "Vibration of Frames and other Structures with Banded Stiffness Matrix," *International Journal for Numerical Methods in Engineering*, Vol. 2, pp. 221-228, 1970.

[24] Lanczos, C., "An Iteration Method for the Solution of the Eigenvalue Problem of Linear Differential and Integral Operators," *Journal of Research of the National Bureau of Standards*, Vol. 45, No. 4, October 1950.

[25] Lanczos, C., *Applied Analysis*, Englewood Cliffs, NJ. Prentice Hall, 1964.

[26] Hughes, T. J. R., *The Finite Element Method – Linear Static and Dynamic Finite Element Analysis*, Englewood Cliffs, NJ. Prentice Hall, 1987.

[27] Gupta, K. K., and C. L. Lawson, "Implementation of Block Lanczos Algorithm for Eigen solution of Gyroscopic System," NASA TM 88290, April 1987.

[28] DeSalvo, G. J. and Gorman, R. W., "ANSYS Engineering Analysis System User's Manual," Swanson Analysis Systems Inc., Houston, Pennsylvania, May 1989.

[29]Gupta, K.K., and Lawson, C. L., "Structural Vibration Analysis by a Progressive Simultaneous Iteration Method", *Proceedings of the Royal Society of London, Series A: Mathematical and physical Sciences*, Vol. 455, pp. 3415–3424, 1999.

[30] Yurkovich, R. N., Liu, D. D. and Chen, P. C., "The State-of-the Art of Unsteady Aerodynamics for High Performance Aircraft," AIAA 2001-0428, 39th AIAA Aerospace Sciences Metting & Exhibit, January 2001.

[31] Smilg, B., and Wasserman, L. S., "Application of Three Dimensional Flutter Theory to Aircraft Structures," *AIAA Journal*, Vol. 15, No. 1, January 1977.

[32] Yates, C. Jr., "Modified-Strip-Analysis Method for Predicting Wing Flutter at Subsonic to Hypersonic Speeds," *AIAA Journal of Aircraft*, Vol. 3, No. 1, January-February 1966.

[33] Rodden, W. P., "The Development of the Doublet-Lattice Method," International Forum on Aeroelasticity and Structural Dynamics, 1997.

[34] Giesing, J. P., Kalman, T. P. and Rodden, W. P., "Subsonic Unsteady Aerodynamics for General Configurations, Part II – Application of the Doublet-Lattice Method and the Method of Images to Lifting-Surfaces/Body Interference," USAF FDL-TR-5, Part II, 1972.

[35] Roden, W. P., Taylor, P. F. and McIntosh, S., "Further Refinement of the Non-Planar Aspects of the Subsonic Double-Lattice Lifting Surface Method," ICAS-96-2.8.2, 1996.

[36] Rodden, W. P., Taylor, P. F., McIntosh, S. C. and Baker, M. L., "Further Convergence Studies of the Enhanced Subsonic Doublet-Lattice Oscillatory Lifting Surface Method," International Forum on Aeroelasticity and Structural Dynamics, 1997.

[37] Blair, M., "A Compilation of the Mathematics Leading to the Doublet-Lattice Method," USAF WL-R 95-3022, 1994.

[38] Stark, V., "Aerodynamic Forces on a Combination of a Wing and a Fin Oscillating in Subsonic Flow," *SABB TN 54,* 1964.

[39] Davies, D. E., "Generalized Aerodynamic Forces on a T-tail Oscillatin in Subsonic Flow," Royal Aircraft Establishment Report Structures 295, 1964.

[40] Berman, J. H. et al., "Unsteady Aerodynamc Forces for General Wing/Control-Surface Configurations in Subsonic Flow," USAF FDL-TR-67-117, 1968.

[41] Zatarian, G. and Hsu, P. T., "Theoretical Studies on the Prediction of Unsteady Air Loads on Elastic Wings," WADC TR 56-97, December 1955.

[42] Danato, V. and Huhn, C., "Supersonic Unsteady Aerodynamics for Wings with Trailing Edge Control Surfaces and Folded Tips," AFFDL-TR-68-30, 1968.

[43] Li, J. M., Borland, C. J., and Hogley, J. R., "Prediction of Unsteady Aerodynamic Loading of Non-Planar Wings and Wing-Tail Configurations in Supersonic Flow," AFFDL-TR-71-158, 1972.

[44] Giesing, J. P. and Kalman, T. P., "Oscillatory Supersonic Lifting Surface Theory Using a Finite Element Doublet Representation," AIAA 75-761, 1975.

[45] Cunningham, A. M., "Oscillatory Supersonic Kernel Function Method for interfering Surfaces," *Journal of Aircraft*, Vol. 11, No. 11, pp. 664-670, April 1974.

[46] Cunningham, A. M., "Oscillatory Supersonic Kernel Function Method for Isolated Wings," *Journal of Aircraft*, Vol. 11, No. 10, p 609-615, April 1974.

[47] Jones, W. P. and Appa, K., "Unsteady Supersonic Aerodynamic Theory by the Method of Potential Gradient," *AIAA Journal*, Vol. 15, No. 1, Jan 1977.

[48] Jones, W. P. and Appa, K., "Unsteady Supersonic Aerodynamic theory for Interfering Surface by Method of Potential Gradient," NASA CR2892-1977.

[49] Jones, W. P. and Appa, K., "Integrated Potential Formulation of Unsteady Supersonic Aerodynamics for Interacting Wings," AIAA 16th Structures, Structural Dynamics, and Materials (SDM) Conference, Denver, Colorado, May 27-29, 1975.

[50] Brock, B J. and Griffin, J. A. Jr., "The Supersonic Doublet-Lattice Method-A Comparison of Two Approaches," AIAA 75-760, May 1975.

[51] Harder, R. L. and Rodden, W. P., "Kernel Function for Non planar Oscillating Surfaces in Supersonic Flow," *Journal of Aircraft*, Vol. 8, August 1971.

[52]Albano, J. P.and Rodden, W. P," A Doublet-Lattice Method for Calculating Lift Distribution on Oscillating Surface Subsonic flows," AIAA Journal, Vol. 7, No. 2, pp. 279-285, February 1969.

[53] Landahl,M. T., "Kernel Function for Nonplanar Oscillating Surfaces in a Subsonic Flow,"AIAA Journal, Vol. 5, No. 5, May 1967.

[54] Scanlan, R. and Rosenbaum, R., *Introduction To The Study of Aircraft Vibration And Flutter*, The MacMillan Company, New York, 1951.

[55] Meurovitch, L., *Analytical Methods in Vibrations*, The MacMillan Company, Collier-MacMillan Limited London, 1967.

[56] Hassig, H. J., "An Approximate True Damping solution of the Flutter Equation by Determinant Iteration", *Journal of Aircraft*, vol. 8, No. 11, pp. 885-889, November 1971.

[57] Gupta, K. K., Brenner, M. J., and Voelker, L. S., "Development of an Integrated Aeroservoelastic Analysis Program and Correlation With Test Data," NASA Technical Paper 3120, May 1991.

[58] Ogata, K., *Modern Control Engineering*, Prentice Hall, Englewood Cliffs, New Jersey, 1987.

[59] Lesoinne, M. and Farhat, C., "Geometric Conservation Laws for Aeroelastic Computation Using Structured Dynamic Meshes," AIAA 95-1709, 12th AIAA Computational Fluid Dynamics Conference, San Diego, California, June19-22 1995.

[60] Etkin, B., *Dynamics of Flight-Stability and Control*, Wiley, New York,1982.

[61] Shankar, V. and Ide, H.," Aeroelastic Computaions of Flexible Configurations," *Computers & Structures*, Vol. 30, No. 1/2, pp. 15-28, May 1988.

[62] Lohner, R.," An Adaptive Finite Element Solver for Transient Problems with Moving Bodies," *Computer & Structures,* Vol. 30, No. 1/2, page 303-317, May 1988.

[63] Farhat, C. and Lin, T. Y.," Transient Aeroelastic Computations Using Multiple Moving Frames of Reference," AIAA 90-3053, AIAA 8th Applied Aerodynamics Conference, Portland, Oregon, August 20-22, 1990.

[64] Thomas, P.D. and Lombard, C. K., "Geometric Conservation Law and its Application to Flow Computations on Moving Grids," *AIAA Journal*, Vol. 17, pp. 1030-1037, October 1979.

[65] Koobus, B. and Farhat, C.,"Second Order Time- Accurate and Geometrical Conservative Implicit Schemes for Flow Computations on Unstructured Dynamic Mesh," *Comp. Methods App. Mech. Engineering*, pp. 103-129, 170, 1999.

[66] Lesoinne, M. and Farhat, C., " Geometric Conservation Law for Flow Problem with Moving Boundaries & Deformable Mesh and Their Impact on Aeroelastic Computation," *Comp. Meths. App. Mech. Engineering*, pp. 71-90,134, 1996.

[67] Rausch, R. D., Batina, J. T. and Yang, H. T. Y.," Euler Flutter Analysis of Airfoils Using Unstructured Dynamic Meshes," *Journal of Aircraft*, Vol. 27, No. 5, pp. 436-443, May 1990.

[68] Robinson, B. A., Batina, J. T. and Yang, H. T. Y.," Aeroelastic Analysis of Wings Using the Euler Equations with a Deforming Mesh," *Journal of Aircraft*, Vol. 28, No. 11, pp. 781-758, May 1991.

[69] Jameson, A. and Mavriplis, D. J., "Finite Volume Solution of the Two-Dimensional Euler Equations on a Regular Triangular Mesh," *AIAA Journal*, Vol. 24, pp. 611-618, April 1986.

[70] Mavriplis, D. J., "Multigrid Solution of the Two-Dimensional Euler Equations on Unstructured Triangular Meshes," *AIAA Journal*, Vol. 26, pp. 824-832, July 1988.

[71] Jameson, A., Baker, T.J. and Weatherill N. P., "Calculation of Inviscid Transonic Flow Over a Complete Aircraft," AIAA 86-0103, January 1986.

[72] Morgan, K. and Peraire, J., "Finite Element Methods for Compressible Flow," Von Karman Institute for Fluid Dynamics Lecture Series 1987-07, Computational Fluid Dynamics, March 2-6, 1987.

[73] Lohner, R., "Finite Elements in CFD: What Lies Ahead," *International Journal for Numerical Methods in Engineering*, Vol. 24, pp. 1741-1756, April 1987.

[74] Morgan, K., Peraire, J., Thareja, R. R., and Stewart, J. R., "An Adaptive Finite Element Scheme for the Euler and Navier-Stokes Equations," AIAA 87-1172, June 1987.

[75] Peraire, J., Peiro, J., Formaggia, L. and Morgan, K., "Finite Element Euler Computations in Three Dimensions," AIAA 88-0032, January 1988.

[76] Lighthill, M. J., "On Displacement Thickness," *Journal of Fluid Mechanics*, pp. 383-392, June 1958.

[77] Sankar, N. L., Ruo, S. Y. and Malone, J. B., "Application of Surface Transpiration in Computational Aerodynamics," AIAA 86-0511, 1986.

[78]Gupta, K. K., "Development of a Finite Element Aeroelastic analysis Capability," *Journal of Aircraft,* Vol. 33, No. 5, pp. 995-1002,1992.

[79] Raj, P. and Harris, B., " Using Surface Transpiration with an Euler Method for Cost-effective Aerodynamic Analysis," AIAA 93-3506, 1996.

[80] Fisher, C. F. and Arena, A. S. Jr., " On the Transpiration Method for Efficient Aeroelastic Analysis Using an Euler Solver," AIAA 96-3436, 1996.

[81] Hunter, J. P. and Arena, A. S. Jr., "An Efficient Method for Time-Marching Supersonic Flutter Predictions Using CFD," AIAA 97-0733, 1997.

[82] Ashley, H. and Zartarian, G.,"Piston Theory – A New Aerodynaimc Tool for the Aeroleastician," *Journal of Aeronautical Sciences*, pp. 1109-1116, December 1956.

[83] Lighthill, M. J., "Oscillating Airfoils at High Mach Number," *Journal of Aeronautical Science*, Vol. 20, No. 6, pp. 402-406, June 1953.

[84] Pittman, J. L., "Application of Supersonic Linear Theory and Hypersonic Impact Methods to Three Dimensional Non-slender Hypersonic Airplane Concepts at Mach Numbers from 1.10 to 2.86,", NASA TP-1539, 1979.

[85]Lo, S. H., "A New Mesh Generation Scheme for Arbitrary Planar Domains," *International Journal for Numerical Methods in Engineering*, Vol. 21, pp. 1403–1426, August 1985.

[86] Peraire, J., Peiró, J., Formaggia, L., Morgan, K., and Zienkiewicz, O. C., "Finite Element Euler Computations in Three Dimensions, *International Journal for Numerical Methods in Engineering,* Vol. 26, pp. 2135–2159, Oct. 1988.

[87] Peraire, J., Vahdati, M., Morgan, K., and Zienkiewicz, O. C., "Adaptive Remeshing for Compressible Flow Computations," *Journal Comput. Phys.*, Vol. 72, 1987.

[88] Gupta, K. K., Petersen, K. L., and Lawson, C. L., "Multidisciplinary Modeling and Simulation of a Generic Hypersonic Vehicle," AIAA 91-5015, December 1991.

[89] Gupta, K. K., Petersen, K. L., and Lawson, C. L., "On Some Recent Advances in Multi-disciplinary Analysis of Hypersonic Vehicles," AIAA 92-5026, December 1992.

[90] Ljung, L., *System Identification: Theory For The User*, Printice Hall Inc., NJ,1987.

[91] Hollkamp, J. J. and Battill, S. M., "Automated Parameter Identification and Order Reduction for Discrete Time Series Models," *AIAA Journal*, Vol. 29, No. 1, pp. 96-103, 1991.

[92] Pinkelman, J. K., Batill, S. M. and Kehoe, M. W., "Total least Squares Criteria in Parameter Identification for Flight Flutter Testing," Journal of Aircraft, Vol. 33, No. 4, pp. 784-792, 1996.

[93] Hollkamp, J. J. and Battil, S. M., "A Recursive Algorithm For Discrete Time Domain Parameter Identification," AIAA 90-26805, 1990.

[94] Hamel, P. G. and Jategaonkar, R. V., "Evolution of Flight Vehicle System Identification," *Journal of Aircraft*, Vol. 33, No. 1, pp. 9-28, 1996.

[95] Cowan, T. J. Arena, A. S. and Gupta, K. K., "Accelerating CFD-Based Aeroelastic Prediction Using System Identification," AIAA 98-4152, August 1998.

[96] Stephens, C. H., ., "CFD Based Aeroservoelastic Predictions with comparisons to Benchmark experimental Data," *AIAA Journal of Aircraft*, Vol. 38, No. 1, pp. 81-87, January-February 2001.

[97]Cowan, T. J., "Development of a Discrete-time Aerodynamic Model for CFD-Based Aeroelastic Analysis," *AIAA Journal of Aircraft* (In Press 2001).

[98] Peiro′, J., Peraire, J., and Morgan, K., *FELISA System Reference Manual: Part 2-User Manual*, December 3, 1993.

[99] Engelund, W. C., Holland, S. D., Cockrell, C. E. Jr. and Bittner, R. D., "Aerodynamic Database Development for the Hyper-X Airframe Integrated Scramjet Propulsion Experiment," AIAA 2000-4006, 18th AIAA Applied Aerodynamics Conference, Denver, Colorado, August 2000.

[100] Cockrell, C. E., Jr., Engelund, W. C., Bittner, R. D., Dilley, A. D., Jentink, T. N., and Frendi, A., "Integrated Aero-Propulsive CFD Methodology for the Hyper-X Flight Experiment," AIAA 2000-4010, 18th AIAA Applied Aerodynamics Conference, Denver, Colorado, August 2000.

[101] Gupta, K. K., Voelker, L. S., Bach, C., Doyle, T. and Hahn, E., "CFD-Based Aeroelastic Analysis of the X-43 Hypresonic Flight Vehicle," AIAA 2001-0712, 39th Aerospace Sciences Meeting & Exhibit, Reno, Nevada, 8-11 January 2001.

[102] Gupta, K. K., Voelker, L. S., and Bach, C., "Finite Element CFD-Based Aeroservoelastic analysis," AIAA 2002-0953, 40th Aerospace Sciences Meeting & Exhibit, Reno, Nevada, 14-17 January 2002.

[103] Bailey, C., Taylor, G. and Cross, M., "Discretisation Procedures for Multi-Physics Phenomena," *Journal of Computational and Applied Mathematics*, Vol. 103, pp. 3-17, 1999.

[104] Wheeler, D., Bailey, C. and Cross, M., "Numerical Modeling and Validation of Marangoni and Surface Tension Phenomena Using the Finite Volume Method," *International Journal for Numerical Methods in Fluids*, Vol. 32, pp. 1021-1047, 2000.